REACTIONS OF METHYLFLUOROSILANES WITH SINGLET METHYLENE AND WITH NITRIC OXIDE ($^4\pi$)

by

Gabriela E. Soto-Garrido

Bachiller en Quimica, Universidad de Concepcion, (Chile), 1972.

Licenciado en Quimica, Universidad de Concepcion, (Chile), 1974.

A THESIS SUBMITTED IN PARTIAL FULFILLMENT

OF THE REQUIREMENTS FOR THE DEGREE OF

DOCTOR OF PHILOSOPHY

in the Department

of

Chemistry

SIMON FRASER UNIVERSITY

January, 1984

APPROVAL

Name: Gabriela E. Soto-Garrido

Degree: Doctor of Philosophy

Title of Thesis: **"Reactions of MethylFluoro Silanes with Singlet Methylene and with Nitric Oxide ($^4\pi$)"**

Examining Committee:

Chairman: Dr. C.H.W. Jones

Dr. T.N. Bell, Professor
Co-Senior Supervisor

Dr. A.G. Sherwood, Associate Professor, Co-Senior Supervisor

Dr. D. Sutton, Professor
Supervisory Committee

Dr. B.L. Funt, Professor
Internal Examiner

Dr. O.P. Strausz, Professor
External Examiner
Chemistry Department, University of Alberta

Date Approved: February 9, 1984

PARTIAL COPYRIGHT LICENSE

I hereby grant to Simon Fraser University the right to lend my thesis, project or extended essay (the title of which is shown below) to users of the Simon Fraser University Library, and to make partial or single copies only for such users or in response to a request from the library of any other university, or other educational institution, on its own behalf or for one of its users. I further agree that permission for multiple copying of this work for scholarly purposes may be granted by me or the Dean of Graduate Studies. It is understood that copying or publication of this work for financial gain shall not be allowed without my written permission.

Title of Thesis/Project/Extended Essay

"Reactions of MethylFluoro Silanes with Singlet Methylene and with Nitric Oxide ($^4\pi$)"

Author: _____
(signature)

Gabriela E. Soto-Garrido
(name)

27 Feb, 1991
(date)

ABSTRACT

This thesis describes two separate studies of the gas phase reactions of methylfluorosilanes.

The first comprises the reactions of compounds of general formula Me_xSiF_{4-x} with electronically excited NO, namely $^4\pi$ NO.

It was found that the decomposition of NO photosensitized by Hg $6(^3P_1)$ atoms shows enhanced formation of the decomposition products, N_2 and N_2O, in the presence of the silanes Me_2SiF_2 and $MeSiF_3$.

A mechanism is proposed involving the formation of two different silane-NO intermediate complexes. This mechanism satisfies the experimental observations and incorporates the accepted mechanism for the Hg-sensitized decomposition of NO itself.

The second series of reactions studied was that of methylene (CH_2) produced from the photolysis of ketene at 313 nm with, again, the series of compounds of general formula Me_xSiF_{4-x}. These reactions were carried out in the presence and absence of NO.

The experimental observations of the products formed leads to the conclusion that singlet methylene inserts into the C-H bonds of $MeSiF_3$, Me_2SiF_2 and Me_3SiF to give the respective

ethyl derivatives, and in the case of Me_2SiF_2 inserts into the Si-F bond to yield $Me_2Si(CH_2F)F$.

The rate constants for insertion into the different silanes were determined with respect to the known reaction:

$$^1CH_2 + CH_2CO \longrightarrow C_2H_4 + CO$$

The relative rates, so determined, for insertion into C-H by singlet methylene are as follows:

Reactant	Relative Rates
$MeSiF_3$	1
Me_2SiF_2	2.4
Me_3SiF	6.6
Me_4Si	8.8

Insertion into the Si-F bond of Me_2SiF_2 is 6.5 times slower than the corresponding insertion into the C-H bond.

These results are discussed in terms of bond energy and steric effects.

TO MY HUSBAND, VICTOR

AND MY PARENTS

ACKNOWLEDGEMENTS

I would like to thank Dr. T.N. Bell and Dr. A.G. Sherwood for their helpful and patient supervision, as well as for their continuous advice.

Sincere thanks are also extended to:

Dr. D. Sutton for his time as member of my supervisory committee;

Dr. K.E. Newman and Ms. Kim Adamson-Sharpe for help with the computing aspects of data analysis;

The technical staff of the Chemistry Department for their cooperation and assistance;

Miss Pat Doidge for kindly typing this manuscript.

This work was performed during a leave-of-absence from Universidad de Concepción, Chile.

TABLE OF CONTENTS

LIST OF TABLES

LIST OF FIGURES

General Introduction

The research work presented in this thesis continues a series of studies in this laboratory with the organosilicon compounds of general formula Me_xSiF_{4-x} (x = 0,1,2,3,4).

The present work was undertaken to obtain further information on the reactivity of these substances. Previous work has clearly shown that such factors as electronegativity, size, and $d\pi$-$p\pi$ bonding contributions make significant differences in the reactivities of silicon compounds compared to those of their carbon analogues.

The methylfluorosilanes do not absorb light except in the far ultraviolet spectral region (below 180 nm), and thus, their reactions with species produced photochemically outside this spectral region can be conveniently studied.

The work described in this thesis is in two main parts:

PART I - Describes the reactions of the compounds of formula Me_xSiF_{4-x} with electronically excited NO, namely $NO(^4\pi)$. The $NO(^4\pi)$ is produced by reactions of NO with Hg $6(^3P_1)$ atoms, i.e., by the process of mercury photosensitization. The silanes are inefficient quenchers of excited mercury and thus there is no complication from the mercury photosensitization of these compounds. A mechanism is proposed to explain the kinetic data.

PART II - Describes the reactions of the silanes Me_xSiF_{4-x} with methylene (CH_2) produced by the direct photolysis of ketene at 313 nm. Trends in reactivities of the series of silanes towards $^1CH_2$ were established, and relative rate constants measured for the insertion reaction into C-H bonds. General mechanistic proposals are made to account for the products formed.

PART I

THE EFFECT OF SILANES ON THE MERCURY-PHOTOSENSITIZED DECOMPOSITION OF NITRIC OXIDE.

I-1. INTRODUCTION

The reaction of NO with Hg $6(^3P_1)$ is well known, and a mechanism proposed by Strausz and Gunning which involves the participation of an electronically excited NO molecule ($^4\pi$) provides a good kinetic fit to their results.

Our interest in adding methylfluorosilanes was to determine if collisions with NO($^4\pi$) would cause C-Si bond cleavage and yield fluorosilyl radicals. No evidence of such a photosensitized reaction was found. Instead, it was determined that the silanes enhanced the decomposition of NO.

The reactivity of the silanes, $MeSiF_3$ and Me_2SiF_2, with Hg $6(^3P_1)$ was also studied and under our experimental conditions, there was no indication of any reaction products.

In the following literature survey, the literature relating to the work described in Part I is summarized.

I-2. LITERATURE SURVEY

I-2.1 Mercury Photosensitized Reactions

The great majority of studies of atom-photosensitized reactions have involved the use of mercury. Two characteristics of mercury which have made it particularly useful (1) are:

i) a sufficiently high vapor pressure at reasonably low temperatures, i.e., 1.43 mtorr at 22°C.

ii) an excitation energy (468.6 kJ) of the right order of magnitude to be of interest from a chemical point of view.

In other words, mercury-photosensitization provides a convenient means of initiating gas phase chemical reactions.

The excited mercury atom, Hg $6(^3P_1)$ is produced by the absorption of 253.7 nm resonance radiation from a low pressure mercury lamp. This process may be represented:

I-1 Hg $6(^1S_0)$ + $h\nu$ → Hg $6(^3P_1)$

The photoexcited atom may lose its excess energy by the following photophysical and photochemical processes (2a):

Photophysical processes:

a) Resonance phosphorescence

I-2 Hg $6(^3P_1)$ → Hg $6(^1S_0)$ + $h\nu_p$

b) Deactivation to the ground state

I-3 Hg $6(^3P_1)$ + M → Hg $6(^1S_0)$ + Mν, where Mν is a vibrationally excited molecule decaying by a non-radiative physical process.

c) Deactivation to a metastable state, eg.,

I-4 $Hg\ 6(^3P_1) + N_2 \rightarrow Hg\ 6(^3P_0) + N_2^*$ (20.9 kJ)

Photochemical processes:

d) Chemical quenching, via direct dissociation

I-5 $Hg\ 6(^3P_1) + RH \rightarrow Hg\ 6(^1S_0) + R + H$

e) Chemical quenching, to form an electronically excited molecule

I-6 $Hg\ 6(^3P_1) + C_2H_4 \rightarrow Hg\ 6(^1S_0) + C_2H_4^*$

The electronically excited molecule may subsequently react to form new products.

f) Chemical quenching, dissociation via an intermediate

I-7 $Hg\ 6(^3P_1) + RH \rightarrow HgH + R \rightarrow Hg\ 6(^1S_0) + H + R$

The energy levels of the lower excited states of mercury and some relevant transitions are shown in Fig. I-1.

In 1947, Laidler (3) rationalized the experimental results on metal-photosensitized reactions of hydrocarbons by applying the spin conservation rules (2) to these processes. In general, those processes in which the total spin angular momentum remains unaltered, are favored. Furthermore, an energy transfer reaction may take place if the quenching gas has low-lying electronic states of the proper multiplicity.

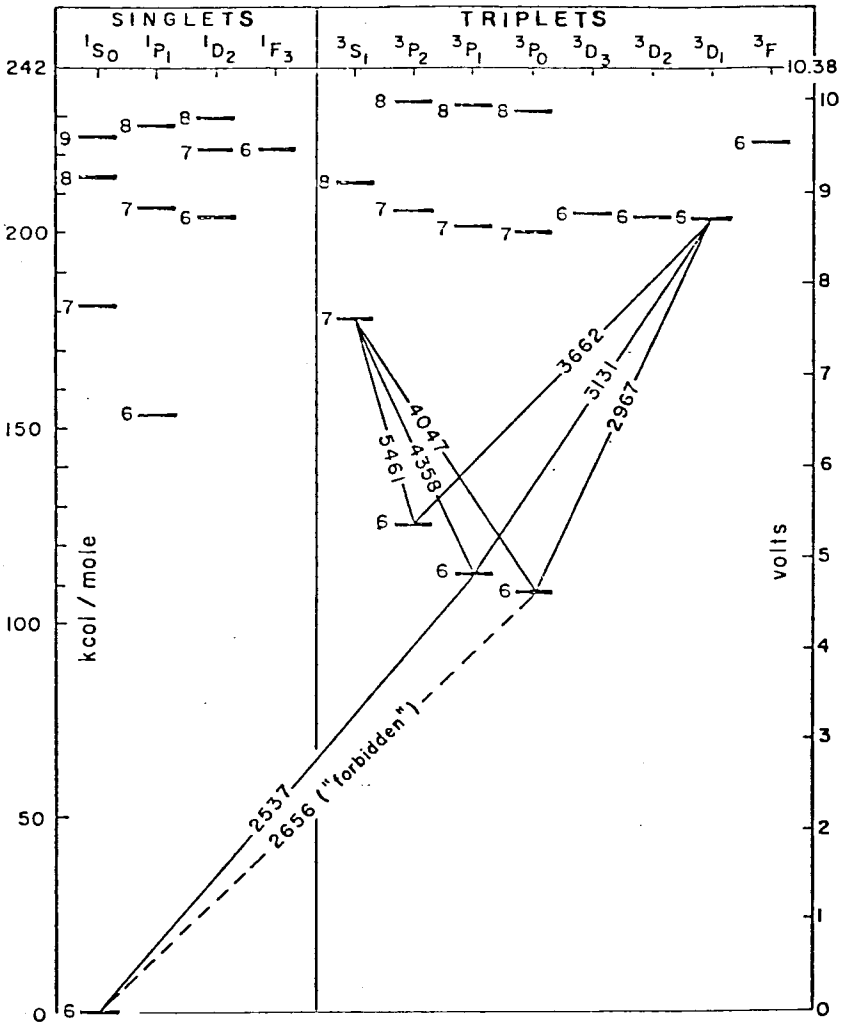

Fig. I-1. Lower Energy Levels of Mercury. Reprinted with permission from (Progress in Reaction Kinetics, Vol 2, R.J. Cvetanovic, G. Porter (Ed.), Mercury Photosensitized Reactions), Copyright (1964), Pergamon Press Ltd.

I-2.2 Quenching Cross Section

The efficiency of the energy transfer process is given in terms of the quenching cross section, σ_Q^2, which is defined by the following expression derived from the kinetic theory of gases:

$$I\text{-}8 \qquad {}_AZ_B = N_A N_B \sigma_Q^2 \{8\pi RT(\frac{1}{M_A} + \frac{1}{M_B})\}^{1/2}$$

where ${}_AZ_B$ represents the frequency of collisions per unit volume between two species A and B of molecular weight M_A and M_B present in concentrations equal to N_A and N_B molecules per unit volume at a temperature T.

In general, the disappearance of Hg* $6(^3P_1)$ atoms by collision with any quencher Q is given by the rate equation I-9:

$$I\text{-}9 \qquad -\frac{d[Hg^*]}{dt} = k_Q N_{Hg^*} N_Q$$

Assuming that every collision is effective in quenching,

$$I\text{-}10 \qquad k_Q = \sigma_Q^2 \{8\pi RT(\frac{1}{M_{Hg}} + \frac{1}{M_Q})\}^{1/2}$$

The value of σ_Q^2 is usually expressed in $Å^2$.

Quenching cross sections have been obtained by the use of two different methods:

a) Physical Method.

This method was first employed by Zemansky in 1930 (4) and has been subsequently improved by several research groups (5). It is based upon physical measurements of the intensity of resonance phosphorescence in the absence and presence of an added quencher.

Assuming only the following processes are occurring:

I-1 $Hg^\circ + h\nu \rightarrow Hg^*$

I-2 $Hg^* \rightarrow Hg^\circ + h\nu_p$

I-11a $Hg^* + Q \rightarrow Hg\dagger + Q^*$

I-11b $Hg^* + Q \rightarrow Hg^\circ + P_1 + P_2$

where $Hg^* = Hg\ 6(^3P_1)$, $Hg\dagger = Hg\ 6(^3P_0)$, $Hg^\circ = Hg\ 6(^1S_0)$, Q is any quenching gas, Q* is the quenching gas with excess energy and P_1 and P_2 are dissociation products, then reactions I-11a and I-11b represent the total non-radiative consumption of Hg* atoms.

Equation I-12 is obtained when steady state treatment is applied to the above sequence, provided the presence of the quencher does not cause any change in the rate of production of the excited mercury atoms.

I-12 $$\frac{I_P}{I_P^Q} = 1 + k_Q \tau^\circ [Q]$$

where I_P and I_P^Q are the phosphorescence intensities in the absence and presence of the quencher, τ° is the lifetime of Hg* in the absence of quencher, and $k_Q = (k_{11a} + k_{11b})$. I-12 is known as the Stern-Volmer equation. τ° has been determined to be 1.14×10^{-7} s (5d), thus k_Q can be obtained from the slope of plots of I_P/I_P^Q versus pressure of the added quencher, and σ_Q^2 is readily calculated from equation I-10.

Equation I-12 represents an ideal situation which in practice is not always obtained. Thus, certain discrepancies are found in the values of σ_Q^2 reported in the literature (2,4,5) as a result of different approaches used to correct for factors such as Lorentz broadening and radiation imprisonment (2).

b) Chemical Method.

This method developed by Cvetanovic (6) is based upon competitive quenching and is independent of those additional factors which need be considered in the physical method. The method basically consists of irradiating mixtures of nitrous oxide and a substrate S in the presence of mercury vapor. The substrate should react with oxygen atoms to avoid the deposition of HgO on the cell windows and to suppress N_2 formation by reaction I-15.

I-13 $\quad Hg^* + N_2O \rightarrow Hg^\circ + N_2 + O$

I-14 $\quad Hg^* + S \rightarrow Hg^\circ + \text{products}$

I-15 $\quad O + N_2O \rightarrow O_2 + N_2$

If reactions I-13 and I-14 represent the only fate of Hg* Cvetanovic has shown that the following expression for N_2 production is obeyed.

$$\text{I-16} \quad \frac{1}{R_{N_2}} = \frac{1}{I_A}\left\{1 + \frac{k_S}{k_{N_2O}}\frac{[S]}{[N_2O]}\right\}$$

where I_A is the intensity of light absorbed by process I-1. Equation I-16 is independent of the time of irradiation, temperature, circulation or pressure. The ratio k_S/k_{N_2O} is then determined from the slope and intercept of the linear plot of $R_{N_2}{}^{-1}$ against $[S]/[N_2O]$. This ratio is related to the effective quenching cross-sections by the expression I-17 (refer to eq. I-10).

$$\text{I-17} \quad \frac{\sigma_S{}^2}{\sigma_{N_2O}^2} = \frac{k_S}{k_{N_2O}}\frac{\left(1 + M_{Hg}/M_{N_2O}\right)^{1/2}}{\left(1 + M_{Hg}/M_S\right)^{1/2}}$$

Thus, quenching cross sections are determined relative to the cross section of nitrous oxide.

The system has also proved useful as an actinometer. Relation I-16 provides a method for the determination of the amount of light absorbed by mercury atoms. In such instances, mixtures of N_2O-nC_4H_{10} are generally used (8).

I-2.3 The Reactions of Hg $6(^3P_1)$ with Silanes

Silicon hydrides and alkyl silanes, like hydrocarbons, do not absorb light of the near U.V. region, but they are susceptible to dissociation by mercury-photosensitization.

Gunning and coworkers (9) studied the reactions of Hg* $6(^3P_1)$ with various methyl substituted silanes and have shown that the primary process is exclusively the cleavage of an Si-H bond if present; otherwise C-H scission occurs. The following simple sequence of reactions was offered to explain their results, where $\gtrless$Si-H represents the silane.

I-18 $\quad \gtrless Si\text{-}H + Hg^* \rightarrow \gtrless Si + H + Hg^\circ$

I-19 $\quad H + \gtrless Si\text{-}H \rightarrow \gtrless Si + H_2$

I-20 $\quad \gtrless Si + Si\lessgtr \rightarrow \gtrless Si\text{-}Si\lessgtr$

I-21 $\quad H + H + M \rightarrow H_2 + M$

The radicals formed in the primary process will result in hydrogen and the corresponding disilane through 19, 20 and 21. Thus, a compound such as Me_3SiH will provide a clean source of substituted silyl radicals.

Yarwood, Strausz and Gunning (5b) have previously determined the quenching cross section of some silicon derivatives. They proposed that quenching occurs by the Si-H bond which is about 10-500 times more efficient as a quencher than the C-H bond. Their values, presented in Table I-1, also show that the

quenching reactivity of Si-H bonds increases with increasing alkyl substitution and that fluorine substitution strongly suppresses quenching.

The efficiency of the energy transfer process involved in mercury photosensitization has been related to the electrophilic character (10) of the Hg $6(^3P_1)$ atom. Nevertheless, there is, as yet, no clear understanding of the details of the energy-transfer processes.

In their study with the silanes, Gunning and coworkers (9) have also investigated the reactions of the silanes with Hg $6(^3P_1)$ in the presence of NO. Addition of small amounts of

Table I-1 Quenching Cross Section of Silanes and their C-Analog with Hg $6(^3P_1)$ Atoms (5b)

Si Compound	σ_Q^2 / Å^2	C Analog	σ_Q^2 / Å^2
SiH_4	26	CH_4	0.06
$MeSiH_3$	32	C_2H_6	0.10
Me_2SiH_2	33	C_3H_8	1.5
Me_3SiH	30	Me_3CH	6.8
Me_4Si	5.0	Me_4C	1.4
Me_3SiF	2.0		
Me_2SiF_2	0.19		

NO completely suppressed the formation of the disilane (reaction I-20) and markedly increased the hydrogen yields. Moreover, N_2 and a disiloxane containing the primary radical were important products. High quantum yields suggested a chain process. These workers proposed the sequence I-22 to I-25, to explain their semi-quantitative observations.

I-22 $R + NO \rightarrow RON$

I-23 $2\ RON \rightarrow 2RO + N_2$

I-24 $RO + RH \rightarrow ROR + H$

I-25 $H + RH \rightarrow H_2 + R$

The addition of step I-22 was favored by the authors in view of the much higher affinity of silicon atoms for oxygen than for nitrogen, i.e., bond dissociation energies (D) are: D_{Si-O} = 812 kJ/mol in $(Me_3Si)_2O$ and D_{Si-N} = 320 kJ/mol in $(Me_3Si)_2NH$ (12).

I-2.4 The Reactions of Hg $6(^3P_1)$ with NO.

The reaction of Hg* $6(^3P_1)$ atoms with NO was first studied by Noyes (13) who established that the rate of the reaction was

i) first order in light intensity, and

ii) first order in nitric oxide pressure in the range 0.003-0.13 torr. The primary process was found to be adequately described by,

$$\text{I-26} \quad Hg^* + NO \rightarrow NO^* + Hg^\circ$$

where NO* represents a long-lived, vibrationally excited NO molecule. It should be noted that NO only absorbs light at wavelengths shorter than 230 nm (2).

Subsequently, Bates (5a) determined a quenching cross section for NO, σ_Q^2 of 24.7 $Å^2$, which shows that nitric oxide is indeed an efficient quencher of Hg $6(^3P_1)$ atoms.

Later, Fallon and coworkers (14) proposed on energetic grounds that NO* corresponds to one of the lower vibrational levels of the $^4\pi$ state. From spectroscopic data and quantum mechanical theory (15) they had estimated that the lowest vibrational level of the $^4\pi$ state lies 448 ± 10 kJ above the lowest vibrational level of the ground state ($^2\pi$). Improved calculations have placed the $^4\pi$ state of NO 453.5 kJ above the ground state. Fig. I-2 shows the two lowest-lying electronic states of NO as given by Gilmore (16). Thus, the previous equation I-26

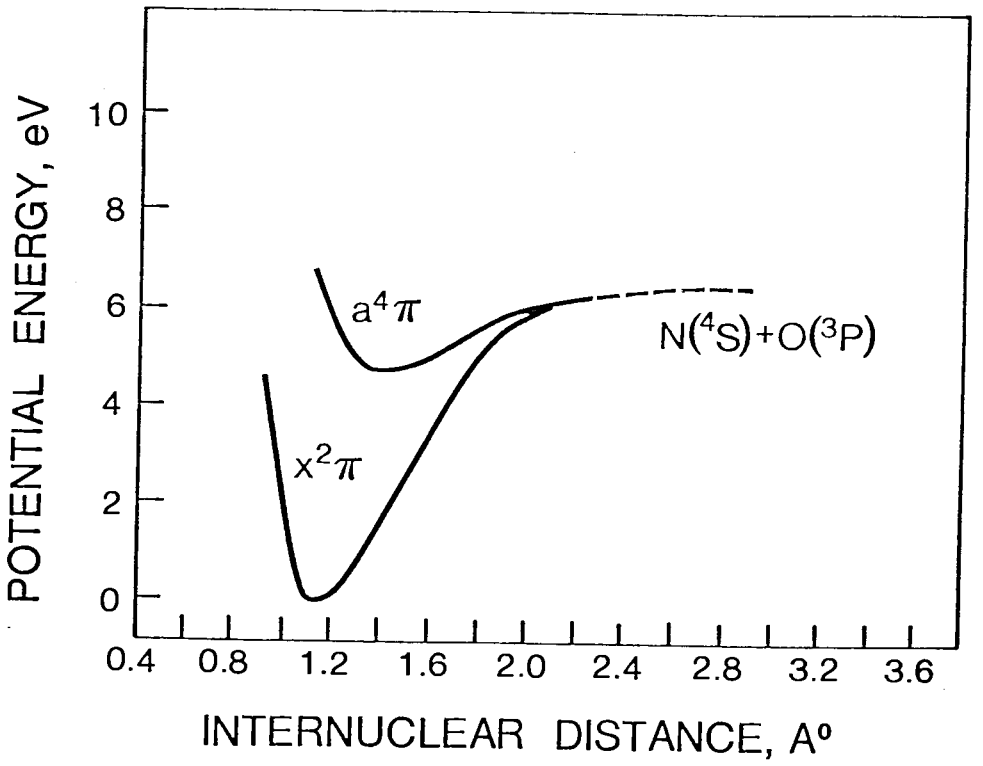

Fig. I-2. Potential Energy Curves for the Lower Electronic States of Nitric Oxide, NO. (1 ev = 96.48 kJ/mol). (Adapted From Reference 16)

represents the process given in equation I-27. Such a process complies with the spin conservation rules.

$$\text{I-27} \quad \text{Hg } 6(^3P_1) + NO(^2\pi) \rightarrow \text{Hg } 6(^1S_0) + NO(^4\pi)$$

More recently, Callear and Norrish (17) proposed that Hg $6(^3P_1)$ must be converted directly to the ground state since no Hg $6(^3P_0)$ was detected in the Hg-NO system. This observation, therefore, excludes the following process from a mechanistic explanation of the reaction of Hg $6(^3P_1)$ atoms with NO:

$$\text{I-28} \quad \text{Hg } 6\ (^3P_1) + NO \rightarrow \text{Hg } 6(^3P_0) + NO^v$$

where NO^v is a vibrationally excited ground state molecule.

Strausz and Gunning (18) presented a detailed study of the reaction of NO with Hg $6(^3P_1)$ and for the first time, the formation of nitrous oxide, N_2O, was reported. The reaction was investigated under static conditions at 30°C over the pressure range 1 to 286 torr in which case N_2, N_2O and higher oxides of nitrogen were the observed products. It was found that above 4 torr, the sum of the quantum yields, $\Phi_{N_2} + \Phi_{N_2O}$, was independent of the NO pressure, while the ratio Φ_{N_2O}/Φ_{N_2} increased linearly with the substrate pressure. The experimental results were consistent with the proposed mechanism:

I-1 $Hg^{\circ} + h\nu \rightarrow Hg^{*}$

I-27 $Hg^{*} + NO \rightarrow NO^{*} + Hg^{\circ}$

I-29 $NO^{*} + NO \rightarrow 2NO$

I-30 $NO^{*} + NO \rightarrow (NO)_2^{*}$

I-31 $(NO)_2^{*} \rightarrow N_2 + O_2$

I-32 $(NO)_2^{*} + NO \rightarrow N_2O + NO_2$

The primary step involves quenching of triplet mercury to yield NO^{*} ($NO^{4}\pi$). This species may be either deactivated by collision with another NO molecule or may form the energy rich dimer $(NO)_2^{*}$. The excited dimer may then produce N_2 or N_2O by two different paths. It should be noted from the low quantum yield of product formation,

$\Phi_{N_2} + \Phi_{N_2O} = 1.9\times10^{-3}$ (moles/einstein) that the deactivation reaction (I-29) constitutes the most important fate of NO^{*}.

I-2.5 The Reactions of NO*($^4\pi$) with Hydrocarbons

Strausz and Gunning (19) studied the reactions of NO($^4\pi$) molecules generated by Hg* 6($^3P_1$) photosensitization with several hydrocarbons: methane, ethane, propane, and neopentane. The hydrocarbons have a small quenching cross section with respect to Hg 6($^3P_1$) atoms. In all cases, a marked increase in the nitrogen and nitrous oxide yields was noticed. A detailed study of the ethane-nitric oxide system gave the following reaction products: N_2, N_2O, H_2O, NO_2, CO, CO_2, C_2H_4, acetaldehyde, nitroethane, ethylnitrite, ethylnitrate, nitroethylene, nitromethane, methylnitrite, methylnitrate and formaldehyde.

The following sequence was proposed to account for the experimental observations:

I-1 $\quad Hg + h\nu \rightarrow Hg^*$

I-27 $\quad Hg^* + NO \rightarrow NO^* + Hg^o$

I-33 $\quad NO^* + RH \rightarrow R + H + NO$

where NO* is acting as the sensitizer which causes the breaking of a C-H bond.

This reaction scheme is further complicated by the secondary reactions of the alkylradicals produced in I-33 which will react with nitric oxide to form the corresponding nitroso compounds:

I-34 $R + NO \rightarrow RNO$

These compounds may undergo a series of reactions which form the observed products.

I-3. EXPERIMENTAL

A. Vacuum Apparatus

In these studies, a conventional Pyrex high-vacuum apparatus was used (Figs. I-3, I-4). A combination of a DuoSeal (Welch model 1402) vacuum pump with a two stage mercury diffusion pump gave a vacuum of 10^{-6} torr or better. A liquid nitrogen trap was placed between the two pumps.

The apparatus was provided with facilities for gas introduction, measurement, purification and storage (Fig. I-3). It was attached to a Gas Chromatograph (Fig. I-4) to allow product analysis, separation and collection. Distillations were performed in a train of "U" traps interconnected through mercury float valves. Pressures were indicated by a four station LKB Autovac Vacuum gauge (Model 3294B) calibrated against a McLeod gauge which was connected to the high vacuum manifold by a mercury float valve.

A secondary vacuum line with an independent mechanical pump provided a rough vacuum which was used to lower the mercury from the mercury float valves, Toepler pump, doser and manometers and to evacuate sections of the vacuum line in order to avoid pumping large quantities of materials through the primary pump.

Fig. I-3. Schematic Diagram of Vacuum Apparatus.

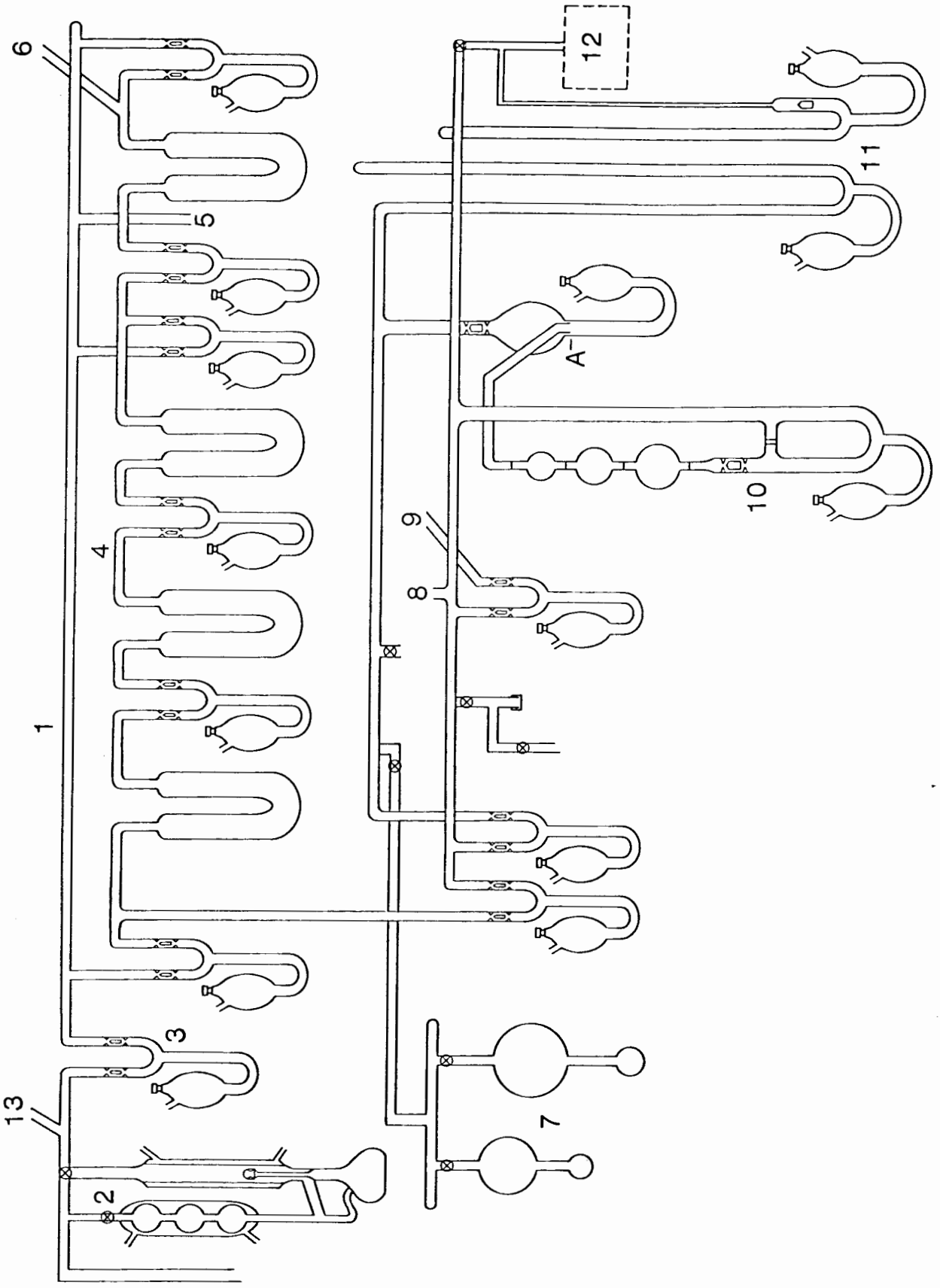
6
5
4
1
3
13
2
7
9
8
12
11
A⁻
10

Fig. I-4. Schematic of Analytical System.

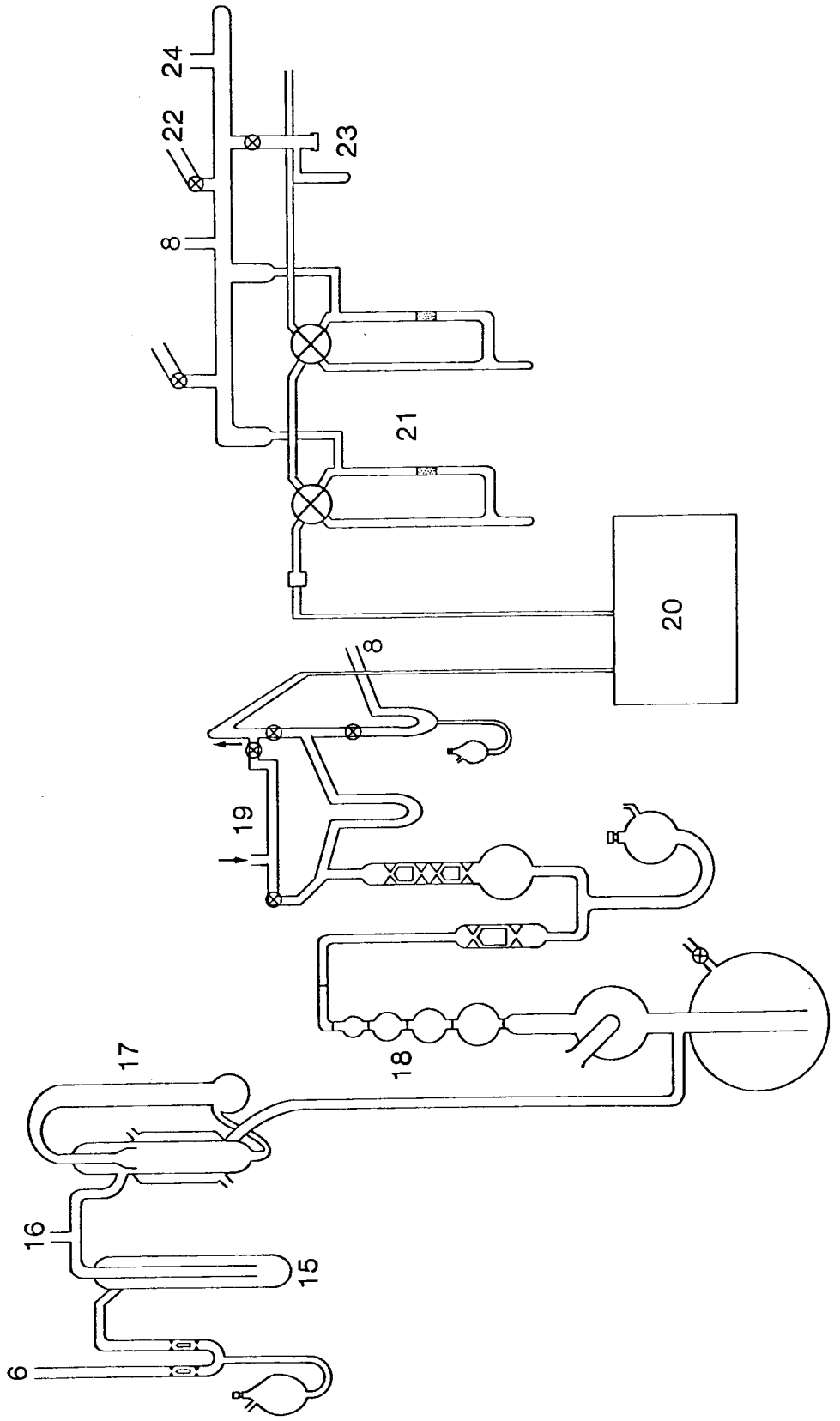
24
22
23
8
21
20
8
19
18
17
16
15
6

Key to Figures

Figure I-3

1. Main vacuum manifold
2. Mercury diffusion pump
3. Mercury float valve
4. Distillation train
5. Connection to McLeod gauge
6. Connection to analytical system
7. Storage bulbs
8. Pirani gauge head
9. Connection to analytical system
10. Gas metering device
11. Mercury manometers
12. Reaction system
13. Connection to analytical system

Figure I-4

15. Cold trap to prepare solid nitrogen
16,24. Pirani gauge head
17. Mercury diffusion pump
18. Toepler gas burette
19. Sample loop
20. Gas chromatograph
21. Traps
22. Connection to secondary vacuum
23. Analytical outlet

Three reaction vessels were used in the course of this research. The first one was cylindrical (5 cm diameter, 10 cm length), total volume 215 ± 3 cc, made of quartz and with a cold finger. The second vessel, used in the pyrolysis studies, was made of quartz, total volume 169 ± 1 cc and is shown in Fig. I-5. Each vessel was individually connected to the high vacuum apparatus and used in static experiments.

A third vessel, made of Pyrex with Suprasil windows was 5 cm in diameter and 2.2 cm long and was used in closed loop flow experiments where a circulatory system was employed.

All vessels were attached in position by Cajon stainless steel fittings.

The circulatory apparatus, Fig. I-6a, with a total volume of 238 ± 1 cc was connected to the high vacuum system. This apparatus comprised the reaction vessel, a gas circulating pump and a mercury saturator.

Key to Figure I-6a

1. Reaction cell
2. Mercury saturator
3. Condenser
4. Circulatory gas pump

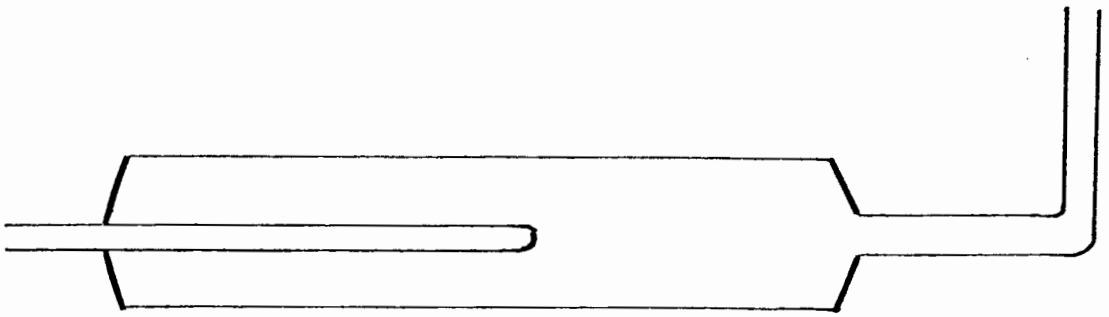

Fig. I-5. Vessel Used at High Temperatures.

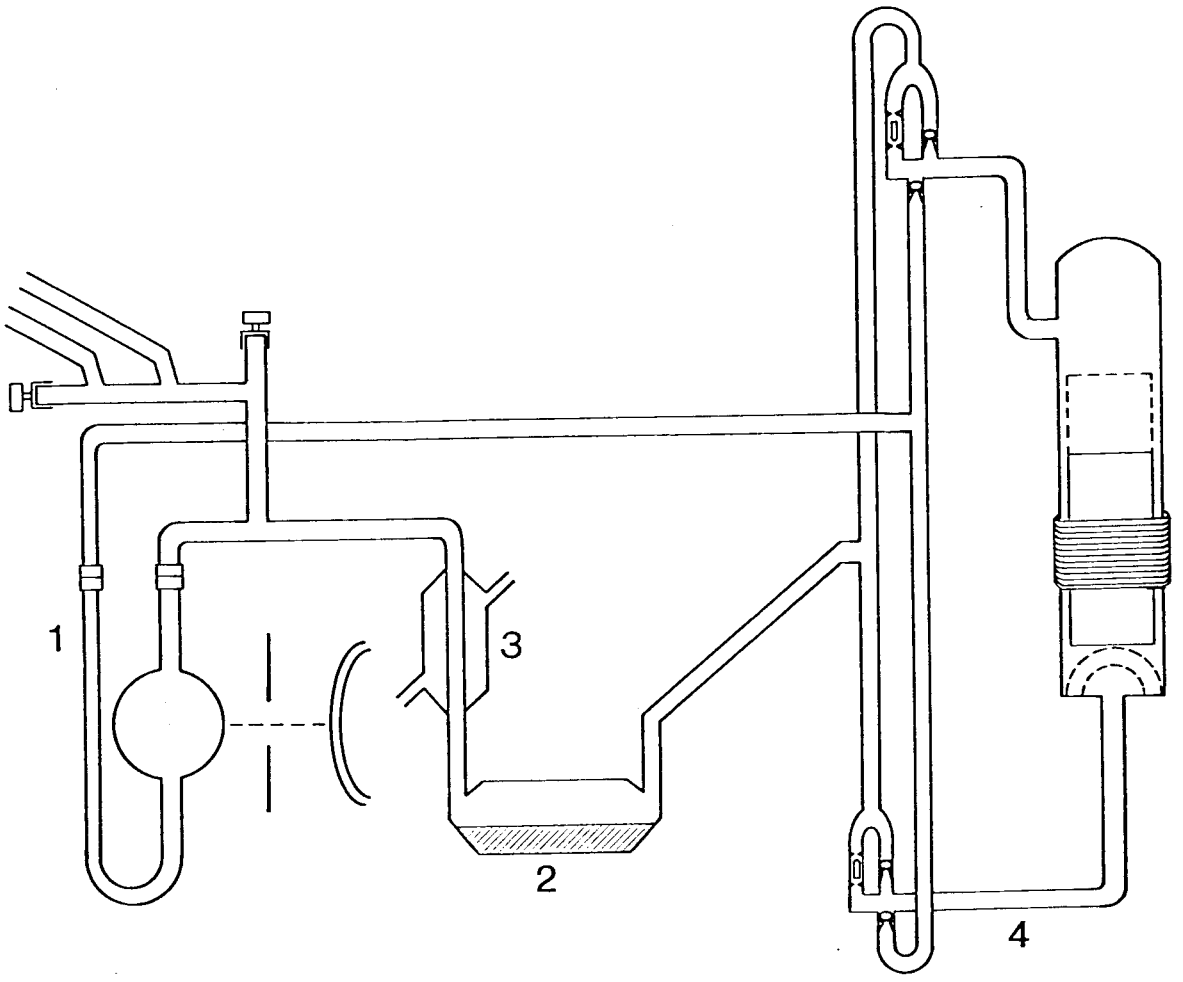

Fig. I-6a. Circulatory Apparatus.

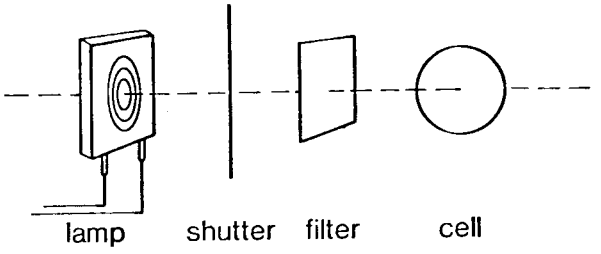

Fig. I-6b. Optical Train.

B. Radiation Source and Optical Train

The 253.7 nm radiation was obtained from a low pressure mercury resonance lamp which was supplied with 50 mA of current at a potential of 5000 volts from a transformer. A Vycor 7910 filter 2 mm thick was used to remove the 185 nm resonance line. A schematic diagram of the optical train is shown in Fig. I-6b.

The lamp intensity was determined using nitrous oxide-n-butane actinometry, as mentioned in Section I-2.2b. A typical plot of $R_{N_2}^{-1}$ versus $P_{n\text{-}C_4H_{10}}/P_{N_2O}$ is shown in Fig. I-7. Intensities of absorbed light of 13.2 ± 0.1, 11.2 ± 0.1 and 5.43 ± 0.05 μeinstein/min were used throughout this research.

The decrease in intensity was achieved by adding an extra filter, Vycor 7900 2 mm thick, which was calibrated on a Unicam (SP800) U.V. spectrophotometer.

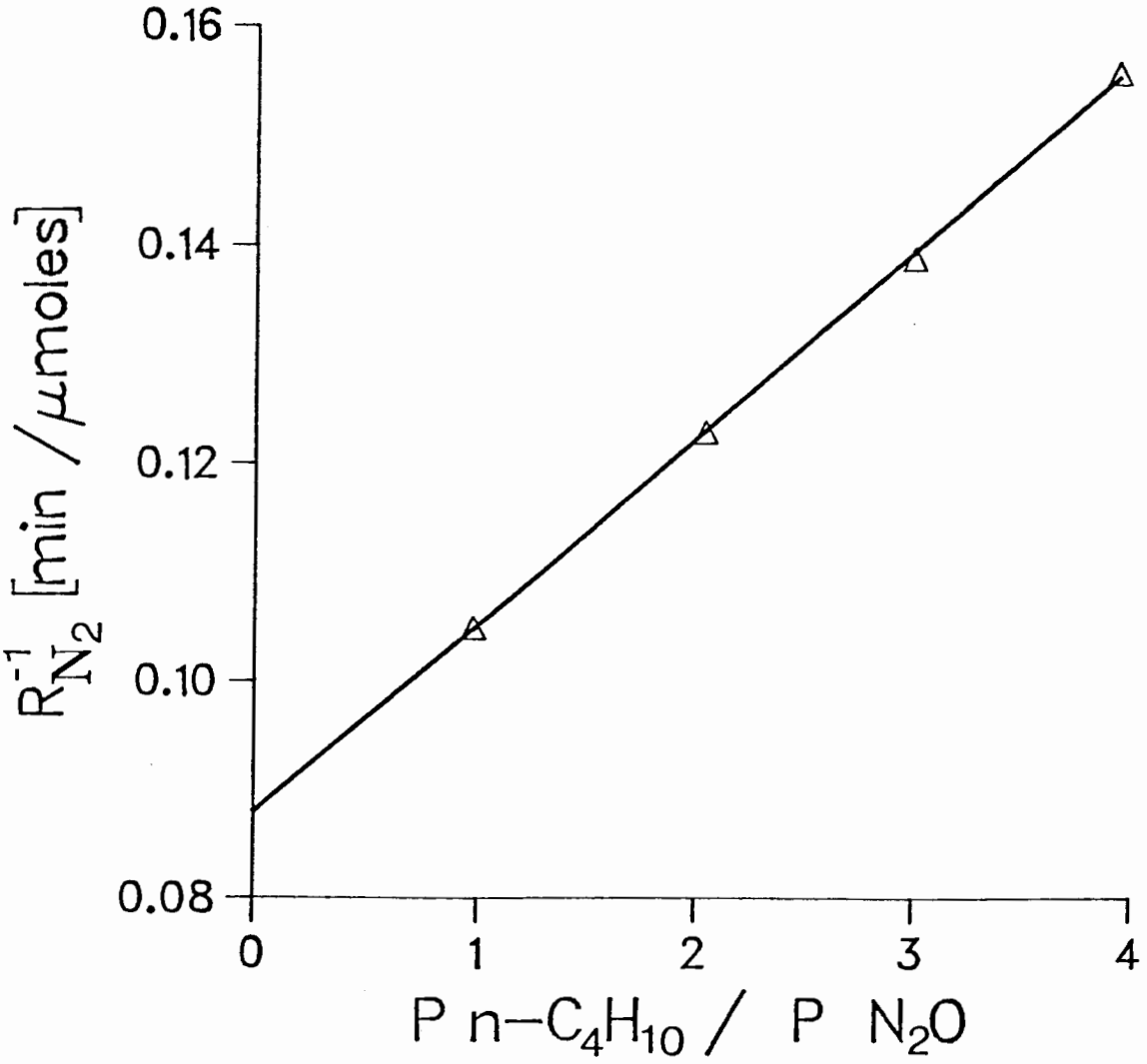

Fig. I-7. Determination of Light Intensity.

C. Reactants

Methyltrifluorosilane: obtained from PCR Research Chemicals, Inc. had CO_2 and small amounts of Me_2SiF_2 as impurities. The sample was degassed, distilled, and collected at -160°C. The purified gas contained less than 0.01% of Me_2SiF_2.

Dimethyldifluorosilane: obtained from PCR Research Chemicals Inc. contained CO_2 which was completely removed when the sample was degassed, distilled and collected at -130°C.

Tetrafluorosilane: obtained from the Matheson Co., was degassed and distilled. The purified reagent was collected at -160°C and contained an impurity which was not identified. The impurity showed chromatographically as a broad peak and did not interfere with product analysis.

Nitric Oxide: obtained from the Matheson Co., was prepurified before being introduced into a storage bulb. The predistillation took place in additional traps which were connected to the main vacuum apparatus. There, the gas was introduced and trapped at -196°C. After being degassed, it was evaporated from -186°C and condensed again at -196°C while the system was continuously pumped. The final portion collected at -196°C was introduced to the storage bulb and was redistilled. Fractions obtained at -196°C and -210°C were collected.

The gas purified in the above manner contained a small amount of nitrous oxide. The exact amount was not determined because quantitative results for small amounts of nitrous oxide in a large excess of nitric oxide were not reproducible.

D. Product Analysis

All analyses were performed on a Gow-Mac (Model 24-377) temperature regulated thermistor catharometer coupled to a Gow-Mac (Model 40-05 D) power supply.

The carrier gas controls, oven and oven controls, and sample injection port of a Perkin Elmer chromatograph (Model 900) were used in conjunction with the above detection system.

This arrangement was preferred after it was determined that response factors obtained from the hot wire detector operated at 225 mA and 250°C with a He flow of 50 cc/min were nearly half the value of those obtained from the thermistor detector operated at 7.5 mA and 50°C under the same carrier gas conditions.

The signal from the detector was recorded with a Texas Instrument Servo/Riter II (Model FT03W6D) recording potentiometer. The sample injection port was adapted to introduce gaseous mixtures. It was connected to the sample loop, shown in Fig. I-4 (item 19), through stainless steel tubing (1.6 mm o.d.) and Swagelock fittings. The carrier gas flow was measured with a soap bubble flow-meter. Helium (Matheson 99.999% pure) used as the carrier gas, was dried by passing it through a molecular sieve 13X column kept at -80°C which was conditioned from time to time at 470°C.

The columns were made from thin wall stainless steel tubing (4.8 mm o.d.) of the desired length. They were filled using standard packing procedures and were conditioned with carrier gas flowing for at least 12 hours at the maximum temperature recommended. The columns used are detailed in Table I-2 and their specific applications in Table I-3.

A calibration was made for all reagents used and products obtained. Firstly, the individual response factors were determined: various quantities of pure substance were measured by means of the gas burette, transferred to the sample loop and flushed into the appropriate column of the G.C. The detector response translated into a peak-area was measured with a planimeter (Gelman 39321). The slope of a plot of the peak areas against moles of material introduced yielded the molar response, r_i, for each compound.

Secondly, a relative response factor, R_i, was calculated using nitrous oxide as the reference compound. These values are included in Table I-3.

In this manner, corrections could be made for day to day deviations in the detector sensitivity due to small changes in its temperature and flow rate. By measuring the daily molar response of N_2O, the corrected number of moles of the different compounds could be evaluated from the following relation:

Table I-2. Chromatographic Columns

Column	Packing	Manufacturer	Particle Size (mesh)	Length (m)	Tube o.d. (mm)
1	Molecular Sieves, 5A	Coast Engineering Lab.	30-60	2	4.8
2	Porapak Q	Waters Assoc., Inc.	50-80	4	4.8

Table I-3. Gas Chromatographic Analysis Conditions

He flow = 50 [cc/min]

Substance	Column	t_R' (min)	Operating Conditions	Relative Response, R_i
N_2	1	t_R=2.00	Room temperature	0.686
NO	1	t_R=3.20	Room temperature	0.660
CH_4	1	t_R=4.20	Room temperature	0.619
CO	1	t_R=8.00	Room temperature	0.706
N_2O	2	7.6	Room temperature	1.00
$MeSiF_3$	2	19.6	12 min at ≈30°C, 10°/min up to 200°C	1.29
Me_2SiF_2	2	26.0	12 min at ≈30°C, 10°/min up to 200°C	1.43
SiF_4	2	2.4	Room temperature	0.907

t_R' = retention time of the given substance - retention time of air peak.

$$n_i = \frac{A_i}{R_i r_s}$$

where

n_i = moles of the compound i.

A_i = area under the peak due to compound i.

r_s = molar response of N_2O (internal standard).

$R_i = r_i/r_s$.

The variation in the r_s value was 2% with respect to the mean value obtained from a set of eight experiments carried out during a three week period.

In addition to gas chromatography, mass spectrometry and IR spectroscopy were used to check the purity and identity of products and reagents.

E. Irradiation Procedure

Preliminary experiments carried out with $MeSiF_3$-NO mixtures in a static system showed very small yields of products. This was due to the depletion of mercury vapor in the cell through its reaction with NO_2 formed during the reaction. Thereafter, a gas-circulating closed reaction system was used (Fig. 6a). In this, the reactants were circulated over a pool of liquid mercury held at 50°C. A condenser downstream from the mercury kept at 25°C ensured a constant pressure of mercury vapor. The detachable cell was cleaned with nitric acid after each run and was left over night under high vacuum pumping.

The general procedure followed in these experiments was to measure, mix and irradiate the reactants. Afterwards, reactants and products were separated into different fractions through distillation. Each faction was analyzed quantitatively by gas chromatography. Each of the separated products could be trapped from the GC eluent and collected for further analysis (IR, MS, NMR).

In order to produce pressures smaller than 10 torr in the reaction vessel, the appropriate gas was measured using the calibrated volumes of a doser (Fig. I-3) and then transferred into the reaction vessel. For pressures higher than 10 torr, the desired pressure in the reaction vessel was obtained by direct dosing from the storage bulb. The gas pressures were read from a mercury manometer.

i) Experiments in the Static System

The static system was used with preliminary experiments. These include the mercury sensitized reaction of $MeSiF_3$, the competitive quenching of Hg $6(^3P_1)$ with $MeSiF_3$-N_2O mixtures and the pyrolysis of $MeSiF_3$.

Photosensitized reactions were carried out in the presence of a drop of clean mercury which was added to the reaction cell before it was attached to the vacuum system (Fig. I-3).

Pyrolysis temperatures were attained by surrounding the reaction vessel with a tubular furnace whose temperature was controlled with a Variac transformer and read by means of a chromel-alumel thermocouple.

ii) Procedure Followed in Studying the Reactions of Me_xSiF_{4-x} with NO.

Known pressures of Me_xSiF_{4-x} and NO were mixed in the reaction vessel. Irradiation times of 2 to 10 min were chosen so that the extent of decomposition of NO was generally less than 1%, although up to 3% decomposition occurred in experiments with low NO concentrations.

After irradiation, the contents of the reaction vessel were divided into a fraction condensable at -196°C, and a volatile fraction consisting of mainly N_2 with some NO. The latter was further fractionated at -210°C to remove any NO. The remaining N_2 was measured and quantitatively analyzed by gas chromatography (Molecular Sieve).

The first fraction condensable at -196°C was further separated by distilling the mixture through traps maintained at -160°C, -196°C and -210°C.

The fraction collected at -210°C consisted of unreacted NO which was combined with the NO from the first fraction and measured in a gas burette.

The fraction collected at -196°C was mainly N_2O. It was measured and quantitatively analysed by gas chromatography (Porapak Q).

The fraction collected at -160°C contained the unreacted silane and some N_2O. An aliquot of this fraction was analyzed with the Porapak Q column; the N_2O found in this fraction accounted for 10-20% of the total amount produced in the reaction.

No other volatile products were found in any of the systems studied.

I-4 EXPERIMENTAL RESULTS

A - Preliminary Experiments

Three different types of reactions were carried out with $MeSiF_3$ at the beginning of this research work. These experimental results will be described briefly.

1. The Reaction of Hg $6(^3P_1)$ with $MeSiF_3$.

Methyltrifluorosilane was irradiated for 15 min in the presence of mercury vapor at a pressure of approximately 51 torr. The analysis of the different fractions by GC yielded no products from the system.

A final experiment under similar conditions was done in which the irradiation at 253.7 nm was extended to 12 hrs. The mass spectrum of the total mixture condensed at -196°C was identical to that of $MeSiF_3$.

2. Quenching Cross Section of $MeSiF_3$

Mixtures of about 50 torr of N_2O and varying pressures of $MeSiF_3$ (50-300 torr) were irradiated at 253.7 nm for 15 min in the presence of mercury vapor. The nitrogen produced was quantitatively determined by gas chromatography. From several experiments it was found that the amount of N_2 produced in these experiments was irreproducible. The results in Table I-4 demonstrate this irreproducibility. Therefore, a reliable value for the cross section could not be obtained.

Table I-4

Attempts to Determine σ_Q^2 for $MeSiF_3$ with Hg $6(^3P_1)$

I_A = 0.565 [μeinstein/min]

Run	P_{total} [torr]	P_{MeSiF_3}/P_{N_2O}	Φ_{N_2} [einstein/mol]
7	300.2	5.93	2.34
9	291.2	5.93	1.23
12	293.2	6.07	2.57
13	299.1	6.08	2.65
14	301.4	6.23	3.69
15	298.7	6.09	1.21
16	298.0	6.13	1.53

3. Pyrolysis of $MeSiF_3$

About 50 torr of methyltrifluorosilane was heated to various temperatures and for different periods of time. The compound did not show appreciable decomposition at temperatures lower than 700°C, as evidenced by no change in the pressure of the system and no products as determined by GC analysis.

Decomposition products from 50 torr of $MeSiF_3$ found at 714 ± 1°C which were identified from their GC retention times and MS are: CH_4, H_2, C_2H_6 and SiF_4. The formation of other products cannot be discounted since no further pyrolysis experiments were performed with this system.

B. The Reactions of Electronically Excited Nitric Oxide with Me_xSiF_{4-x}.

The reaction of $NO(^4\pi)$ molecules was examined with three compounds in the series Me_xSiF_{4-x}. These corresponded to ($x = 0,1,2$).

Preliminary experiments carried out under static conditions had shown that the amount of N_2 produced from the mercury photosensitation of NO in the presence of $MeSiF_3$ (reactant ratio 1:18) had increased by a factor of 4 compared to that obtained in the reaction of NO alone. These results suggested that further studies should be made of this system. At this point, the gas circulatory-mercury saturation apparatus (Fig. I-6a) was connected to the high vacuum system.

The results presented in Table I-5 demonstrate the effect on the rates of formation of N_2 and N_2O caused by the presence of the different silanes.

Table I-5

The Effect of Me_xSiF_{4-x} on the Rates of Formation of N_2 and N_2O in the Reaction of NO with Hg $6(^3P_1)$.

Me_xSiF_{4-x}	P_{Sil} (c)	P_{NO}	N_2	N_2O
	[torr]		[μmoles/min]×10^2	
-		100.4 (a)	0.09	3.15
SiF_4 (a)	298.0	101.5	1.31	not measured
$MeSiF_3$ (a)	304.8	98.1	31.7	57.5
Me_2SiF_2 (b)	71.9	99.1	54.2	58.6

(a) Irradiation time = 10.00 min.

(b) Irradiation time = 5.00 min.

(c) Sil = Me_xSiF_{4-x}.

Several experiments, with the Me_xSiF_{4-x} compounds were carried out to search for products other than N_2 and N_2O. In neither case, were products found additional to those formed in the NO/Hg system. Furthermore, there was no observed decrease in the amount of silane during the experiments. The magnitude of the observed effects is such that the enhanced decompositions of NO caused by the silanes is in the order $Me_2SiF_2 > MeSiF_3 >> SiF_4$.

Systematic studies of the NO/$MeSiF_3$ and the NO/Me_2SiF_2 systems were undertaken to determine the effects of time, light intensity, and varying pressures of silane at constant NO pressures and vice-versa.

1. The Reaction of NO($^4\pi$) with $MeSiF_3$.

Fig. I-8 presents the results obtained when mixtures of NO/$MeSiF_3$ were subjected to different irradiation times. Pressures of silane and NO were 188.4 ± 0.1 and 98.1 ± 0.8 torr, respectively. I_{Abs} = 13.2 [μeinstein/min]. The longest irradiation time produced 3.1% of NO decomposition.

The effect of light intensity was studied for 1:1 mixtures of NO/$MeSiF_3$. Average values of two determinations at each light intensity are summarized in Table I-6. The quantum yields of N_2 and N_2O appear independent of light intensity within experimental error.

The effect of the composition of the reaction mixture on the quantum yields of the products is shown in Table I-7 and I-8. At constant pressure of NO, the quantum yields of N_2 and N_2O increase markedly with increasing pressures of $MeSiF_3$. But, while the quantum yield of N_2 reaches a constant value at pressures of silane of about 200 torr, that of N_2O continues to increase steadily with the pressure of the added silane. At constant pressure of $MeSiF_3$ with varying NO, the quantum yield of N_2 remains virtually unchanged while that of N_2O decreases rapidly to reach a constant value at pressures of NO higher than 200 torr.

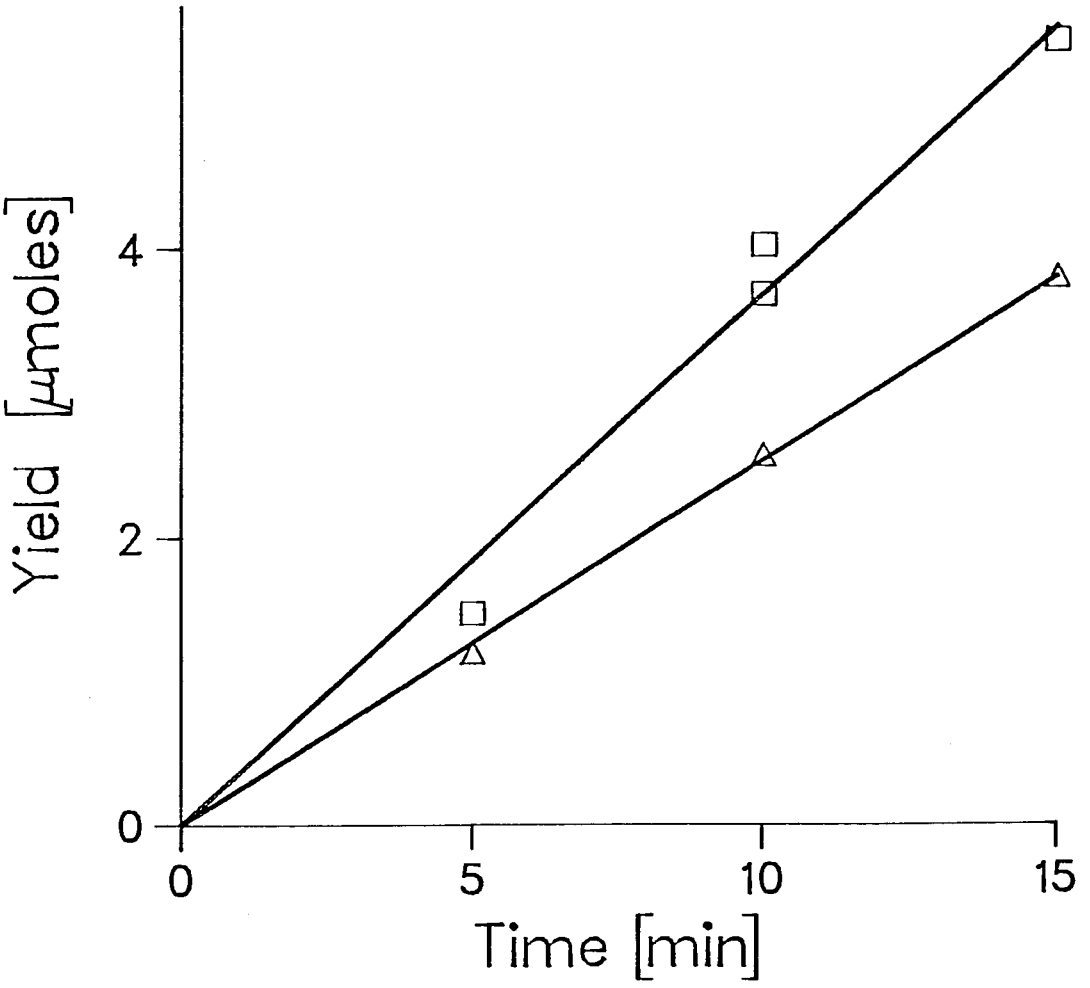

Fig. I-8. Time Dependence of N_2 and N_2O Yields from $MeSiF_3$-NO Mixtures: □, N_2O; Δ, N_2.

Table I-6

Product Quantum Yields of $MeSiF_3$-NO Mixtures as a Function of Light Intensity.

$P_{MeSiF_3} = P_{NO} = 99.6$ [torr]

I_{Abs} [μeinstein/min]	Φ_{N_2} [mol/einstein]×10^2	Φ_{N_2O} [mol/einstein]×10^2
11.2	1.84±0.17	1.55±0.07
5.43	2.11±0.16	1.63±0.07

Table I-7

Product Quantum Yields of $MeSiF_3$-NO Mixtures at

$P_{NO} = 98.4 \pm 0.3$ [torr]

$I_{Abs} = 13.2$ [μeinstein/min]

Run	P_{MeSiF_3} [torr]	Φ_{N_2} [mol/einstein]×10^2	Φ_{N_2O} [mol/einstein]×10^2
62	0	0.077	0.22
61	76.3	1.12	1.35
66	99.1	1.36	2.00
63	135.8	1.58	2.92
65	160.2	1.45	2.97
59	188.5	1.95	3.05
64	235.4	1.85	4.03
60	291.0	2.05	4.72

Table I-8

Product Quantum Yields of $MeSiF_3$-NO Mixtures at

P_{MeSiF_3} = 100.2 ± 0.4 [torr]

I_{Abs} = 11.2 [μeinstein/min]

Run	P_{NO} [torr]	Φ_{N_2} [mol/einstein]×10^2	Φ_{N_2O} [mol/einstein]×10^2
83	10.4	2.40	6.91
80	31.4	1.65	4.57
78	50.5	1.80	2.82
79	79.8	1.80	2.14
77	101.0	2.13	1.64
75	203.0	2.02	1.09
76	300.3	2.09	0.93

2. The Reaction of NO($^4\pi$) with Me_2SiF_2.

The results obtained are analogous to those already described for $MeSiF_3$. Table I-9 shows that the quantum yields of the products appear independent of light intensity. Table I-10 shows that both quantum yields of N_2 and N_2O increase markedly with increasing Me_2SiF_2 pressures and from Table I-11 it can be seen that N_2O decreases while N_2 increases with increasing pressures of NO at a fixed pressure of Me_2SiF_2.

Table I-9

Product Quantum Yields of Me_2SiF_2-NO Mixtures as a Function of Light Intensity.

$P_{Me_2SiF_2}$ = 50.6 ± 0.4 [torr]

P_{NO} = 100.5 ± 0.2 [torr]

I_{Abs} [μeinstein/min]	Φ_{N_2} [mol/einstein]×10^2	Φ_{N_2O} [mol/einstein]×10^2
11.2	4.16±0.16	3.34±0.10
5.43	5.15±0.17	3.38±0.03

Table I-10

Product Quantum Yields of Me_2SiF_2-NO Mixtures

P_{NO} = 100.7 ± 0.7 [torr]

I_{Abs} = 11.2 [μeinstein/min]

Run	$P_{Me_2SiF_2}$ [torr]	Φ_{N_2} [mol/einstein]×10^2	Φ_{N_2O} [mol/einstein]×10^2
103	5.1	0.96	0.11
101	12.7	2.14	1.15
96	25.2	3.34	2.34
94	50.0	4.42	3.70
112	71.9	5.45	5.23

Table I-11

Product Quantum Yields of Me_2SiF_2-NO Mixtures

$P_{Me_2SiF_2}$ = 50.5 ± 0.5 [torr]

I_{Abs} = 11.2 [μeinstein/min]

Run	P_{NO} [torr]	Φ_{N_2} [mol/einstein]×10^2	Φ_{N_2O} [mol/einstein]×10^2
107	26.4	1.77	6.63
105	50.6	3.15	4.96
94	100.7	4.42	3.69
106	192.2	5.75	2.62

I-5. DISCUSSION

A. Preliminary Experiments

Exploratory experiments carried out at the beginning of this work were aimed at the possibility of producing SiF_3 radicals from CH_3SiF_3. Various methods were attempted:

1. Mercury Photosensitized Decomposition at 253.7 nm:

No decomposition was found under our experimental conditions, presumably due to the low quenching efficiency of this molecule for Hg* $6(^3P_1)$ atoms. Therefore, the plausible chemical reactions, I-35 and I-36, did not occur.

I-35 $\quad MeSiF_3 + Hg^* \rightarrow CH_3 + SiF_3 + Hg^\circ$

I-36 $\quad MeSiF_3 + Hg^* \rightarrow H + CH_2SiF_3 + Hg^\circ$

So far, no value of the quenching cross section of $MeSiF_3$ has been reported in the literature. Gunning and coworkers (5b) did, however, measure the cross sections of Me_2SiF_2 (0.19 $Å^2$) and Me_3SiF (1.0 $Å^2$) using the physical method. Since there is a clear reduction in the quenching cross section when methyl groups are replaced by fluorine atoms (Table I-1), it would be expected that the effective cross section of $MeSiF_3$ will be much smaller than 0.19 $Å^2$. Our attempts to determine the quenching cross section of $MeSiF_3$ by the chemical method did not, as

mentioned above, yield reproducible results. No further attempts were made to measure the quenching cross sections.

2. Pyrolysis:

$MeSiF_3$ proved to be thermally stable up to temperatures of 700°C. Above this temperature the products, which were readily detected were: methane, hydrogen, ethane and tetrafluorosilane.

It might be expected that the initial step is scission of the C-Si bond, eg., I-37.

I-37 $MeSiF_3 \rightarrow CH_3 + SiF_3$

followed by a series of free radical reactions. These processes might be expected to include reactions such as:

I-38 $CH_3 + MeSiF_3 \rightarrow CH_4 + CH_2SiF_3$

I-39 $CH_3 + CH_3 \rightarrow C_2H_6$

The primary step, scission of the C-Si bond, is in accord with that suggested by Davidson and coworkers (21) for the pyrolysis of trimethylchlorosilane. The formation of tetrafluorosilane can be explained if reactions I-40 and I-41 are incorporated with the above sequence:

I-40 $2SiF_3 \rightarrow Si_2F_6$

I-41 $Si_2F_6 \rightarrow SiF_4 + SiF_2$

It has been shown that hexafluorodisilane decomposes thermally at 700°C and the formation of difluorosilylene has been suggested as a product from the primary process (22).

Thus, the thermal decomposition of $MeSiF_3$ proved to be an impractical source of SiF_3 radicals due to the high temperatures required for decomposition and to the obvious complexity of the reaction mechanism.

3. Energy Transfer from the $^4\pi$ State of NO:

From energetic considerations, $NO^4\pi$ may be expected to cause Si-C bond cleavage. Recent estimates of Si-C bond dissociation energies (20,23) yield values of

$$D_{Me_3Si-CH_3} = 374.0 \text{ and } D_{Cl_2MeSi-CH_3} = 355.6 \text{ [kJ/mol]}$$

Our experiments showed that Si-C bond splitting did not occur. Instead, it was found that the silane causes substantial increases in the yields of products of the mercury photosensitized decomposition of NO.

B. The Effect of Silanes on the Mercury-Photosensitized Decomposition of Nitric Oxide.

The observed enhancement in the production of N_2 and N_2O from NO-Hg $6(^3P_1)$-Me_xSiF_{4-x} mixtures can be accounted for by the following scheme:

I-1	$Hg^\circ + h\nu \rightarrow Hg^*$	I_{Abs}
I-27	$Hg^* + NO \rightarrow NO^* + Hg^\circ$	
I-29	$NO^* + NO \rightarrow 2NO$	
I-30	$NO^* + NO \rightarrow (NO)_2^*$	
I-31	$(NO)_2^* \rightarrow N_2 + O_2$	
I-32	$(NO)_2^* + NO \rightarrow N_2O + NO_2$	
I-42	$NO^* + Sil \rightarrow SilNO\dagger$	
I-43	$NO^* + Sil \rightarrow SilNO\dagger\dagger$	
I-44	$SilNO\dagger \rightarrow Sil + NO$	
I-45	$SilNO\dagger + NO \rightarrow Sil + N_2 + O_2$	
I-46	$SilNO\dagger + NO \rightarrow Sil + 2NO$	
I-47	$SilNO\dagger + Sil \rightarrow 2Sil + NO$	
I-48	$SilNO\dagger\dagger \rightarrow Sil + NO$	
I-49	$SilNO\dagger\dagger + NO \rightarrow Sil(NO)_2\dagger\dagger \xrightarrow{NO} Sil + N_2O + NO_2$	
I-50	$SilNO\dagger\dagger + NO \rightarrow Sil + 2NO$	
I-51	$SilNO\dagger\dagger + Sil \rightarrow 2Sil + NO$	

where: Hg° = Hg $6(^1S_o)$; Hg^* = Hg $6(^3P_1)$, NO^* = $NO^4\pi$, Sil = $MeSiF_3$ or $MeSiF_2$, and SilNO† and SilNO†† are two diferent Me_xSiF_{4-x}-NO intermediate complexes.

This mechanism incorporates the accepted mechanism for the Hg-sensitized decomposition of NO itself and is consistent with our experimental observations.

As mentioned previously, in Section I-2.4, Strausz and Gunning (18) in their study of the Hg $6(^3P_1)$-NO mixtures, proposed reactions I-1, I-27 and I-29 to I-32 as the most plausible route by which the observed products are formed. Their data also showed that the sum of the quantum yields of N_2 and N_2O are independent of NO pressure in the complete quenching region. This observation indicates that there is no interaction of the excited NO dimer to regenerate NO either via unimolecular dissociation or by collision with another molecule. Thus, the enhancement of N_2 and N_2O when the silanes are added cannot result from the reaction of the Me_xSiF_{4-x} compounds with $(NO)_2$* since this process would not increase the yields of N_2 and N_2O. It seems likely that the silanes intervene in the mechanism through competition with reaction I-29 and I-30. The interpretation of the data requires the participation of two different Me_xSiF_{4-x}-NO intermediate complexes, each capable of initiating a series of reactions to yield one of the products of the reaction. Furthermore, it must be assumed that these intermediate complexes are not interconvertible. Thus, in the proposed mechanism SilNO† leads to N_2 while SilNO†† leads to N_2O formation.

From the above mechanism, the rate of N_2 formation is given by:

I-53 $$R_{N_2} = k_{31}[(NO)_2^*] + k_{45}[SilNO\dagger][NO]$$

but since the quantum yield of N_2 in the absence of Me_xSiF_{4-x} is very small (Table I-5) $k_{45} >> k_{31}$, hence,

I-54 $$R_{N_2} = k_{45}[SilNO\dagger][NO].$$

Applying the steady state approximation to the intermediate SilNO†, the quantum yield of N_2 production is given by the following expression:

I-55
$$\Phi_{N_2} = \frac{k_{42}k_{45}[NO][Sil]}{\{(k_{29}+k_{30})[NO]+(k_{42}+k_{43})[Sil]\}\{k_{44}+(k_{45}+k_{46})[NO]+k_{47}[Sil]\}}$$

Similarly, the rate of N_2O formation is expressed by:

I-56 $$R_{N_2O} = k_{32}[(NO)_2^*][NO] + k_{49}[SilNO\dagger\dagger][NO]$$

since $k_{49} >> k_{32}$

I-57 $$R_{N_2O} = k_{49}[SilNO\dagger\dagger][NO]$$

and the expression for the quantum yield is

I-58
$$\Phi_{N_2O} = \frac{k_{43}k_{49}[NO][Sil]}{\{(k_{29}+k_{30})[NO]+(k_{42}+k_{43})[Sil]\}\{k_{48}+(k_{49}+k_{50})[NO]+k_{51}[Sil]\}}$$

A detailed derivation of Equations I-55 and I-58 is included in the Appendix.

The effects of the silanes $MeSiF_3$ and Me_2SiF_2 need to be discussed separately due to differences in the quantitative measurements resulting in the observed trends obtained for each system. These are described in the Experimental Results section.

1. $MeSiF_3$ + NO ($^4\pi$).

A plot of $\Phi_{N_2}^{-1}$ against $P_{MeSiF_3}^{-1}$ is shown in Figure I-9. It is a straight line described by Equation I-55 if it is presumed that

$$(k_{29} + k_{30})[NO] >> (k_{42} + k_{43})[Sil]$$

$$(k_{44} + k_{47})[Sil] >> (k_{45} + k_{46})[NO].$$

Thus, Equations I-55 and I-58 are reduced to

$$\text{I-59} \qquad \Phi_{N_2} = \frac{k_{42}k_{45}}{(k_{29} + k_{30})} \quad \frac{[Sil]}{(k_{44} + k_{47}[Sil])}$$

$$\text{I-60} \qquad \Phi_{N_2O} = \frac{k_{43}k_{49}}{(k_{29} + k_{30})\{k_{48} + (k_{49} + k_{50})[NO] + k_{51}[Sil]\}}$$

Rearrangement of equation I-59 gives:

$$\text{I-61} \qquad \Phi_{N_2}^{-1} = \frac{(k_{29} + k_{30})}{k_{42}k_{45}} \left\{\frac{k_{44}}{[Sil]} + k_{47}\right\}$$

Equation I-61 is thus consistent with the linear dependence of $\Phi_{N_2}^{-1}$ on $P_{MeSiF_3}^{-1}$. From Equation I-61, the slope to intercept ratio yields k_{44}/k_{47} for which a value of $(6.1 \pm 1.8)\times10^3$ mol L^{-1} is obtained.

A plot of Φ_{N_2O} versus P_{MeSiF_3} (Equation I-60) at constant P_{NO} is shown in Figure I-10. A straight line with

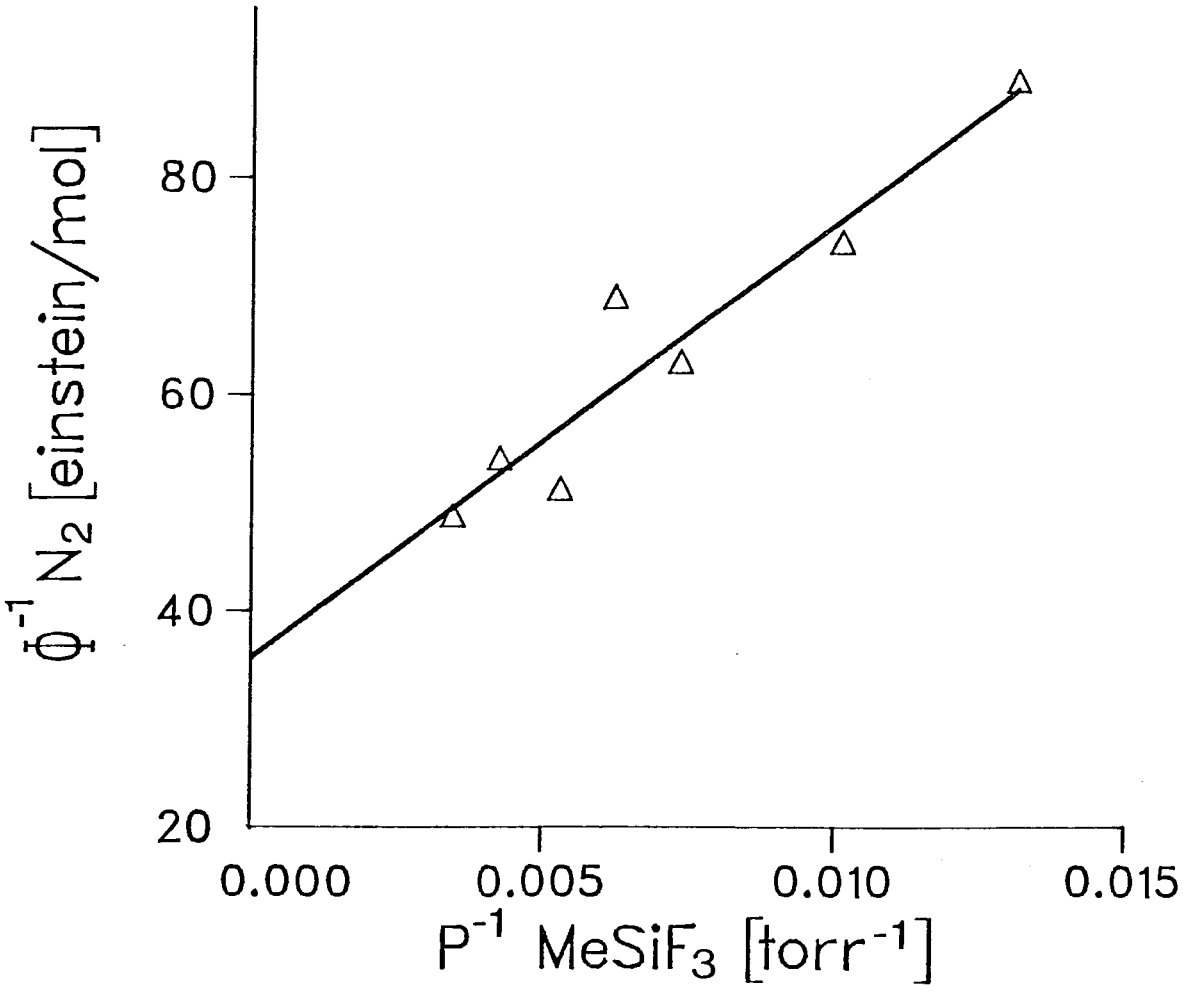

Fig. I-9. Reciprocal Quantum Yield of N_2 vs. Reciprocal of $MeSiF_3$ Pressure: P_{NO} = constant.

intercept zero is a good representation of the experimental data and indicates that the term k_{51}[Sil] may be neglected and Equation I-60 may be rewritten as follows:

$$\text{I-62} \qquad \Phi_{N_2O} = \frac{k_{43}k_{49}}{(k_{29} + k_{30})} \frac{[Sil]}{\{k_{48} + (k_{49} + k_{50})[NO]\}}$$

which upon rearrangement becomes:

$$\text{I-63} \qquad \Phi_{N_2O}^{-1} = \frac{(k_{29} + k_{30})}{k_{43}k_{49}[Sil]}\{k_{48} + (k_{49} + k_{50})[NO]$$

A plot of $\Phi_{N_2O}^{-1}$ vs. P_{NO} at constant pressure of $MeSiF_3$ is shown in Figure I-11. It shows that a straight line is obtained at low pressures of NO as expected from Equation I-63, but at pressures higher than about 150 torr, the results show distinct curvature indicating that the amount of N_2O formed is larger than that predicted by Equation I-63. This suggests that the yield of N_2O from reaction I-32 becomes an important source of the compound at higher pressures of NO. This source of N_2O is not considered in the derived expression (I-63). A plot of the straight line portion is shown in Figure I-12 from which the slope to intercept ratio yields $(k_{49} + k_{50})/k_{48}$ which value is $(1.2 \pm 0.4)\times10^3$ L mol^{-1}.

2. Me_2SiF_2 + NO ($^4\pi$)

In the case of Me_2SiF_2, there is a distinct dependence of the quantum yield of N_2 on the pressure of NO (Table I-11) which indicates that the term $(k_{42} + k_{43})$[Sil] cannot be neglected compared to $(k_{29} + k_{30})$[NO] in contrast to the case of $MeSiF_3$.

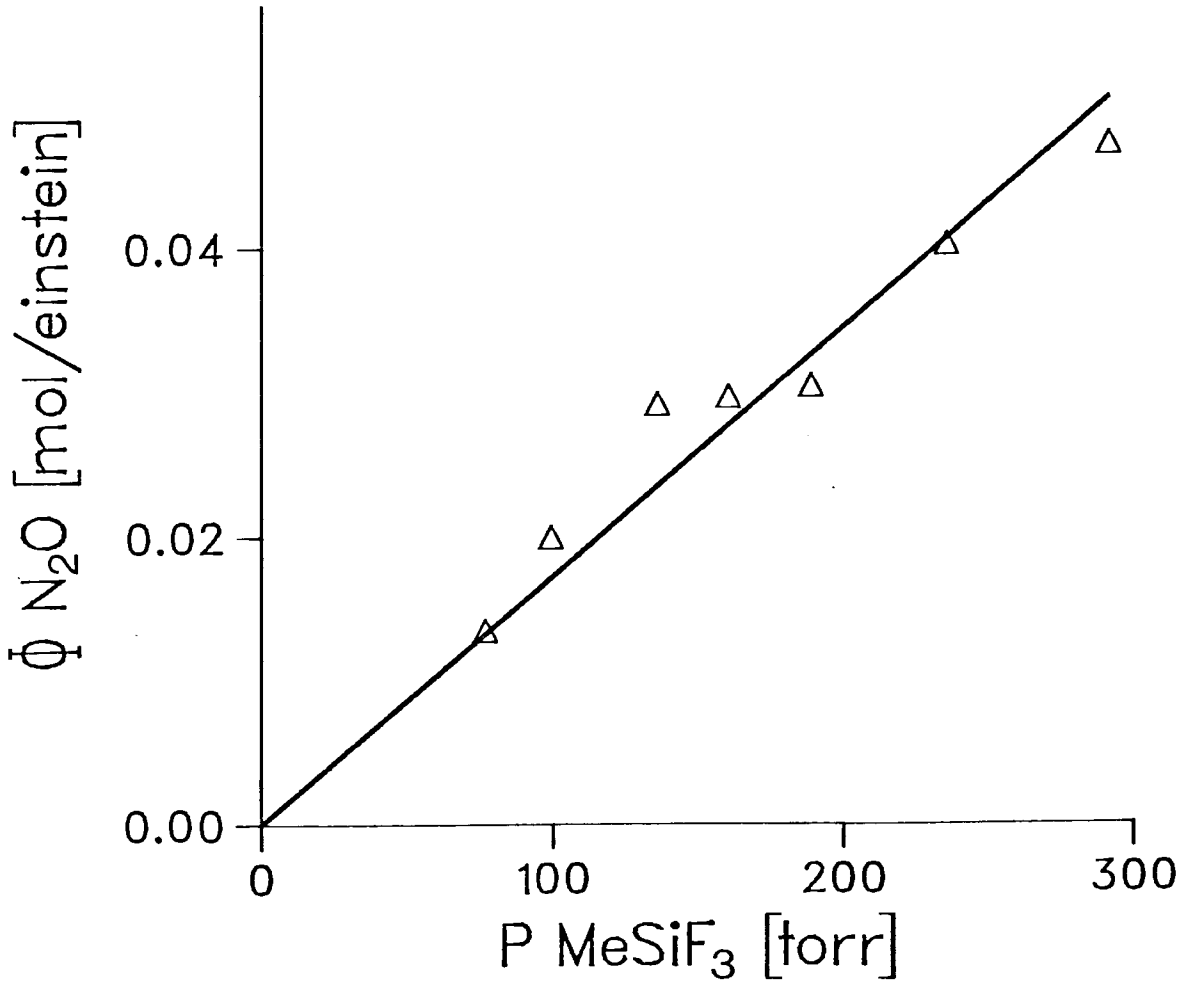

Fig. I-10. A Plot of Quantum Yield of N_2O vs. $MeSiF_3$ Pressure: P_{NO} = 98.4 ± 0.3 [torr].

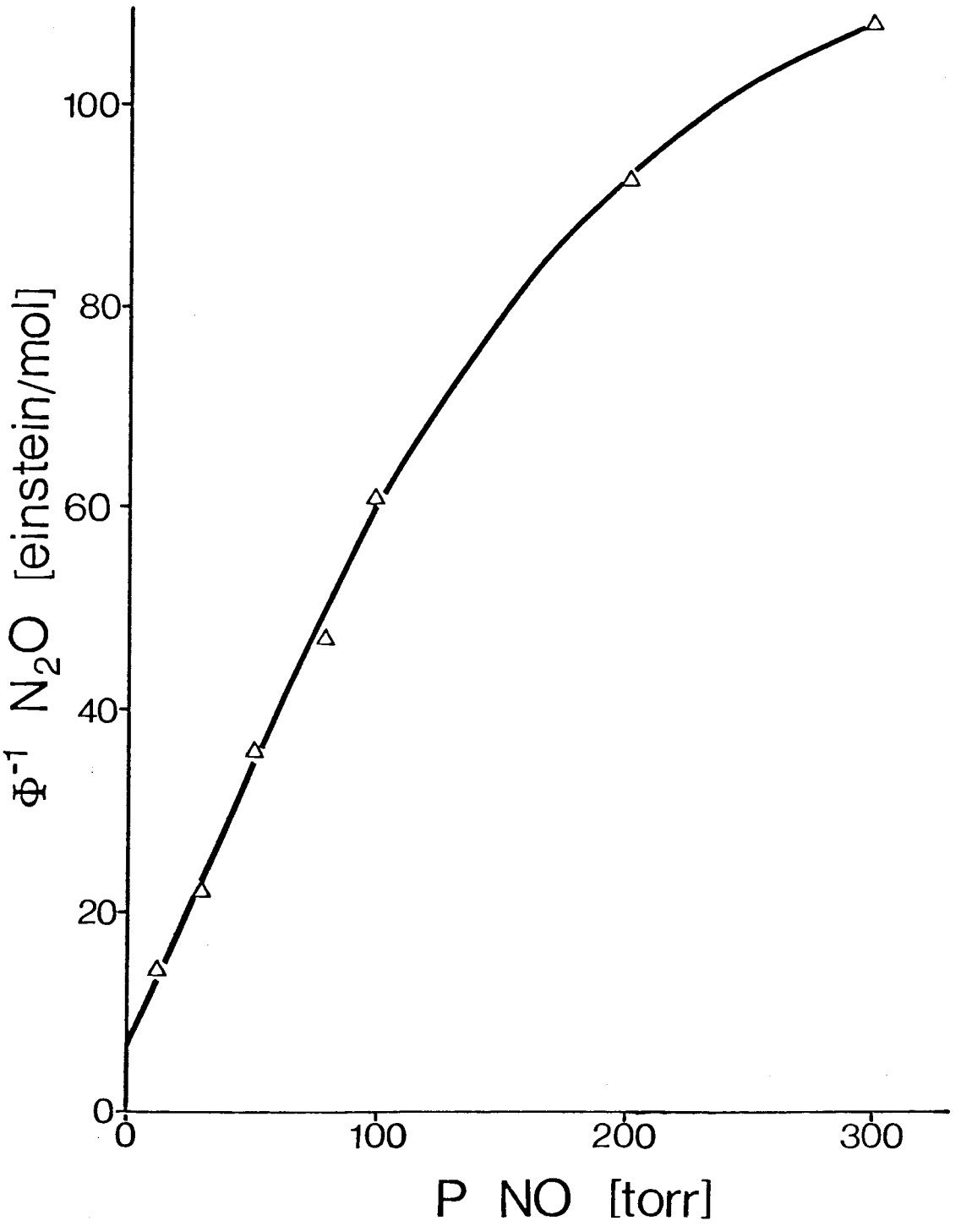

Fig. I-11. Plot of Reciprocal of Quantum Yield of N_2O vs. NO pressure: P_{MeSiF_3} = 100.2 ± 0.4 [torr]. I_{Abs} = 11.2 [μeinstein/min].

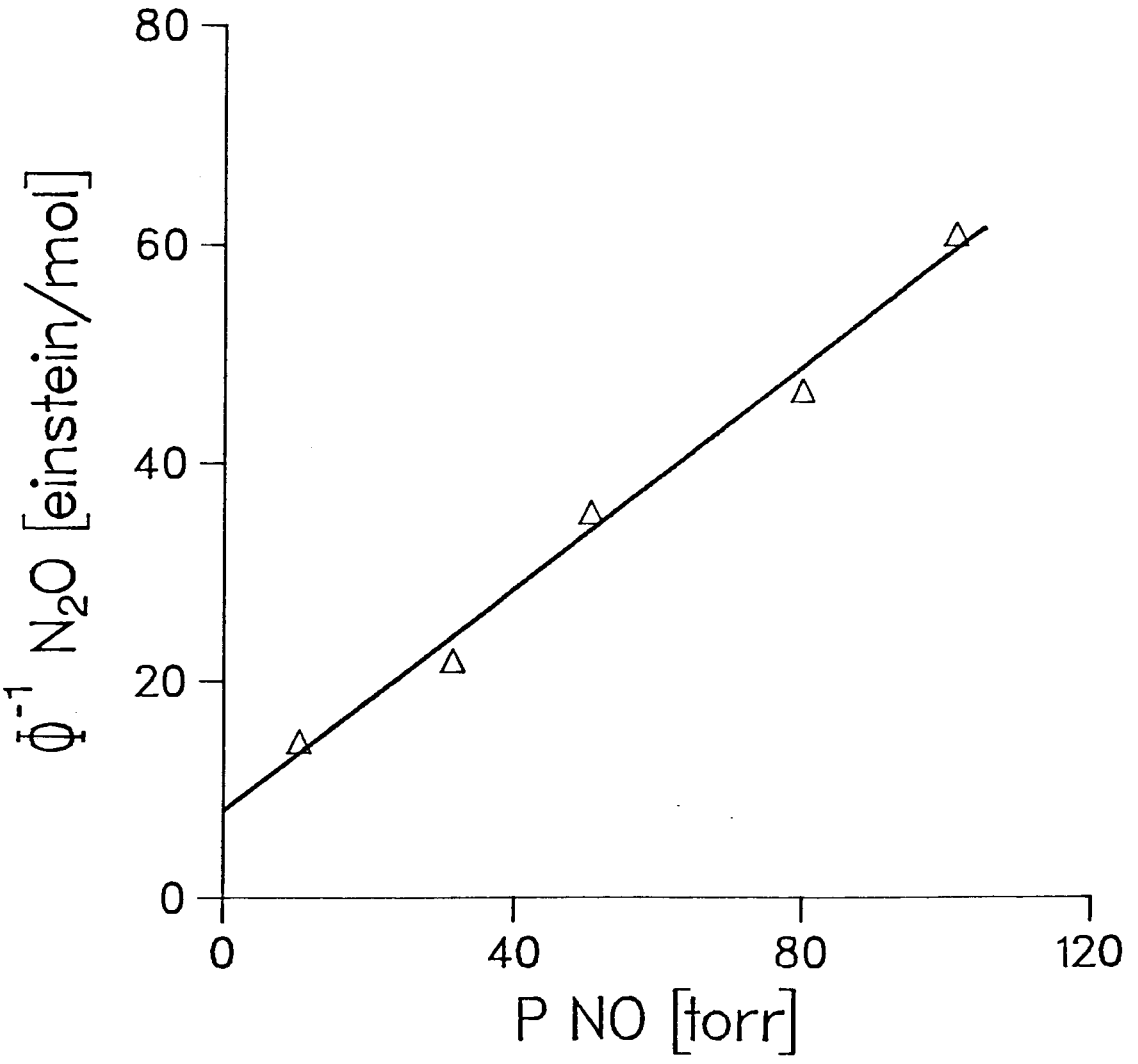

Fig. I-12. A Plot of Quantum Yield of N_2O vs. NO Pressure: The Lower Pressure Region.

Retaining the arguments that $k_{44} + k_{47}[Sil] >> (k_{45} + k_{46})[NO]$ and including the assumption that $k_{47}[Sil]$ is sufficiently small to be neglected relative to k_{44}, the expression for Φ_{N_2} (I-55) becomes:

$$\text{I-64} \qquad \Phi_{N_2} = \frac{k_{42}k_{45}[NO][Sil]}{k_{44}\{(k_{29} + k_{30})[NO] + (k_{42} + k_{43})[Sil]\}}$$

from which,

$$\text{I-65} \qquad \frac{[NO]}{\Phi_{N_2}} = \frac{k_{44}}{k_{42}k_{45}}\{(k_{42} + k_{43}) + (k_{29}+k_{30})\frac{[NO]}{[Sil]}\}$$

A plot of P_{NO}/Φ_{N_2} versus P_{NO} at constant pressure of Me_2SiF_2 is shown in Figure I-13. The data points fall on a straight line in accord with Equation I-65.

Similarly from I-64 the appropriate equation for the dependence of Φ_{N_2} on Me_2SiF_2 is:

$$\text{I-66} \qquad \frac{[Sil]}{\Phi_{N_2}} = \frac{k_{44}}{k_{42}k_{45}}\{(k_{29} + k_{30}) + (k_{42} + k_{43})\frac{[Sil]}{[NO]}\}$$

A plot of $P_{Me_2SiF_2}/\Phi_{N_2}$ versus $P_{Me_2SiF_2}$ at constant NO pressure is a straight line and is shown in Figure I-14.

Arguments for deriving a rate equation for the formation of N_2O must retain those mechanistic assumptions used to describe N_2 production, i.e., $(k_{42} + k_{43})[Sil]$ cannot be neglected. Thus, deactivation and product formation via I-49 and I-50 are more important than the unimolecular decomposition of SilNO††:

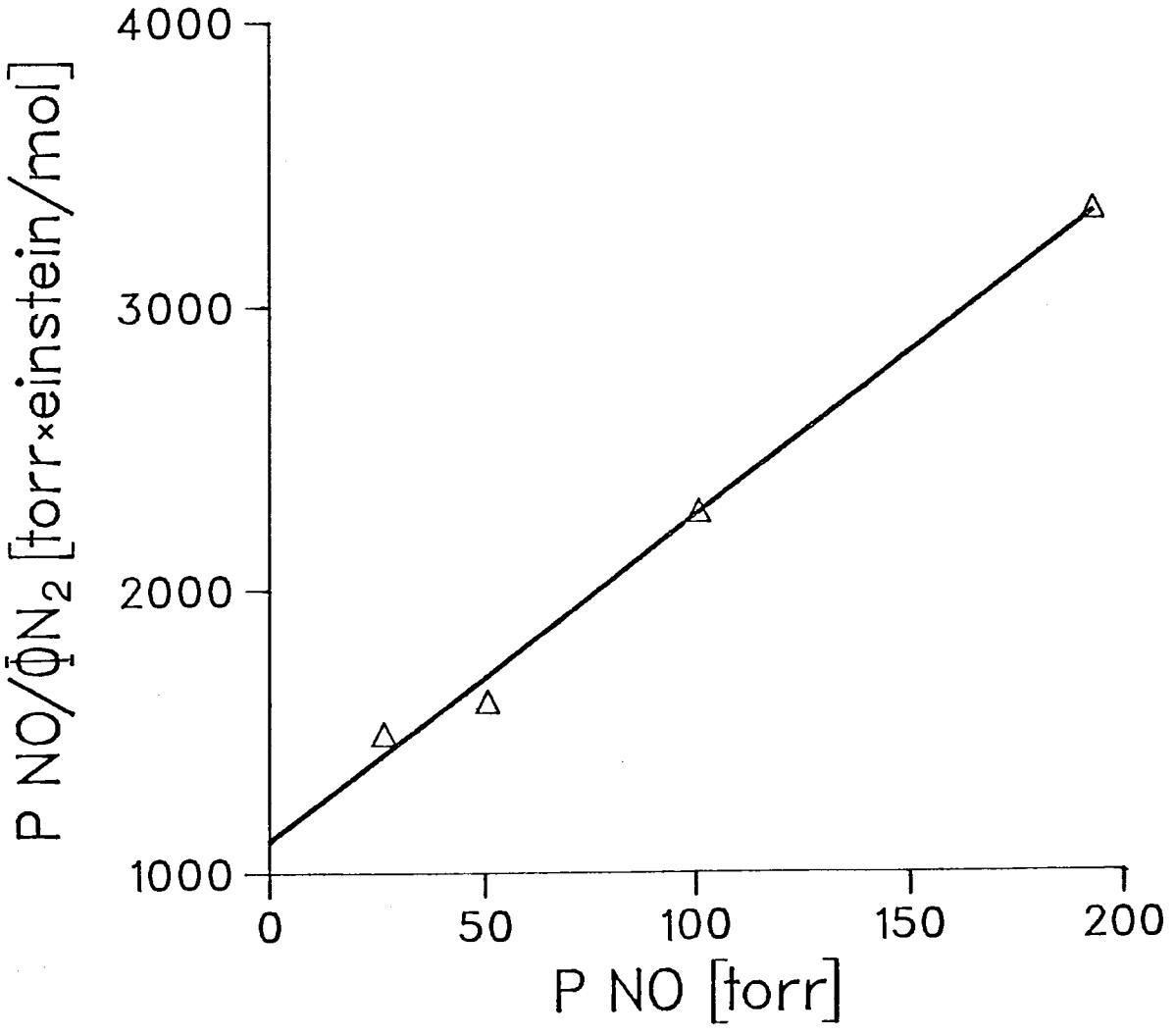

Fig. I-13. A Plot of P_{NO}/Φ_{N_2} vs. NO Pressure: $P_{Me_2SiF_2}$ = 50.5 ± 0.5 [torr].

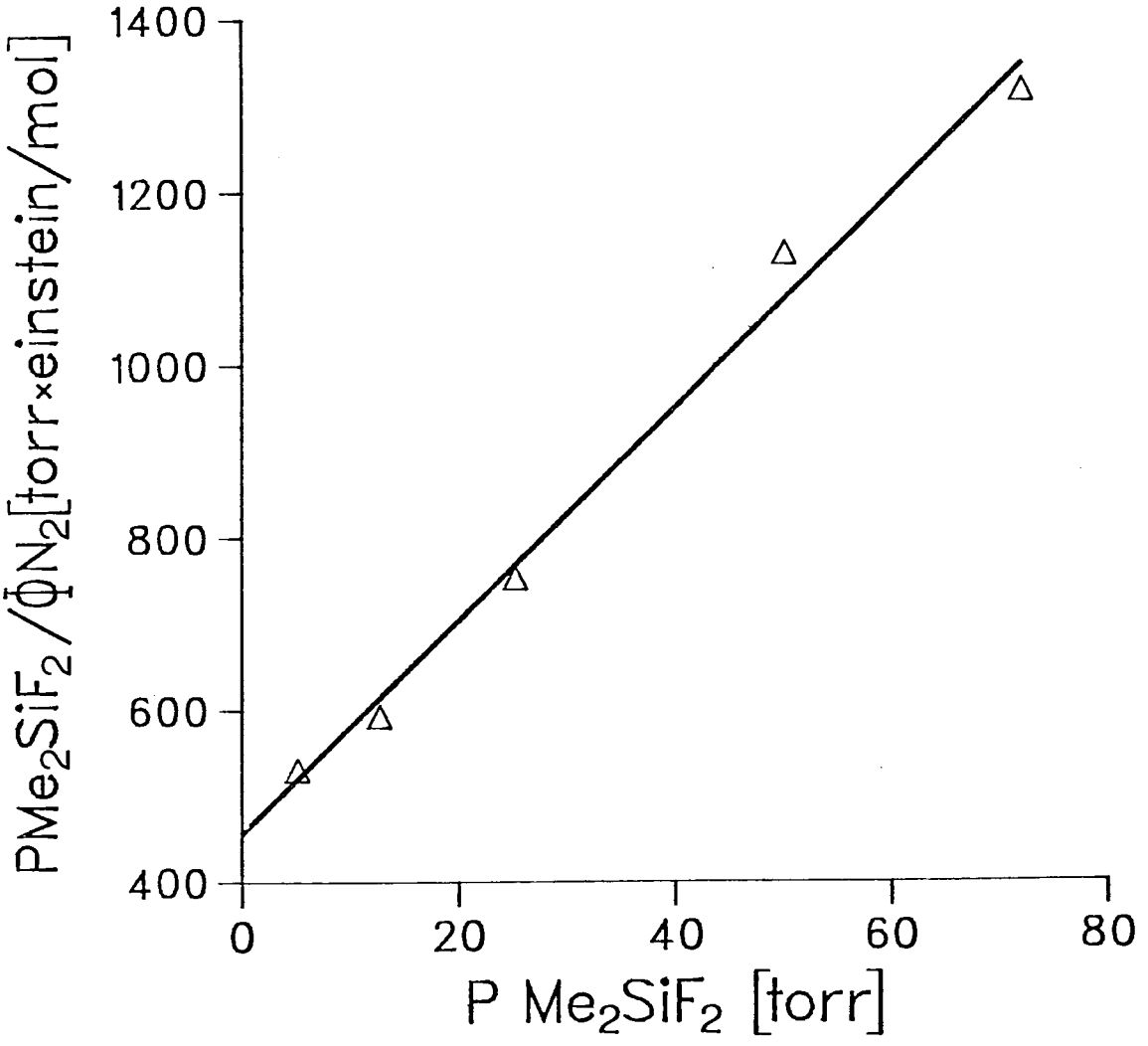

Fig. I-14. A Plot of $P_{Me_2SiF_2}/\Phi_{N_2}$ vs. Me_2SiF_2 Pressure: P_{NO} = 100.7 ± 0.7 [torr].

i.e., $k_{48} << (k_{49} + k_{50})[NO]$. In such case, the expression for the quantum yield of N_2O (I-58) becomes:

I-67

$$\Phi_{N_2O} = \frac{k_{43}k_{49}[Sil]}{(k_{49} + k_{50})\{(k_{29} + k_{30})[NO] + (k_{42} + k_{43})[Sil]\}}$$

from which,

I-68 $$\Phi_{N_2O}^{-1} = \frac{(k_{49} + k_{50})}{k_{43}k_{49}}\{(k_{42} + k_{43}) + (k_{29} + k_{30})\frac{[NO]}{[Sil]}\}$$

A plot of $\Phi_{N_2O}^{-1}$ versus P_{NO} at constant pressure of Me_2SiF_2 is shown in Figure I-15 and is a straight line as required by the above expression.

Figure I-16 shows that a plot of Φ_{N2O}^{-1} against $P_{Me2SiF2}^{-1}$ at constant NO pressure is also linear. The datum point for the lowest value of $P_{Me_2SiF_2}$ is not plotted. It lies far beyond the portion of the graph shown and the value predicted by Equation I-68 would be considerably smaller than the actual Φ_{N2O}. This difference may be explained by the increasing importance of reaction I-32 as a source of N_2O at low pressures of the silane.

From the slopes and intercepts of graphs I-13, I-14 and I-15, the following values of the ratio $(k_{42} + k_{43})/(k_{29} + k_{30})$ and their standard deviations were obtained: 1.9 ± 0.3, 2.7 ± 0.4 and 1.8 ± 0.3.

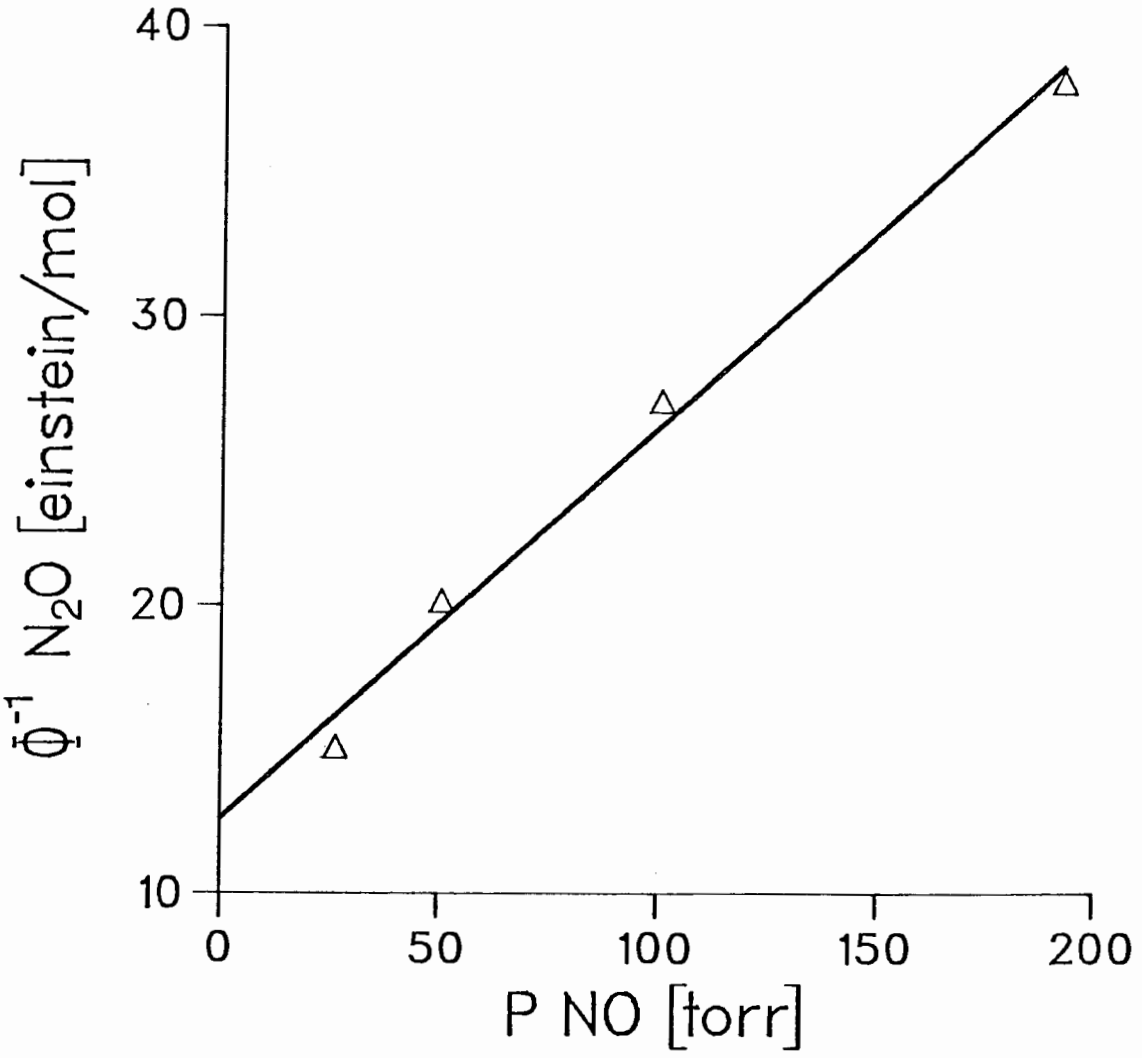

Fig. I-15. A Plot of Reciprocal of Quantum Yield of N_2O vs. NO Pressure: $P_{Me_2SiF_2}$ = 50.5 [torr].

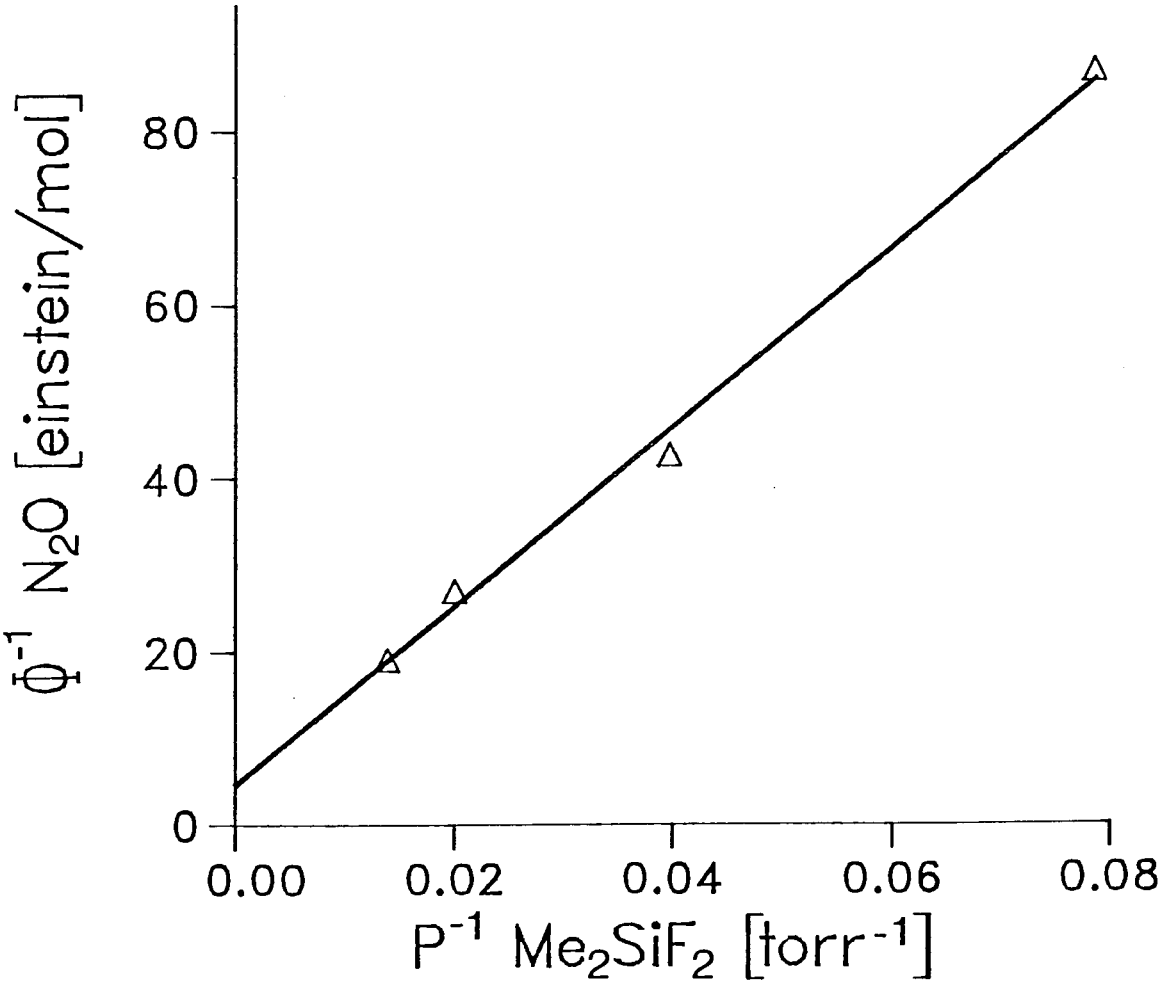

Fig. I-16. A Plot of Reciprocal of Quantum Yield of N_2O vs. Reciprocal of Me_2SiF_2 Pressure: P_{NO} = 100.7 ± 0.7 [torr].

3. The Nature of the Proposed Intermediate Complexes

The proposed mechanism involves the formation of two non-interconvertible complexes of $NO^4\pi$ with the silanes. These are denoted SilNO† and SilNO††

The $^4\pi$ state of nitric oxide lies 453.5 kJ above the ground state, with $\nu = 1$ at 464 kJ (16). The energy available from Hg $6(^3P_1)$ is only sufficient to populate the level $\nu = 1$ of this state. The fact that the energy available is sufficient to populate only $NO^4\pi$ ($\nu = 1$), suggests that these complexes must be structurally rather than energetically different.

Much of the chemistry of silicon, which is different from that of carbon, arises from its ability to expand its coordination number through the use of d orbitals. We propose that the two intermediate complexes may be formed through Si-N and Si-O bonding of the nitric oxide to the silicon center as is schematically shown in Figure I-17, but we do not conjecture upon which one leads to N_2 formation.

Theoretical support to the above postulate is obtained from calculations by P.G. and K.A. Perkins (24). They calculated the stability of the Sil-NO and Sil-ON complexes relative to the separate reactants, silane + $NO(^4\pi)$.

The Sil-ON complexes are 88 ($x = 2$), 21 ($x = 1$) and 10 ($x = 0$) kJ more stable than the isolated reactants. On the

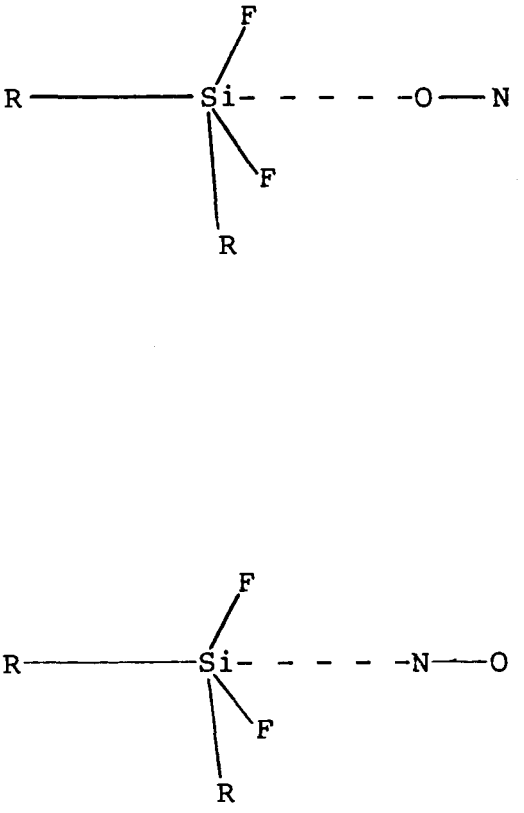

Fig. I-17. Schematic Representation of the Two Silane-NO Complexes.

other hand, the Sil-NO complex is 49 kJ more stable for the Me_2SiF_2-NO system while the corresponding complexes involving $MeSiF_3$ and SiF_4 have about the same stability as that of the isolated silane and $NO^4\pi$. In all cases, the Sil-ON complex is more stable than the Sil-NO complex for the same silane. For the series of silanes, the order of stability of the complexes was found to be $Me_2SiF_2 > MeSiF_3 > SiF_4$ which is in the same order as the experimentally observed reactivity with $NO^4\pi$.

I-6. CONCLUSIONS

The conclusions of this part of the present work may be summarized as follows:

1. $MeSiF_3$ does not provide an efficient source of SiF_3 radicals through its thermal decomposition, which occurs at too high a temperature to be practical as a clean source of the radicals. Si-C bond cleavage through mercury photosensitization at 253.7 nm is not observed; nor is Si-C bond cleavage with NO*.

2. The enhancement found in the production of N_2 and N_2O from NO-Hg $6(^3P_1)$-Me_xSiF_{4-x} mixtures may be explained if two different intermediate complexes are formed by reaction of nitric oxide in the $^4\pi$ state with the Me_xSiF_{4-x} compounds. The enhancement effects of the silanes are in the order

$$Me_2SiF_2 > MeSiF_3 >> SiF_4.$$

The proposed mechanism yields rate equations which satisfy the experimental observations for the two systems which were studied in detail. The differences observed are due to differences in the rate constants. For example,

reactions I-42 and I-43, in which the complexes are formed, are faster in the Me_2SiF_2 case. Moreover, they appear to compete with the deactivation reaction I-29 which still is the main fate of $NO^4\pi$.

PART II

THE REACTION OF METHYLENE WITH COMPOUNDS OF THE GENERAL FORMULA Me_xSiF_{4-x}

II-1. INTRODUCTION

The concurrent production of methylene in its singlet and triplet electronic states is well documented. The presence of the triplet state may be suppressed by the use of a radical scavenger; thus, oxygen has been widely used for this purpose.

Our interest was to determine if singlet methylene inserts into the different bonds of the Me_xSiF_{4-x} compounds. To simplify the kinetic scheme, nitric oxide was added to ketene-silane mixtures as a triplet methylene scavenger.

The following survey summarizes the literature related to this part of the thesis.

II-2 LITERATURE SURVEY

II-2.1 Ketene ($H_2C=C=O$), Spectrum and Photodissociation.

Since an early investigation of the photochemistry of ketene by R.G.W. Norrish and coworkers (26), a large number of publications have appeared in the literature (27). Some of the results which relate to this research work are presented below.

The absorption spectrum of ketene has been measured by several workers (28). The near U.V. region shown in Figure II-1 consists of two absorption bands:

i) a weak band which extends from 260-370 nm with a maximum at approximately 325 nm ($\varepsilon_{max} \simeq 9.3$[L/mol×cm]).

ii) a much stronger absorption from 195-215 nm with $\varepsilon_{max} \simeq 3000$[L/mol×cm].

Fluorescence of ketene following absorption in the near ultraviolet has not been observed, which indicates that the excited singlet state of ketene is extremely short-lived. An upper limit lifetime of $\tau \lesssim 4\times10^{-10}$ s has been estimated by Zabransky and Carr (29).

Despite numerous reports (30,31) which have appeared in the literature related to ketene photodissociation to methylene and carbon monoxide, the details of the electronic processes have not, as yet, been well established.

Zabransky and Carr (29) have proposed a mechanism for the near ultraviolet photodissociation of ketene which is in accord with their own observations and those of other workers (30,31).

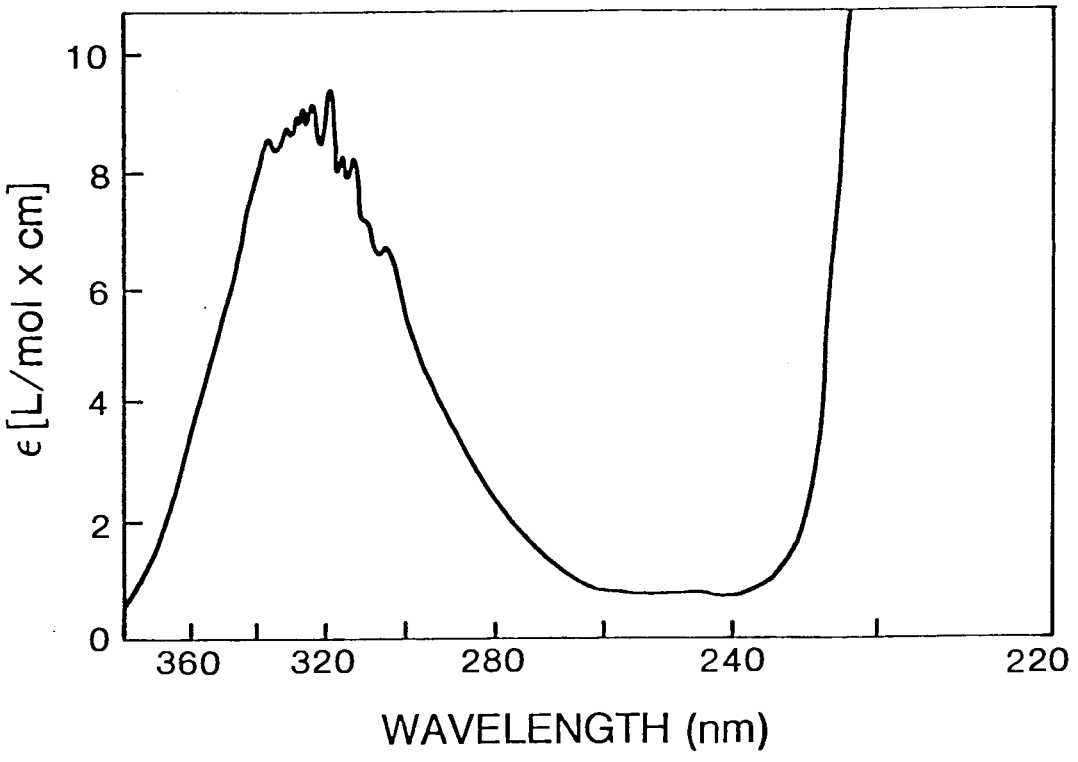

Fig. II-1. Absorption Spectrum of Ketene

(Adapted from Ref. 28c, p.97.)

A summarized account of the experimental work leading to the proposed mechanism is presented below:

i) The quantum yield of ketene decomposition (30,31) is a function of the radiation wavelength, the temperature and the pressure. At the shorter wavelengths (260-270 nm) the quantum yield is unity and pressure independent. At 313 nm and low pressures (17-60 torr), the quantum yield is also unity, but decreases at higher pressures. At 334 nm and at low pressures (≈26 torr), a value less than unity is reported. At this wavelength, the quantum yield decreases more rapidly with pressure than was observed at 313 nm. At 366 nm the primary quantum yield, extrapolated to zero ketene pressure, is much smaller than unity and decreases further as the pressure is increased.

ii) The photolysis of ketene in the 260-370 nm region yields both triplet ($^3CH_2$) and singlet ($^1CH_2$) methylene.

iii) The proportion of $^3CH_2$ formed increases with increasing wavelength. Thus at wavelength, 270-280 nm, about 85% of the methylene formed is singlet while at 366 nm it is mainly triplet. Various studies at 313 nm yield a value of 71% for the $^1CH_2$ with almost no pressure dependence. Thus, Rowland and coworkers (32a) and Zabransky and Carr (29) obtained a value of 70 ± 3% for the formation of $^1CH_2$ at 313 nm and 0-1 atm.

iv) Spin conservation rules require that triplet ketene be the precursor of triplet methylene and that singlet ketene be the source of singlet methylene (30b,c).

Equations II-1 to II-6 were proposed by Zabransky and Carr to account for ketene photodissociation at 313 nm.

II-1 $S_o \xrightarrow{h\nu,\ 313\ nm} {}^{i}S_1$

II-2 ${}^{i}S_1 \longrightarrow {}^{m}S_o$

II-3 ${}^{m}S_o \longrightarrow {}^{1}CH_2 + CO$

II-4 ${}^{m}S_o \longrightarrow {}^{k}T_1$

II-5 ${}^{k}T_1 \longrightarrow {}^{3}CH_2 + CO$

II-6 $M + {}^{m}S_o \longrightarrow S_o + M$

where S_o and S_1 are the ground and first excited singlet states, and T_1 is the lowest lying triplet state of ketene; i, m, k are vibrational levels of the corresponding electronic states.

The inclusion of steps II-1 and II-6 are based on Zabransky and Carr's estimated value for the lifetime of the excited ketene molecule ($\lesssim 4\times10^{-10}$ s). The overall photodissociation lifetimes, derived from the work of Stratchan and Thornton (30c) and Porter and Connelly (31a), were found to be considerably

longer than this value; viz., 3.5×10^{-7} s at 366 nm and 1.3×10^{-9} s at 334 nm. The rapid internal conversion process (II-2) proposed by Zabransky and Carr may involve an oxirene intermediate as shown by the ^{14}C labeling studies of Russell and Rowland (32b).

The photochemistry of ketene in the 260-370 nm region is characterized by the presence of both singlet and triplet methylene. The major products observed from ketene photolysis in this wavelength region are ethylene and carbon monoxide, but at longer wavelengths, small amounts of propylene, ethane and acetylene are also formed.

In pure ketene photolytic systems, ethylene is mainly formed by reaction II-7 (33).

II-7 $\quad {}^1CH_2 + CH_2CO \rightarrow C_2H_4 + CO$

Two different mechanistic sequences have been proposed to account for the reactions of triplet methylene. The first originated from the work of Kistiakowsky and Walter (34). They assumed that triplet methylene reacts with ketene to produce CH_3 and CHCO radicals and that these radicals participate in a sequence of reactions which leads to ethane and acetylene production. Reactions II-8 to II-11 were proposed.

II-8 $\quad {}^3CH_2 + CH_2CO \rightarrow CH_3 + CHCO$

II-9 $\quad CHCO + CHCO \rightarrow C_2H_2 + 2CO$

II-10 $\quad CH_3 + CHCO \rightarrow C_2H_4 + CO$

II-11 $\quad CH_3 + CH_3 \rightarrow C_2H_6$

An alternative proposal, based on experiments with labelled ketene, is that of Russell and Rowland (35). They favored ethane and acetylene formation through the following set of reactions:

II-12 $^3CH_2 + {}^3CH_2 \rightarrow C_2H_2 + 2H$

II-13 $H + CH_2CO \rightarrow CH_3 + CO$

II-14 $^3CH_2 + CH_3 \rightarrow C_2H_4 + H$

II-11 $CH_3 + CH_3 \rightarrow C_2H_6$

Both alternatives lead to the formation of equal amounts of acetylene and ethane in accord with experimental observations. Arguments in favor of the Russell and Rowland mechanism are supported by results from an earlier flash-photolysis study of ketene (36). This study shows that the reaction of $^3CH_2$ with ketene must be very slow compared to the reaction of $^3CH_2$ with another $^3CH_2$. Rowland and coworkers (37) have estimated the collision efficiency of reaction II-8 to be $<10^{-7}$. At the same time, they have found that methyl radical attack on ketene is not important.

II-2.2 Methylene (CH_2).

The first chemical evidence for methylene formation was given in the early nineteen thirties (26). Since then, it has been one of the most thoroughly studied of reactive intermediates. It has been a focus of interest not only of organic chemists, but also of theoretical chemists, spectroscopists and

chemical kineticists. Even though there are still some uncertainties as to its behaviour, the general aspects of the properties of methylene are well established. Those considered to be more relevant are listed below (2a,2b,38).

a) Methylene has a triplet ground state, $CH_2(^3B_1)$, which is bent with an H-C-H angle of about 136°. The lowest-lying excited state is a singlet, $CH_2(^1A_1)$, with an H-C-H angle of about 102°.

b) The energy separation between the lowest singlet and triplet states is still under dispute. Thus, while Herzberg (39) suggested an energy gap of less than 96.2 kJ/mol, Halberstadt and McNesby (40) provided an estimate of 10.5 kJ/mol. In the last few years, many experimental and theoretical studies have been carried out to determine this energy difference. The results fall into two groups (41), those in the range of 33.9 to 56.5 kJ/mol and those near 81.6 kJ/mol.

c) The chemical reactivities of the two species, $^1CH_2$ and $^3CH_2$, are different. Only singlet methylene inserts into the C-H bonds of hydrocarbons, i.e.,

II-15 $$^1CH_2 + R\text{-}H \rightarrow R\text{-}CH_3$$

This reaction has a small selectivity towards the different

types of C-H bonds. Rates are in the order:

tertiary > secondary > primary

Triplet methylene abstracts H-atoms from hydrocarbons, i.e.:

II-16 $^3CH_2 + R\text{-}H \rightarrow CH_3 + R$

d) Singlet methylene is collisionally deactivated to the triplet state by inert gases

II-17 $^1CH_2 + M \rightarrow {}^3CH_2 + M$

II-2.2.1 Reactions of Singlet Methylene with Silanes.

Several studies of methylene with silanes have been reported. Kramer and Wright (42) first investigated its reactions in solution with compounds containing Si-H bonds. Subsequently, Simons and coworkers (43) examined its reactions with various silanes, i.e.: SiH_4, Me_xSiH_{4-x}. It is now known that:

a) Singlet methylene does not insert into C-Si bonds.

b) Singlet methylene inserts 7 to 9 times faster into the Si-H bonds than into the C-H bonds of methylsilanes.

c) The relative rates of singlet methylene insertion into the Si-H and C-H bonds of Me_xSiH_{4-x} compounds are in the order

$$MeSiH_3 \approx Me_2SiH_2 > Me_3SiH \approx Me_4Si$$

d) Singlet methylene inserts into the C-H bonds of tetramethylsilane (TMS) to yield ethyltrimethylsilane. The total reactivity for insertion of TMS relative to that of methane (k_{TMS}/k_{CH_4}) as reported by Simons and Hase (43d) is six.

e) Due to the exothermic character of the insertion reaction, the insertion products are vibrationally excited, and will undergo unimolecular decomposition which will compete with collisional stabilization.

II-2.2.2 Reaction of Methylene with NO.

Nitric oxide is used to scavenge alkyl radicals in hydrocarbon systems. Laufer and Bass (36) found that NO is also an excellent scavenger of $^3CH_2$. Thus, they determined that NO is ten times more efficient than O_2 in suppressing the concentration of $^3CH_2$. They reported a rate constant $k_{18} = 9.6\times10^9$ L mol^{-1} s^{-1}.

II-18 $^3CH_2 + NO \rightarrow (CH_2NO)$

The final products of reaction II-18 have not been established. A rate constant of 6.0×10^9 L mol^{-1} s^{-1} was recently published by Pilling and Robertson (44) for this reaction.

Laufer and Bass also determined that NO reacts with $^1CH_2$ and an upper limit of 2×10^{10} L mol^{-1} s^{-1} was calculated for

the rate constant. The reaction products are also unknown. Thus, when nitric oxide is used to scavenge triplet methylene, singlet methylene as well may be scavenged. However, nitric oxide will be very effective in reducing the ratio $[^3CH_2]/[^1CH_2]$ because the reaction of the triplet with NO is much faster than competing reactions such as, for example, the abstraction reaction II-16. Braun and coworkers (45) estimated a value of $<3\times10^7$ L $mol^{-1}s^{-1}$ for H abstraction by triplet methylene from both H_2 and CH_4. Singlet methylene, on the other hand, reacts with comparable efficiency with hydrocarbons and with nitric oxide and will not be appreciably affected by small concentrations of NO scavenger.

II-3 EXPERIMENTAL

A. Vacuum Apparatus.

Gas handling was performed in the standard all-glass vacuum system described in Section I-3.

B. Radiation Source and Optical Train.

The optical train is shown in Figure II-2. The 313 nm radiation was obtained from a 200 W high pressure mercury arc (PEK) in a ventilated housing with the appropriate optics to provide a parallel beam. The desired wavelength was isolated using a filter system composed of a Pyrex cell (5 cm in diameter, 1 cm in length) containing distilled water to absorb infrared radiation, a 3 mm thick Corning glass filter CS#7-54, and a cylindrical three-compartment Pyrex cell (5 cm in diameter) containing the following solutions (2a):

1. 1.05 M $NiSO_4$ aqueous solution — 5 cm
2. 0.299 M $CoSO_4$ aqueous solution — 5 cm
3. 0.0245 M potassium biphthalate aqueous solution — 1 cm
   This solution was changed prior to each irradiation.

The photolysis reaction vessel was made of quartz, cylindrical (5 cm diameter, 10 cm length) with planar windows, and total volume 215 ± 3 cc.

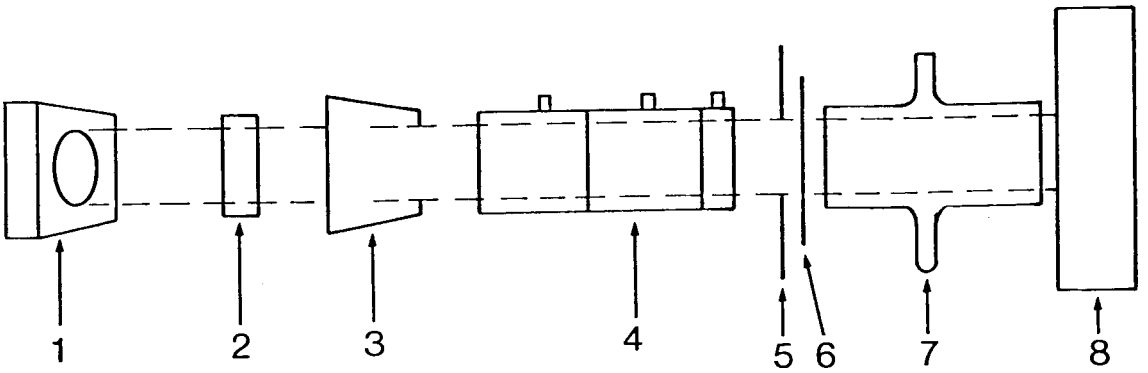

Fig. II-2. Optical Train

Key to Figure II-2.

1. Radiation source with housing
2. Distilled water filter
3. Corning glass filter (CS#7-54)
4. Three compartment Pyrex filter cell
5. Light stop
6. Shutter
7. Photolysis vessel
8. Jarrel-Ash monochromator

A scanning monochromator (Jarrel-Ash model #82-410) in conjunction with a photomultiplier, power supply and recorder was used to check the transmission of the filter system. The light transmitted through the reaction cell was also checked prior to and during each irradiation.

C. Reactants.

Ketene: Prepared using a ketene generator as described by Vogel (46). Acetone vapor (Fisher spectra grade) was decomposed on a glowing resistance wire to yield ketene. The vapors were directed through a series of traps at 0°C to collect any unreacted acetone and ketene was collected at -80°C. The ketene was then degassed and purified by several trap-to-trap distillations. The purified gas was collected at -186°C. Gas chromatographic analysis of the purified ketene showed small amounts of impurities which were not identified, but which did not interfere with product analysis.

The absorption spectrum of ketene in the 200-400 nm region was obtained with a Cary 17 spectrophotometer. The extinction coefficient at 325 nm was 9.7 L $mol^{-1}cm^{-1}$ which agrees within experimental error with values reported in the literature (28). The ketene was stored in the dark at -196°C.

Methyltrifluorosilane: Obtained from K & K Laboratories Inc. It was reported to be 99% pure. Its major impurities were CO_2 and Me_2SiF_2. The material was further purified as described in Section I-3. This procedure left small quantities of Me_2SiF_2 which would have interfered with product analysis and was therefore removed by preparative gas chromatography.

Trimethylfluorosilane: Obtained from PCR Research Chemicals Inc. It contained CO_2 and Me_2SiF_2 in small quantities. The material was degassed, distilled and collected at -98°C. Impurities were undetectable after this procedure.

Tetramethylsilane: Obtained from Alfa Inorganics (NMR grade). It was degassed at -186°C and used without further purification.

The sources and purification procedures of dimethyldifluorosilane, tetrafluorosilane and nitric oxide are the same as those described in Section I-3.

D. Product Analysis and Identification.

All analyses were performed by gas chromatography as described in Section I-3. Products were collected from the GC eluent and characterized by IR, MS and ^{1}H-NMR spectrometry.

The IR spectra were obtained with a Perkin Elmer 599B spectrophotometer. Each purified compound was collected in a specially adapted air-tight gas cell provided with NaCl windows with 13 cc total volume and 5 cm optical path.

The mass spectra were obtained with a Hewlet Packard 5985 GC-MS spectrometer. Each purified gas was condensed into an evacuated capillary tube (3 mm o.d. diameter) which was transferred into the sample injector in the inlet system of the mass spectrometer.

The ^{1}H-NMR spectra were obtained with a Bruker WM-400 NMR spectrometer. Each purified sample was collected in a capillary tube containing degassed $CDCl_3$ under vacuum. The tube was then sealed and removed for analysis.

Three different GC columns were used to quantitatively analyze the gaseous mixtures. The Molecular Sieves (5A) and the Porapak Q columns were those described in Table I-2. The third column made of thin wall stainless steel tubing, 4.8 mm o.d. and 5.3 m in length contained Porapak N (Waters Assoc. Inc., 80-100 mesh). The details of the applications of the Porapak Q and N columns are shown in Table II-1. The analysis conditions with the Molecular Sieves column are shown in Table I-3.

The silicon-containing products were not commercially available and were prepared by the reaction of methylene with the corresponding Me_xSiF_{4-x} compound. Isolation and purification was accomplished by preparative gas chromatography. The GC molar responses were determined using these purified materials. The values obtained and respective standard deviations, are shown in Table II-1. The molar responses of ethane, ethylene and acetylene are also included in this table.

Table II-1

Gas Chromatographic Analysis Conditions

He flow = 50 [cc/min]

Substance	t_R' [min] (a)	Operating Conditions	Molar Response, r_i [Area/mol] $\times 10^{-9}$
Porapak N Column:			
C_2H_4	6.7	50°C	1.70±0.03
C_2H_6	9.1	50°C	1.81±0.03
C_2H_2	14.8	50°C	1.44±0.02
CH_2CO	25.2	20 min at 50°C, 10°/min up to 180°C	
NO	$t_{R=2.3}$	50°C	
Porapak Q Column:			
$MeSiF_3$	3.7	5 min at 110°C, 10°/min up to 230°C	
$EtSiF_3$	11.1	5 min at 110°C, 10°/min up to 230°C	
Me_2SiF_2	10.5	5 min at 110°C, 10°/min up to 230°C	
$EtSi(Me)F_2$	15.6	5 min at 110°C, 10°/min up to 230°C	2.84±0.04

Table II-1, continued

Substance	t_R' [min](a)	Operating Conditions	Molar Response, r_i / [Area/mol]$\times 10^{-9}$
$Me_2Si(CH_2F)F$	17.1	5 min at 110°C 10°/min up to 230°C	1.76±0.03
Me_3SiF	15.3	5 min at 110°C, 10°/min up to 230°C	
$Et(Me)_2SiF$	19.5	5 min at 110°C, 10°/min up to 230°C	3.54±0.05
SiF_4	0.63	5 min at 110°C, 10°/min up to 230°C	
CH_2CO	4.7	5 min at 110°C, 10°/min up to 230°C	
Me_4Si	9.0	5 min at 190°C, 10°/min up to 230°C	
$EtSiMe_3$	13.1	5 min at 190°C, 10°/min up to 230°C	4.12±0.05

(a) $t_R' = t_R - t_{Air}$

E. Photolysis Procedure.

The reaction mixtures for Me_xSiF_{4-x}-ketene photolysis were prepared by first introducing into the reaction cell a known pressure of Me_xSiF_{4-x} and condensing it. Secondly, a known pressure of ketene was also condensed. The gases were then abruptly evaporated and allowed to stand for several minutes to ensure complete mixing.

Reaction mixtures for the Me_4SiF_{4-x}-ketene-NO photolysis were similarly prepared. The nitric oxide could not be quantitatively transferred from the metering device to the reaction cell because its vapor pressure at -196°C is ≈70 microns and so the nitric oxide pressure was calculated by a difference procedure.

All experiments were carried out at room temperature. Irradiation times were chosen so that the extent of ketene decomposition was between 6 and 9%. The rates of formation of products were independent of time of irradiation provided ketene decomposition was less than 10%.

After irradiation the cold finger of the reaction cell was cooled to -196°C and thus the contents of the reaction cell were divided into a condensable fraction and a volatile fraction consisting of CO, some NO (if initially present) and some C_2H_4. The latter fraction was further fractionated at -210°C. The material noncondensable at -210°C consisting of CO was quantitatively measured in a gas burette and checked for purity by gas

chromatography (Molecular Sieves).

The fraction left in the reaction vessel at -196°C was further separated by distilling the mixture through traps maintained at -160°, -196° and -210°C.

All fractions collected at -196°C and -210°C were combined and quantitatively analyzed by gas chromatography (Porapak N). The resultant mixture consisted of unreacted ketene and ethylene and also contained some of the unreacted NO when the reaction was carried out in the presence of this compound. If NO was not initially added, then ethane and acetylene, which are suppressed by NO, were also present in this mixture.

The fraction collected at -160°C contained the unreacted silane and the silane product and was quantitatively analyzed by gas chromatography only for the silane product (Porapak Q).

II-4. EXPERIMENTAL RESULTS

A. Preliminary Studies

Ketene (K) slowly decomposes thermally at room temperature, hence experiments were carried out over short periods of time so that this decomposition was insignificant.

Experiments were also carried out to determine if a dark reaction occurred with ketene and the silanes. Only in the case of SiF_4 was any enhancement observed in the thermal decomposition of ketene.

Preliminary photochemical experiments with silane-ketene mixtures were undertaken to determine the products of the reaction of the Me_xSiF_{4-x} compounds with methylene. Mixtures of the appropriate compound and ketene (ratios 10:1) were photolyzed for 60 min at 22±1°C and the results of these experiments are shown in Table II-2. SiF_4 is not included in this table since no products were found additional to those observed from the photolysis of ketene even after the mixture was irradiated for 180 min.

The silicon-containing products, as indicated in Table II-2, were ethyltrifluorosilane (EtTFS) from $MeSiF_3$, ethyldimethylfluorosilane (EtDMFS) from Me_3SiF, and ethylmethyldifluorosilane (EtMDFS) and much smaller amounts of dimethylfluoromethylfluorosilane (DMFMFS) from Me_2SiF_2. These products were identified from their MS, IR and ^{1}H-NMR spectra. The main

Table II-2

Product Yields for 313 nm Photolysis of 10:1 Me_xSiF_{4-x}-Ketene Mixtures at Room Temperature (22±1°C)

$P_{Me_xSiF_{4-x}}$ = 51±1[torr]

Run	System	CO	$C_2H_4+C_2H_2$	C_2H_6	CH_4	C-H[(a)]	Si-F[(b)]
		[μmoles/60 min]					
PT20	K	31.1	10.5	0.54	0.052	0	0
PT18	$K+MeSiF_3$	23.2	5.5	0.83	0.038	0.85	0
PT21	$K+Me_2SiF_2$	21.1	3.9	0.90	0.033	8.74	1.38
PT19	$K+Me_3SiF$	21.6	2.7	1.04	0.028	13.5	0
1C	$K+Me_4Si$	22.6	1.9	1.17	0	14.3	0

(a) C-H represents the product of general formula $EtMe_{x-1}SiF_{4-x}$.

(b) Si-F represents the product of general formula $Me_xSi(CH_2F)F_{3-x}$.

features of the mass spectra and proton-NMR spectra of these compounds are presented in Tables II-3 and II-4.

Besides the ethylfluorosilanes, the other major products of the reaction were carbon monoxide and ethylene. Minor amounts of hydrogen, methane and ethane were also found. The amount of hydrogen produced was not quantitatively determined. Acetylene, which is also a minor product from ketene decomposition, was not separated from ethylene in these initial experiments.

Once the products were characterized, kinetic studies were undertaken.

Table II-3

Main Mass-Spectral Bands (70 eV)

m/e	Abundance	Assignment	Ref.
	$EtSiMe_3$ (EtTMS)		
102	3.0	M^+	
87	18.1	$EtSiMe_2^+$	
73	100.0	Me_3Si^+	
59	47.9	Me_2SiH^+	
45	9.5	$MeSiH_2^+$	
43	7.6	$MeSi^+$	
	$EtSi(F)Me_2$ (EtDMFS)		47
106	10.6	M^+	
91	26.9	$EtSi(F)Me^+$	
77	100.0	Me_2SiF^+	
63	34.6	$MeSiHF^+$	
49	9.1	SiH_2F^+	
47	18.2	SiF^+	
	$EtSi(F)_2Me$ (EtMDFS)		
110	21.7	M^+	
95	30.4	$EtSiF_2^+$	
81	100.0	$MeSiF_2^+$	

Table II-3, continued

m/e	Abundance	Assignment
67	13.9	$SiHF_2^+$
47	9.7	SiF^+
	$Me_2(F)SiCH_2F$ (DMFMFS)	
81	15.2	$MeSiF_2^+$
77	100.0	Me_2SiF
67	16.0	$SiHF_2^+$
63	9.6	CH_3SiHF^+
49	22.4	SiH_2F^+
47	22.7	SiF^+
	$EtSiF_3$ (EtTFS)	
114	12.9	M^+
113	9.2	$C_2H_4SiF_3^+$
112	10.0	$C_2H_3SiF_3^+$
111	15.4	$C_2H_2SiF_3^+$
95	46.9	$C_2H_5SiF_2^+$
93	33.3	$C_2H_3SiF_2^+$
91	19.1	$C_2HSiF_2^+$
85	100.0	SiF_3^+
67	16.6	$HSiF_2^+$

Table II-3, continued

m/e	Abundance	Assignment
66	18.9	SiF_2^+
47	25.4	SiF^+
29	39.0	$C_2H_5^+$
28	73.0	$C_2H_4^+$
27	43.5	$C_2H_3^+$
26	15.8	$C_2H_2^+$

Table II-4. ^{1}H-NMR Spectral Data

Compound	δ_{CH_3} [ppm]	δ_{CH_2} [ppm]	$^3J_{H-H}$ [Hz]	$^4J_{H-H}$ [Hz]	$^2J_{H-F}$ [Hz]	$^3J_{H-F}$ [Hz]	Ref.
$CH_3CH_2Si(CH_3)_3$	(1) 0.954 t	0.498 q	8.0				
(1)(2) (3)	(3) 0.003 s						
$CH_3CH_2\overset{F}{\underset{}{Si}}-(CH_3)_2$	(1) 0.985 t	0.650 c	7.7			7.5(3)	47
(1)(2) (3)	(3) 0.200 d						
$CH_3CH_2\overset{F}{\underset{F}{Si}}CH_3$	(1) 1.037 t	0.764 c	8.0	0.32(3-2)		6.3(3)	
(1)(2)F (3)	(3) 0.323 t						
$FCH_2\overset{F}{\underset{}{Si}}(CH_3)_2$	(3) 0.358 d	4.475 d of d			46.8	7.2(3)	
(4) (3)						5.4(4)	
$CH_3CH_2SiF_3$	1.138 t	0.975 c	8.0				

s = singlet; d = doublet, t = triplet, q = quartet, c = complex

B. Kinetic Studies

1. Product Yields as a Function of Time.

Yields of products as a function of exposure time at constant light intensity were determined by photolyzing mixtures of Me_3SiF-ketene and Me_2SiF_2-ketene in a 5:1 ratio. The individual reactant pressures in this series of experiments were kept within the limits; ketene, 1.30±0.05 torr and silane, 6.50±0.05 torr. The experimental results are shown in Figures II-3 and II-4 for the major products, and Tables II-5 and II-7 for the minor products.

The results fall on a smooth curve which is essentially linear up to about 10 minutes of irradiation time. All subsequent experiments were carried out in this linear region which corresponds to less than 10% decomposition of ketene.

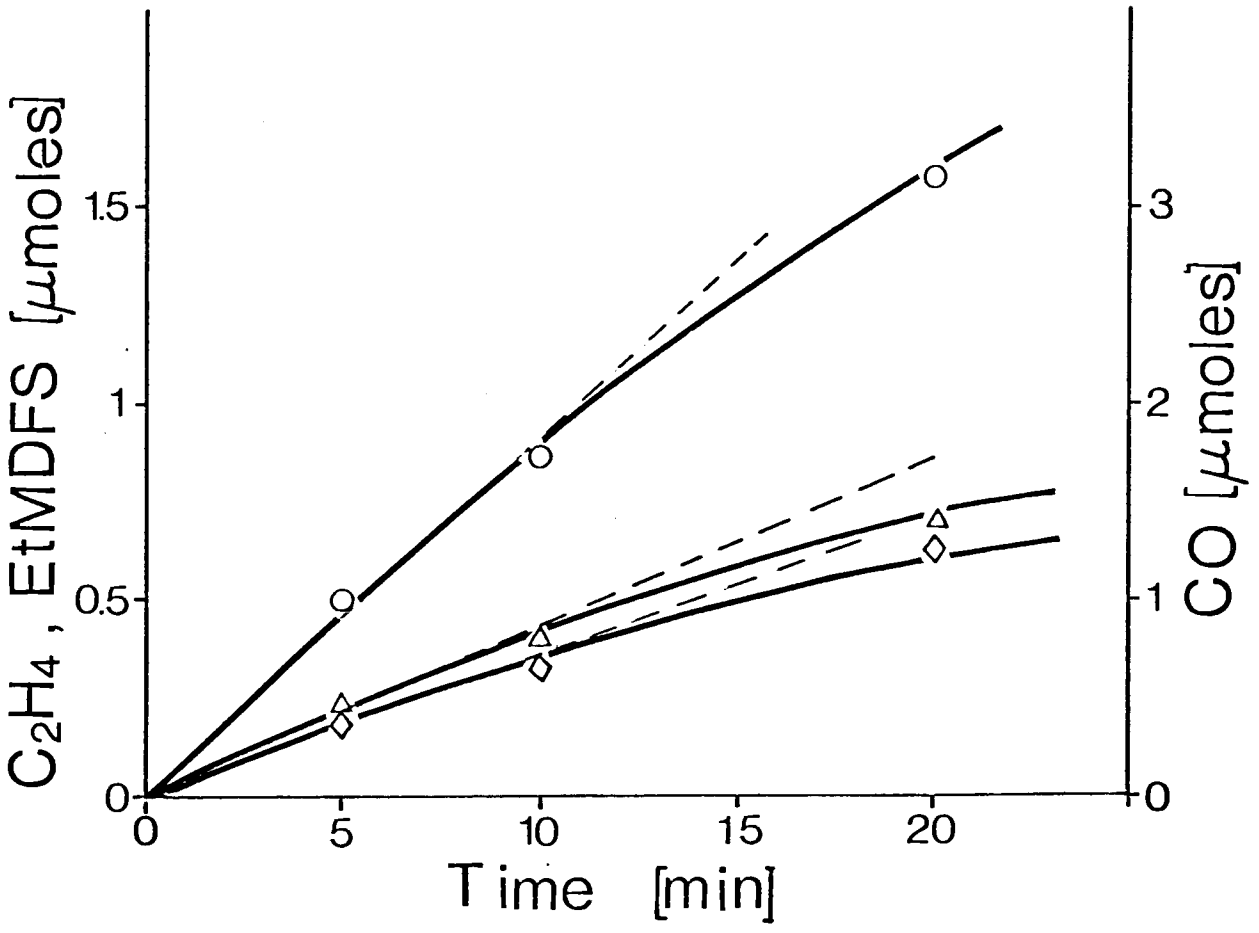

Fig. II-3. Time Dependence of CO (O), C_2H_4 (Δ), and EtDMFS (◇) Yields from 313 nm Me_3SiF-Ketene Photolysis; P_{Me_3SiF}=6.50±0.05 [torr], P_K=1.30±0.05 [torr].

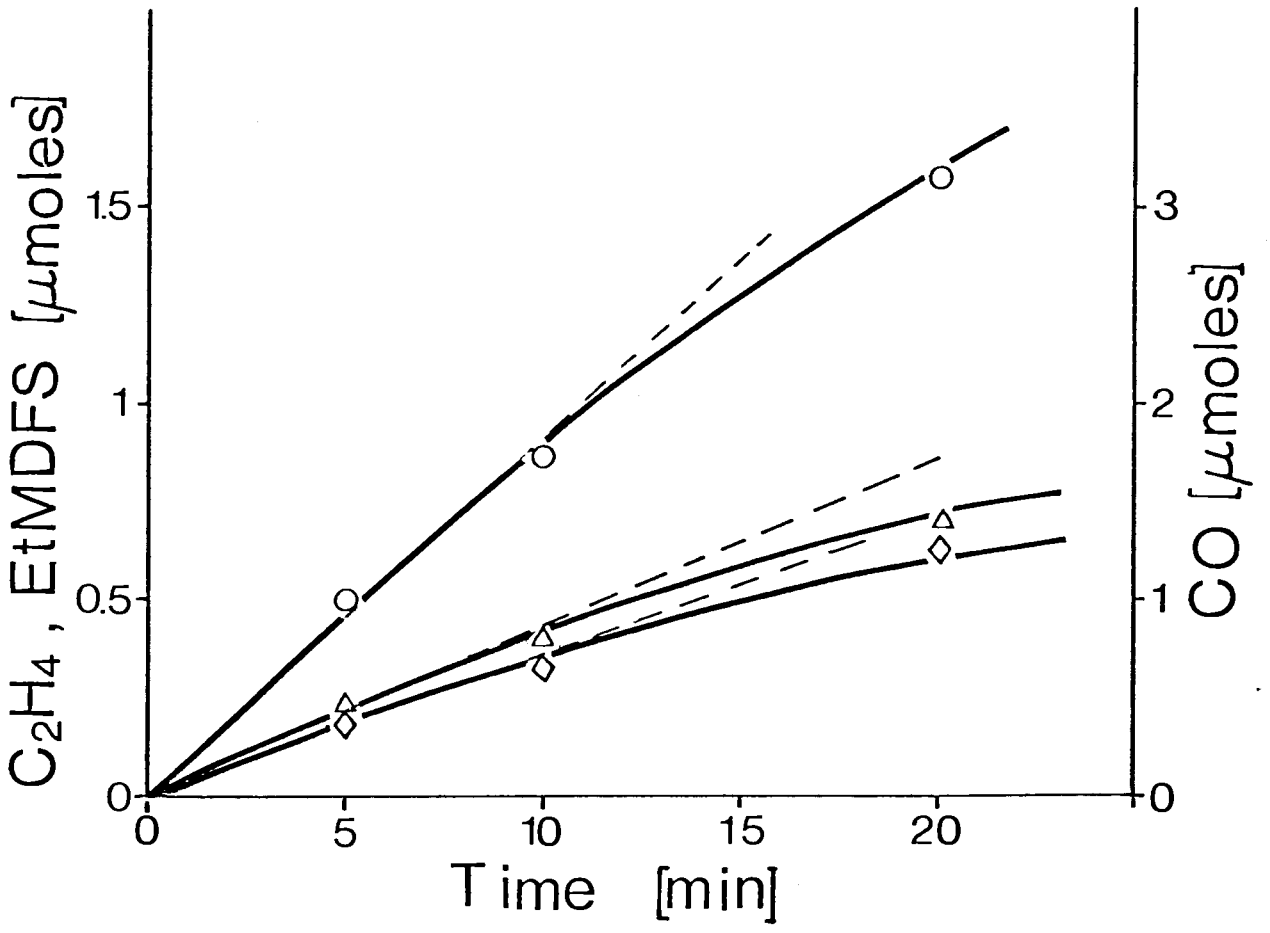

Fig. II-4. Time Dependence of CO (O), C_2H_4 (Δ), and EtMDFS (◇) Yields from 313 nm Me_2SiF_2-Ketene Photolysis; $P_{Me_2SiF_2}$=6.50±0.05 [torr], P_K=1.30±0.05 [torr].

Table II-5

Time Dependence of C_2H_6 and C_2H_2 Yields from 313 nm Me_3SiF-Ketene Photolysis

P_{Me_3SiF} = 6.50±0.05 [torr]

P_K = 1.30±0.05 [torr]

Run	t	C_2H_6	C_2H_2
	[min]	[μmoles]	
6	5.00	0.029	0.007
4	10.00	0.058	0.028
5	10.00	0.050	0.036
3	20.00	0.104	0.072
7	20.00	0.102	0.074

Table II-6

Time Dependence of C_2H_6, C_2H_4 and DMFMFS Yields from 313 nm Me_2SiF_2-Ketene Photolysis

$P_{Me_2SiF_2}$ = 6.50±0.05 [torr]

P_k = 1.30±0.05 [torr]

Run	t	C_2H_6	C_2H_2	DMFMFS
	[min]		[μmoles]	
3A	5	0.037	0.053	0.016
1A	10	0.094	0.080	0.062
2A	20	0.122	0.130	0.109

2. Photolysis of Ketene and Ketene-NO Mixtures.

Ketene (1.3 torr) was irradiated for 5 minutes and the product yields were determined. This ketene pressure was also used in those experiments of ketene with the silanes.

The photolysis of ketene was periodically repeated to monitor the lamp intensity and general reaction conditions. A sample of these experiments covering a period of nearly seven months is shown in Table II-7. The total change in the carbon monoxide yield during this time corresponds to a 15.5% decrease of the lamp intensity. The results from Table II-7 also show that, during the time a given system was studied, the lamp intensity was constant within experimental error.

The effect of added nitric oxide on the products of the ketene photolysis was studied by photolyzing a constant pressure of ketene with various pressures of nitric oxide. Product rates are reported in Table II-8. A pressure of 0.030 torr of nitric oxide was enough to completely suppress the formation of ethane and acetylene. These products are diagnostic of the presence of triplet methylene; thus their absence may be used as an indication of the complete removal of triplet methylene.

Table II-7

Product Rates for Ketene Photolysis at 313 nm

P_K = 1.32±0.03 [torr]

Run	CO	C_2H_4	C_2H_6	C_2H_2	Related System under study
		[μmoles/min]			
2K*	0.316	0.121	0.008	0.012	Me_2SiF_2-K,
3K	0.313	0.105	0.009	0.011	K and K-NO,
4K	0.328	0.120	0.007	0.008	Me_2SiF_2-K-NO,
5K	0.312	0.120	0.007	0.008	& Me_3SiF-K-NO
6K**	0.280	0.111	0.010	0.008	$MeSiF_3$-K-NO,
7K	0.270	0.112	0.007	0.009	Me_4Si-K-NO &
8K	0.267	0.106	0.007	0.009	Me_4Si-K

* Started a new lamp.

** The decrease in the lamp intensity between experiments 5K and 6K was due to the use of the lamp in long irradiations when samples of products (EtTFS and EtTMS) were prepared for calibrations.

Further addition of nitric oxide causes a further decrease in the concentration of ethylene suggesting that some singlet methylene was also being removed. The rate of carbon monoxide formation did not vary significantly, indicating that the extent of ketene decomposition was not affected by the presence of nitric oxide.

Table II-8

Product Rates for Ketene-NO Photolysis at 313 nm

P_K = 1.31±0.02 [torr]

Run	P_{NO}	CO	C_2H_4
	[torr]	[μmoles/min]	
K[a]	0	0.317	0.120
33A	0.030	0.320	0.101
22A	0.073	0.322	0.0968
32A	0.145	0.314	0.0882
31A	0.352	0.304	0.0767
34A	0.744	0.312	0.0680

(a) Average of four determinations.

3. Photolysis of Me_xSiF_{4-x}-Ketene and Me_xSiF_{4-x}-Ketene-NO Mixtures.

Experiments were carried out to study the effect of the composition of the reaction mixture on the product yields. In these experiments, the pressures of ketene and nitric oxide (if added) were kept constant and the pressure of the silane was varied. These mixtures were irradiated for five or six minutes.

In the absence of nitric oxide, the products were carbon monoxide, ethylene, ethane, acetylene, and $EtMe_{x-1}SiF_{4-x}$. Only in the case of the Me_2SiF_2-ketene system was an extra silicon-containing product observed, namely, $Me_2Si(CH_2F)F$.

Owing to differences in the reactivity of the silanes, a larger pressure of ketene (4 torr) was added in the case of $MeSiF_3$-ketene-NO mixtures to obtain quantities of the ethyl derivative which were measurable by gas chromatography.

The product rates corresponding to each of the silane-ketene systems are reported in Tables II-9, II-11, II-13 and II-15. A typical plot of the rates of formation of ethylene and EtMDFS from the data in Table II-9 (Me_2SiF_2-ketene) is shown in Figures II-5 and II-6.

The data from these tables show that for each silane, the rates of carbon monoxide and ethylene both decrease while the rates of $EtMe_{x-1}SiF_{4-x}$, and $Me_2Si(CH_2F)F$ (DMFMFS) in the case of Me_2SiF_2, increase with increasing silane pressure. These rates plateau at high pressures of the silane (Figs. II-5

and II-6). The amount of the silane required to reach this plateau region depended on the silane itself and was in the order:

$$MeSiF_3 > Me_2SiF_2 > Me_3SiF > Me_4Si$$

The rates of the minor products is such that ethane remains essentially constant and acetylene decreases as the pressure of a given silane is increased. The observed decrease of the acetylene yield appeared to be related to the reactivity of the silane. Thus, in the Me_4Si system, the acetylene yield dropped to zero at much smaller pressures of added silane than in the Me_2SiF_2 systems (refer to Tables II-13 and II-9). A typical plot of the rates of formation of ethane and acetylene from the data in Table II-9 (Me_2SiF_2-ketene) is shown in Figure II-7. The rates have considerable uncertainties due to the small amount of product formed.

The data in Tables II-9, II-11, II-13 and II-15 show that the observed trends in the product rates as a function of silane pressure are similar for each of the silane-ketene systems. The differences between the systems are only quantitative, presumably as a result of the different reactivities of the silanes with methylene.

The results of the experiments carried out in the presence of nitric oxide are shown in Tables II-10, II-12, II-14 and II-16. A typical plot of the rates of formation of C_2H_4 and EtMDFS is shown in Figures II-5 and II-6. Also included in

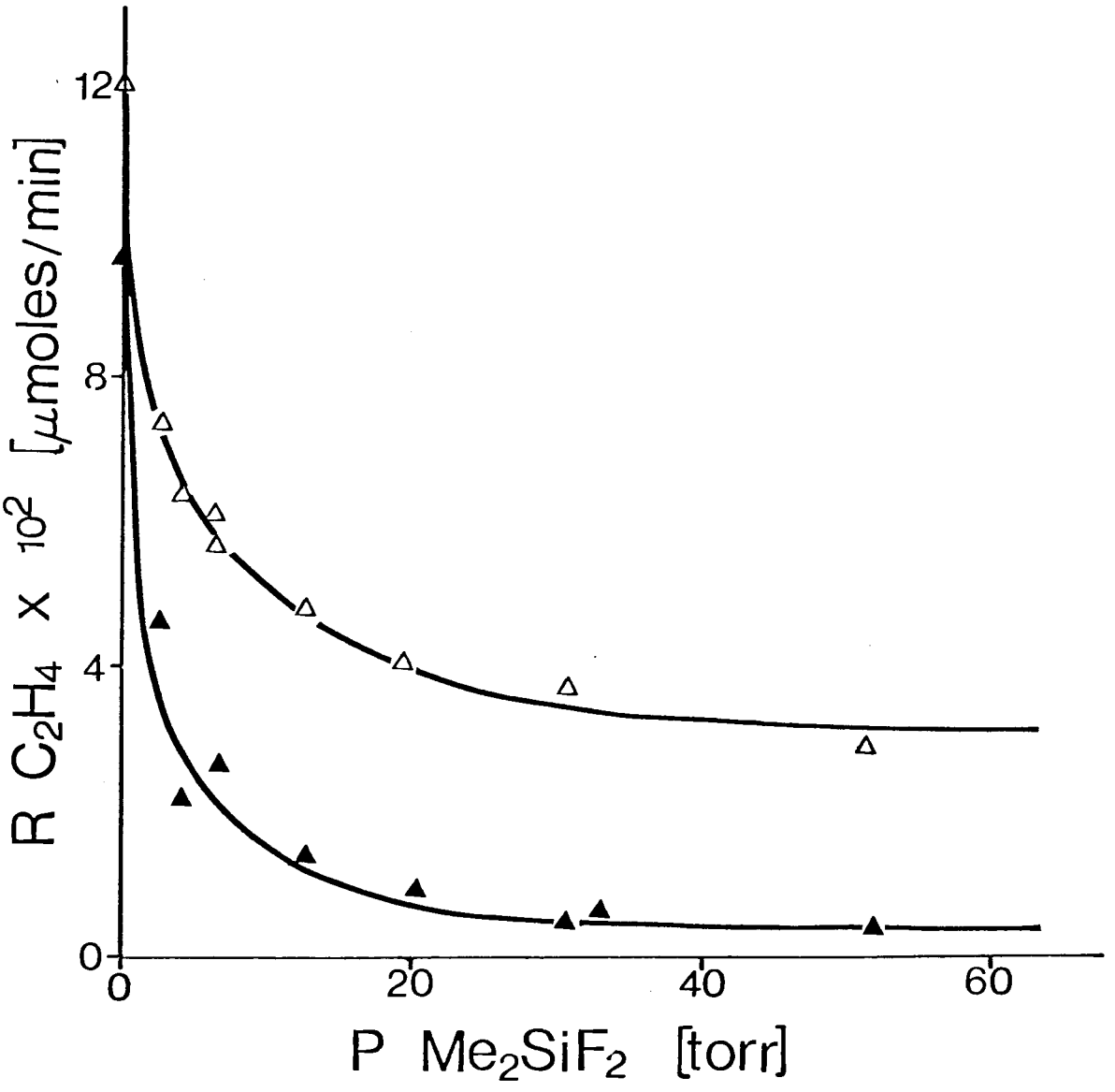

Fig. II-5. Rate of Ethylene Production as a Function of Me_2SiF_2 Pressure from Me_2SiF_2-Ketene (Δ) and Me_2SiF_2-Ketene-NO (▲) Mixtures.

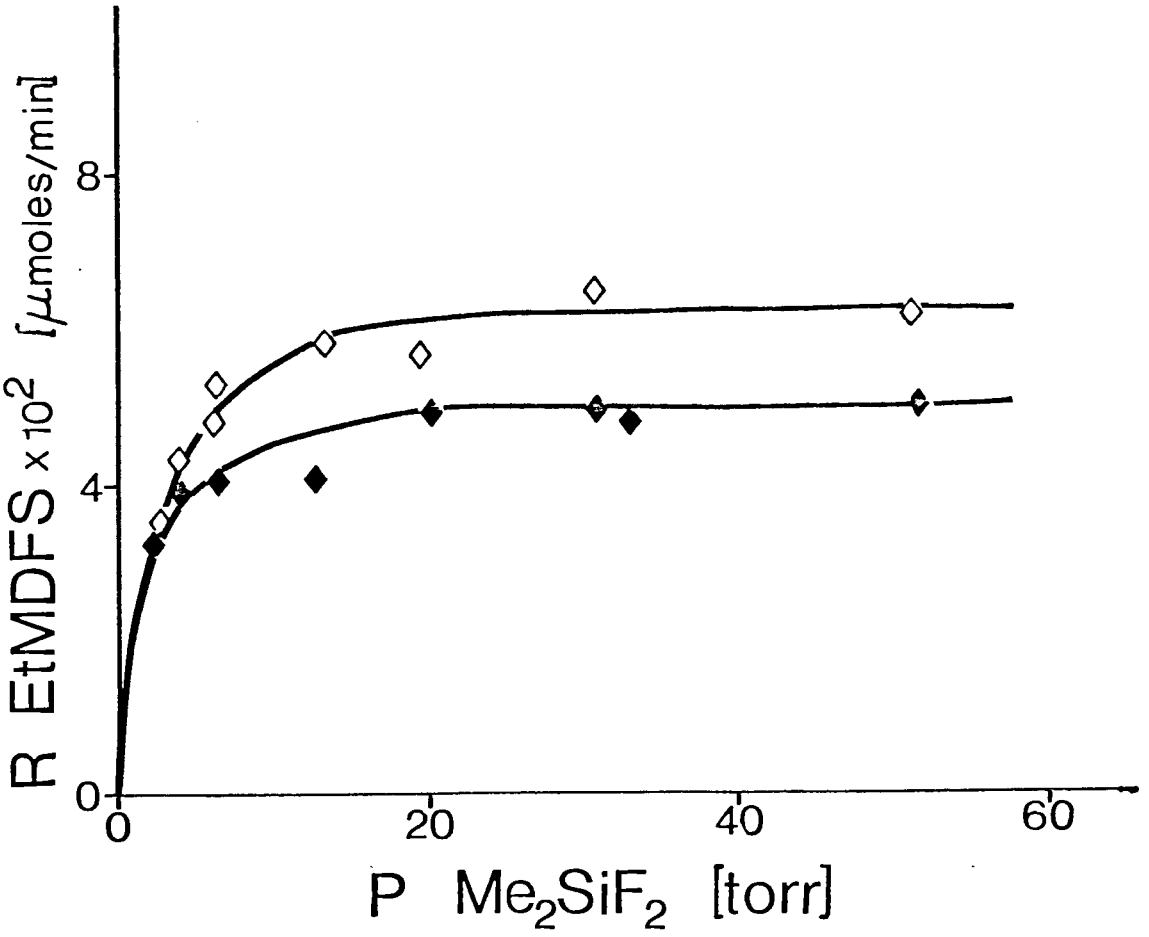

Fig. II-6. Rate of Ethylmethyldifluorosilane Production as a Function of Me_2SiF_2 Pressure from Me_2SiF_2-Ketene (◇) and Me_2SiF_2-Ketene-NO (◆) Mixtures.

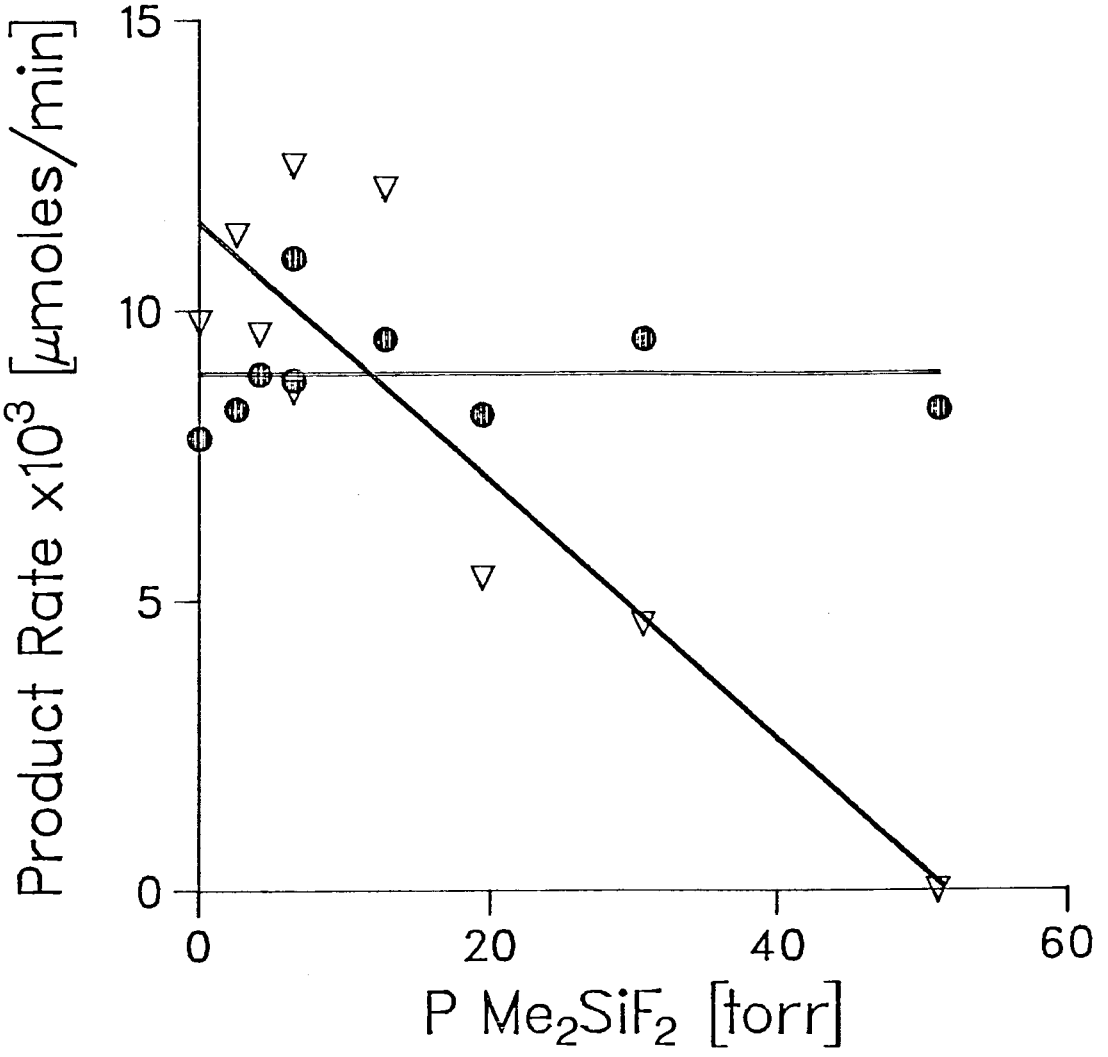

Fig. II-7. Rate of Ethane (●) and Acetylene (▽) Production as a Function of Me_2SiF_2 Pressure from Me_2SiF_2-Ketene Mixtures.

Figures II-5 and II-6 are the data for the Me_2SiF_2-ketene system in the absence of NO. The yields of ethane and acetylene were completely suppressed by the presence of nitric oxide at the concentrations used in these experiments. Carbon monoxide, ethylene and $EtMe_{x-1}SiF_{4-x}$ were the major products of the reaction and in the case of the Me_2SiF_2 system, small quantities of DMFMFS were also formed. The product rates follow the same trends as in the absence of the scavenger but with lower values. Table II-10 also shows experiments carried out at different nitric oxide pressures. These involved a mixture of ≈4 torr of silane and 1.3 torr of ketene together with various pressures (0.072 up to 0.357 torr) of nitric oxide. A small decrease of the products rates was observed as the pressure of nitric oxide was increased, but the ratio (C_2H_4/Σ silane derivatives) was constant, within experimental error.

Table II-9

Product Rates for Me_2SiF_2-Ketene Mixtures

P_K = 1.30±0.02 [torr]

Run	P_{Sil}	CO	C_2H_4	EtMDFS	DMFMFS	C_2H_6	C_2H_2
	[torr]	[μmoles/min]×10^2					
18A	2.54	27.0	7.40	3.58	0.48	0.83	1.13
20A	4.13	25.4	6.36	4.34	0.69	0.89	0.96
13A	6.45	24.2	5.66	5.30	0.74	0.88	0.86
14A	6.45	25.8	6.12	4.80	0.81	1.09	1.25
15A	12.7	24.2	4.80	5.82	0.92	0.95	1.21
16A	19.4	22.0	4.06	5.64	0.97	0.82	0.54
17A	30.6	21.6	3.70	6.48	0.98	0.95	0.46
19A	51.1	18.2	2.88	6.16	0.91	0.83	0
Experiments carried out at $I \neq I_o$							
45A	2.92	19.7	5.82	2.50	0.37	0.62	0.74
44A	15.1	19.8	4.27	5.23	1.00	0.88	0.87
43A	40.9	15.7	2.87	5.05	0.75	0.72	0.13
41A	50.7	15.7	2.70	6.60	1.05	0.77	0

Table II-10

Product Rates for Me_2SiF_2-Ketene-NO Mixtures

P_K = 1.30±0.02 [torr]

Run	P_{Sil}	P_{NO}	CO	C_2H_4	EtMDFS	DMFMFS
	[torr]		[μmoles/min]×10^2			
28A	2.59	0.094	27.0	4.60	3.12	0.46
*40A	3.30	0.209	24.2	3.50	3.46	0.48
*36A	4.14	0.169	26.4	3.48	3.68	0.55
*37A	4.16	0.357	24.6	3.10	3.36	0.51
35A	4.20	0.093	23.8	3.14	3.90	0.59
*38A	4.20	0.072	24.0	3.26	3.70	0.53
27A	6.53	0.091	23.8	2.62	4.06	0.70
*39A	8.16	0.211	23.6	2.04	4.24	0.68
26A	12.83	0.095	21.4	1.36	4.08	0.78
23A	20.15	0.098	20.6	0.90	4.90	0.83
29A	30.69	0.078	20.2	0.46	4.92	0.88
24A	32.99	0.085	21.0	0.61	4.80	0.77
25A	51.71	0.086	18.3	0.36	5.04	0.85

(*) Indicate experiments in which the pressure of NO was varied.

Table II-11. Product Rates for Me_3SiF-Ketene Mixtures

P_K = 1.35±0.02 [torr]

Run	P_{Sil}	CO	C_2H_4	EtDMFS	C_2H_6	C_2H_2
	[torr]	[μmoles/min]×10^2				
21	2.64	18.0	4.82	4.82	0.51	0.54
19	3.00	20.0	5.13	5.40	0.39	0.28
22	5.17	18.7	4.05	6.70	0.63	0.59
18	15.8	16.7	3.02	9.13	0.76	0.28
20	28.3	13.6	1.65	8.35	0.42	0
17	51.2	12.8	1.34	7.94	0.63	0

Table II-12. Product Rates for Me_3SiF-Ketene-NO Mixtures

P_K = 1.30±0.02 [torr]

P_{NO} = 0.143±0.002 [torr]

Run	P_{Sil}	CO	C_2H_4	EtDMFS
	[torr]	[μmoles/min]×10^2		
15	2.20	23.2	3.56	5.26
14	2.87	23.6	3.06	6.16
12	4.23	22.8	2.10	6.84
13	7.72	20.8	1.20	7.54
11	20.18	20.2	0.50	8.34

Table II-13. Product Rates for Me_4Si-Ketene Mixtures

P_K = 1.36±0.02 [torr]

Run	P_{Sil}	CO	C_2H_4	EtTMS	C_2H_6	C_2H_2
	[torr]	[μmoles/min]×10^2				
12C	1.53	22.0	5.97	4.98	0.58	0.59
14C	2.17	20.3	4.77	6.03	0.58	0.59
11C	4.52	19.0	3.83	7.68	0.42	0.12
10C	14.0	16.3	2.08	9.32	0.67	0
13C	30.7	13.2	0.88	7.93	0.51	0
3C	51.6	12.5	0.59	6.94	0.54	0

Table II-14. Product Rates for Me_4Si-Ketene-NO Mixtures

P_K = 1.38±0.04 [torr]

P_{NO} = 0.19±0.03 [torr]

Run	P_{Sil}	CO	C_2H_4	EtTMS
	[torr]	[μmoles/min]×10^2		
6C	2.24	23.3	3.10	6.65
7C	3.33	20.7	2.17	6.70
8C	4.69	21.7	1.82	7.28
9C	6.69	18.0	1.15	7.37
5C	10.13	14.5	0.64	6.57

Table II-15

Product Rates for $MeSiF_3$-Ketene Mixtures[a]

P_K = 1.34±0.05 [torr]

Run	P_{Sil}	CO	C_2H_4	C_2H_6	C_2H_2
	[torr]	[μmoles/min]×10^2			
28B	5.97	23.3	6.58	1.10	1.37
26B	14.1	22.8	5.67	0.86	1.05
2B	16.1	19.7	4.38	0.65	0.63
27B	33.0	18.2	3.63	0.62	0.42
5B	47.4	17.8	3.76	0.92	0.87
25B	51.0	18.5	4.10	0.94	0.92

(a) EtTFS could not be detected under this experimental condition. Small quantities of the compound produced was presumably lost on the column material.

Table II-16

Product Rates for $MeSiF_3$-Ketene-NO Mixtures

$P_K = 4.13 \pm 0.05$ [torr]

$P_{NO} = 0.304 \pm 0.005$ [torr]

Run	P_{Sil}	CO	C_2H_4	EtTFS
	[torr]	[μmoles/min]×10^2		
18B	9.74	75.8	16.0	6.8
19B	13.1	68.8	12.0	7.0
17B	16.4	68.7	11.7	7.2
21B	20.7	72.0	11.3	7.5
16B	29.6	66.2	8.6	7.5
15B	48.4	66.2	5.4	8.6
20B	49.9	62.8	5.0	8.4
13B	50.4	59.5	5.2	8.2

II-5. DISCUSSION

A. The Proposed Mechanism.

The experimental results presented in the previous section indicate that the photolysis of Me_xSiF_{4-x}-ketene mixtures yields various products resulting from the participation of both the lowest singlet and triplet electronic states of methylene. The presence of both methylene states could be inferred from the experimental results obtained in the presence and absence of the scavenger NO. All scavenged experiments showed a complete suppression of ethane and acetylene and a substantial decrease of the ethylene yields. The silicon-containing products were also diminished, but to a lesser extent, by the scavenger NO. In addition, the results show that each silane-ketene system behaved similarly. Therefore, a general mechanism is considered in order to explain the main features of these experiments.

The mechanism proposed below accounts for the major products from each Me_xSiF_{4-x}-ketene system and incorporates reactions II-1 to II-6a (29) to represent the photodissociation of ketene at 313 nm.

II-1 $So \xrightarrow{h\nu} {}^{i}S_1$

II-2 ${}^{i}S_1 \longrightarrow {}^{m}S_o$

II-3 ${}^{m}S_o \longrightarrow {}^{1}CH_2 + CO$

II-4 ${}^{m}S_o \longrightarrow {}^{k}T_1$

II-5 ${}^{k}T_1 \longrightarrow {}^{3}CH_2 + CO$

II-6a $S_o + {}^{m}S_o \longrightarrow S_o + S_o$

II-6b $Me_xSiF_{4-x} + {}^{m}S_o \longrightarrow S_o + Me_xSiF_{4-x}$

II-19 ${}^{1}CH_2 + S_o \longrightarrow {}^{3}CH_2 + S_o$

II-20 ${}^{1}CH_2 + Me_xSiF_{4-x} \longrightarrow {}^{3}CH_2 + Me_xSiF_{4-x}$

II-7 ${}^{1}CH_2 + S_o \longrightarrow C_2H_4 + CO$

II-21a ${}^{1}CH_2 + Me_xSiF_{4-x} \longrightarrow EtMe_{x-1}SiF_{4-x}$ $(x\neq O)$

II-21b ${}^{1}CH_2 + Me_xSiF_{4-x} \longrightarrow Me_xSi(CH_2F)F_{3-x}$

II-22 ${}^{3}CH_2 + S_o \longrightarrow C_2H_4 + CO$

where in the above S_o and S_1 are the ground and first excited singlet states, and T_1 is the lowest triplet state of ketene; i, m, k are vibrational levels of the corresponding electronic states.

Reaction II-6b represents the deactivation of vibrationally excited ketene by the silanes. The production of triplet methylene by collision induced intersystem crossing is a well-established process and thus triplet methylene can be formed not only in the primary process but also through reaction II-19 and II-20. Reactions II-21 represent the well documented insertion of singlet methylene into C-H bonds together with a proposed insertion into the Si-F bond to account for DMFMFS formed from Me_2SiF_2. Reactions II-7 and II-22 are also well documented and represent the formation of ethylene from singlet and triplet methylene.

In the following sections, evidence relating to the above proposals will be provided.

Ethane and acetylene were the minor products of reaction. Addition of the silanes decreases the amount of ketene decomposition (Reaction II-6b) and accordingly a decrease in the yields of both ethane and acetylene is expected whether the mechanism proposed by Kistiakowsky and Walter (p.77) or by Russell and Rowland (p.78) is considered. In the previous section, the experimental results showed that acetylene decreases significantly as the pressure of a given silane was increased. Moreover, the efficiency of the silanes in decreasing acetylene formation was in the order:

$$Me_4Si > Me_3SiF > Me_2SiF_2 > MeSiF_3$$

which is also the observed order of the reactivity of these

compounds towards C-H bond insertion by singlet methylene. On the other hand, the rates of ethane formation showed considerable scatter so it is not possible to ascertain a correlation between the rate of ethane formation and the reactivity of the silanes themselves. However, it is clear that ethane formation is not greatly affected by the addition of the silanes. Qualitative proposals which will account for the formation of the minor products are presented below.

Proposal I.

In order to explain the difference in the behaviour of ethane and acetylene when the silanes are added, Reaction II-23 is included with either the Kistiakowsky and Walter or the Russell and Rowland mechanism. Reaction II-23 represents the abstraction of H atoms by triplet methylene.

II-23 $^3CH_2 + Me_xSiF_{4-x} \rightarrow CH_3 + CH_2Me_{x-1}SiF_{4-x}$

Each of the mechanisms is analyzed separately.

a) Kistiakowsky and Walter

II-8 $^3CH_2 + CH_2CO \rightarrow CH_3 + CHCO$

II-9 $CHCO + CHCO \rightarrow C_2H_2 + 2CO$

II-11 $CH_3 + CH_3 \rightarrow C_2H_6$

Assuming that k_8 and k_{23} are of a similar order of magnitude, at $P_{Sil} >> P_K$ Reaction II-8 will be negligible

compared to Reaction II-23; at the same time, Reaction II-20 will form $^3CH_2$ from $^1CH_2$. Thus a decrease of the C_2H_2 and an increase of the C_2H_6 with increasing pressures of the silanes is predicted. To explain the experimentally observed near constancy of the C_2H_6, a balance between the increase due to Reaction II-23 and the overall decrease due to Reaction II-6b needs to be postulated. With this assumption, Equations II-8, II-9, II-11 and II-23 offer a general explanation of the experimental results.

b) Russell and Rowland

II-12 $^3CH_2 + {}^3CH_2 \rightarrow C_2H_2 + 2H$

II-13 $H + CH_2CO \rightarrow CH_3 + CO$

II-11 $CH_3 + CH_3 \rightarrow C_2H_6$

The rate constant of reaction II-12 has been measured as 3.2×10^{10} L $mol^{-1}s^{-1}$ while rate constants for H abstraction by triplet methylene are $<6\times10^6$ L $mol^{-1}s^{-1}$ (45) and thus an estimate of the ratio of the rates of abstraction (II-23) to combination (II-12) may be made.

II-24 $$\frac{R_{Abs}}{R_{Comb}} = 1.88\times10^{-4}\ \frac{[Sil]}{[^3CH_2]}$$

The acetylene yields from ketene photolysis and the value of k_{12} provides an upper limit of $[^3CH_2] = 1.54\times10^{-10}$ M. Hence, at the lowest silane pressures (1.5 torr) the above ratio is 100 and at

the highest silane pressures (50 torr) is 3.3×10^3 indicating that Reaction II-23 may well be an important source of methyl radicals as the pressure of the silane is increased. Again, similar arguments to those already considered with the Kistiakowsky and Walter mechanism may be used to explain the experimental observations of decreasing acetylene while the ethane is essentially sustained with increasing silane pressure.

Consequently, inclusion of Equation II-23 with either the Russell and Rowland or the Kistiakowsky and Walter mechanisms allows for a qualitative account of the experimental findings. It should be noted, however, that other workers (28a, 45, 48) have suggested that Reaction II-12 produces molecular hydrogen. If this was the case, the Russell and Rowland mechanism will no longer be valid.

Proposal II.

An alternative mechanism which also accommodates the experimental results is proposed below:

II-8 $^3CH_2 + CH_2CO \rightarrow CH_3 + CHCO$

II-25 $^1CH_2 + CHCO \rightarrow C_2H_3CO^* \rightarrow C_2H_2 + CO + H$

II-13 $H + CH_2CO \rightarrow CH_3 + CO$

II-11 $CH_3 + CH_3 \rightarrow C_2H_6$

II-26 $CHCO + Me_xSiF_{4-x} \rightarrow H_2CCO + CH_2(Me)_{x-1}F_{4-x}$

This scheme is based on the observation that increasing silane pressures decreases the formation of acetylene paralleling the decrease in singlet methylene. By analogy with the Kistiakowsky and Walter mechanism, Reaction II-8 produces CH_3 and CHCO radicals, the precursors to C_2H_6 and C_2H_2, respectively. As the pressure of the silane increases, the concentration of singlet methylene will decrease leading to a decrease in C_2H_2 through Reaction II-25 and therefore to a decrease in the concentration of CH_3 radicals formed through Reaction II-13. Simultaneously, the concentration of $^3CH_2$ increases at the expense of $^1CH_2$ via Reaction II-20 and thus the formation of ethane can be sustained through CH_3 production via Reaction II-8. Also, as the pressure of the silane increases, Reaction II-26, H abstraction by CHCO radicals leading to ketene would become an important alternative pathway for the CHCO radicals. The fact that C_2H_2 decreases faster as fluorine substitution on the silane is increased relates to the reactivity found for these compounds in their insertion reactions with singlet methylene. Thus, Equations II-8, II-25, II-13, II-11 and II-26 also offer a qualitative explanation to the results obtained for the formation of the minor products, ethane and acetylene.

B. Mass Balance.

The consumption of ketene in a given experiment can be equated either to the rate of CO produced or to the rate of methylene produced. Thus,

II-27 $R_{CO} = R_{CH_2}$

where,

R_{CO} = no. of CO moles produced per minute.

R_{CH_2} = sum of methylene products from non-scavenged experiments produced per minute.

So

II-28

$$R_{CH_2} = 2R_{C_2H_4} + 2R_{C_2H_6} + 2R_{C_2H_2} + R_{EtMe_{x-1}SiF_{4-x}} + R_{Me_xSi(CH_2F)_{3-x}}$$

Analysis of the data for each silane system, Tables II-17, II-18 and II-19, shows that there is a linear relationship when R_{CO} is plotted against R_{CH_2} (calculated via II-28). In each case, the slope and intercept, and standard deviations are:

Silane	slope	$\frac{\text{intercept}\times 10^2}{[\mu\text{moles/min}]}$
Me_2SiF_2	0.98±0.04	-3.3 ±1.1
Me_3SiF	0.90±0.10	0.39±1.2
Me_4Si	1.02±0.05	-2.8 ±1.0

Thus, within experimental error, the data follow an equation of the form

II-29 $R_{CH_2} = R_{CO} + b$

Figure II-8 is a sample plot of Equation II-29 with the data from Table II-17 (Me_2SiF_2-ketene). The data obtained for the $MeSiF_3$-ketene system did not include a quantitative analysis of EtTFS, this being too small to measure under these comparable experimental conditions.

The value of b is characteristic of a particular system and for Me_3SiF-ketene is zero within error limits. For Me_2SiF_2-ketene and Me_4Si-ketene, the value of b shows that the rate of methylene which is accounted for is less than the rate of carbon monoxide produced. This discrepancy is larger than that expected from random errors and is likely to arise from some systematic error. Two possible sources of systematic error may be considered:

(a) loss of methylene through polymerization;

(b) difficulties in the analysis of silicon-containing products carried out in the presence of large quantities of parent silicon compounds.

In any particular case, the rate of methylene products accounts for approximately 80% or more of the rate of CO produced. Considering the difficulties in separating small amounts of products from the reaction mixture, it is not difficult to justify a discrepancy of the magnitude observed.

Table II-17

Mass Balance: Me_2SiF_2-Ketene System.

P_{Sil}	R_{CO}	R_{CH_2}	$R_{CO\ SEC}$ (a)	$R_{CO\ PRIM}$ (a)
[torr]		[μmoles/min]×10^2		
-	31.7	27.5	13.8	17.9
2.54	27.0	22.8	9.4	17.6
4.13	25.4	21.5	8.2	17.2
6.45	24.2	20.8	7.4	16.8
6.45	25.8	22.5	8.5	17.3
12.7	24.2	20.7	7.0	17.2
19.4	22.0	17.5	5.4	16.6
30.6	21.6	17.7	5.1	16.5
51.1	18.2	14.5	3.7	14.5

(a) The separation of R_{CO} in two parts is discussed below.

Table II-18

Mass Balance: Me_3SiF-Ketene System.

P_{Sil}	R_{CO}	R_{CH_2}	$R_{CO\ SEC}$ (a)	$R_{CO\ PRIM}$ (a)
[torr]		[μmoles/min]×10^2		
-	26.7	24.3	12.2	14.5
2.64	18.0	16.5	5.9	12.1
3.00	20.0	17.0	5.8	14.2
5.17	18.7	17.2	5.3	13.4
15.8	16.7	17.3	4.1	12.6
28.3	13.6	12.5	2.1	11.5
51.2	12.8	11.8	2.0	10.8

(a) The separation of R_{CO} in two parts is discussed below.

Table II-19

Mass Balance: Me_4Si-Ketene System.

P_{Sil}	R_{CO}	R_{CH_2}	$R_{CO\ SEC}$ (a)	$R_{CO\ PRIM}$ (a)
[torr]	[μmoles/min]×10^2			
-	26.7	24.3	12.2	14.5
1.53	22.0	19.3	7.1	14.9
2.17	20.3	17.9	5.9	14.4
4.52	19.0	16.4	4.4	14.6
14.0	16.3	14.8	2.8	13.6
30.7	13.2	10.7	1.4	11.8
51.6	12.5	9.2	1.1	11.4

(a) The separation of R_{CO} in two parts is discussed below.

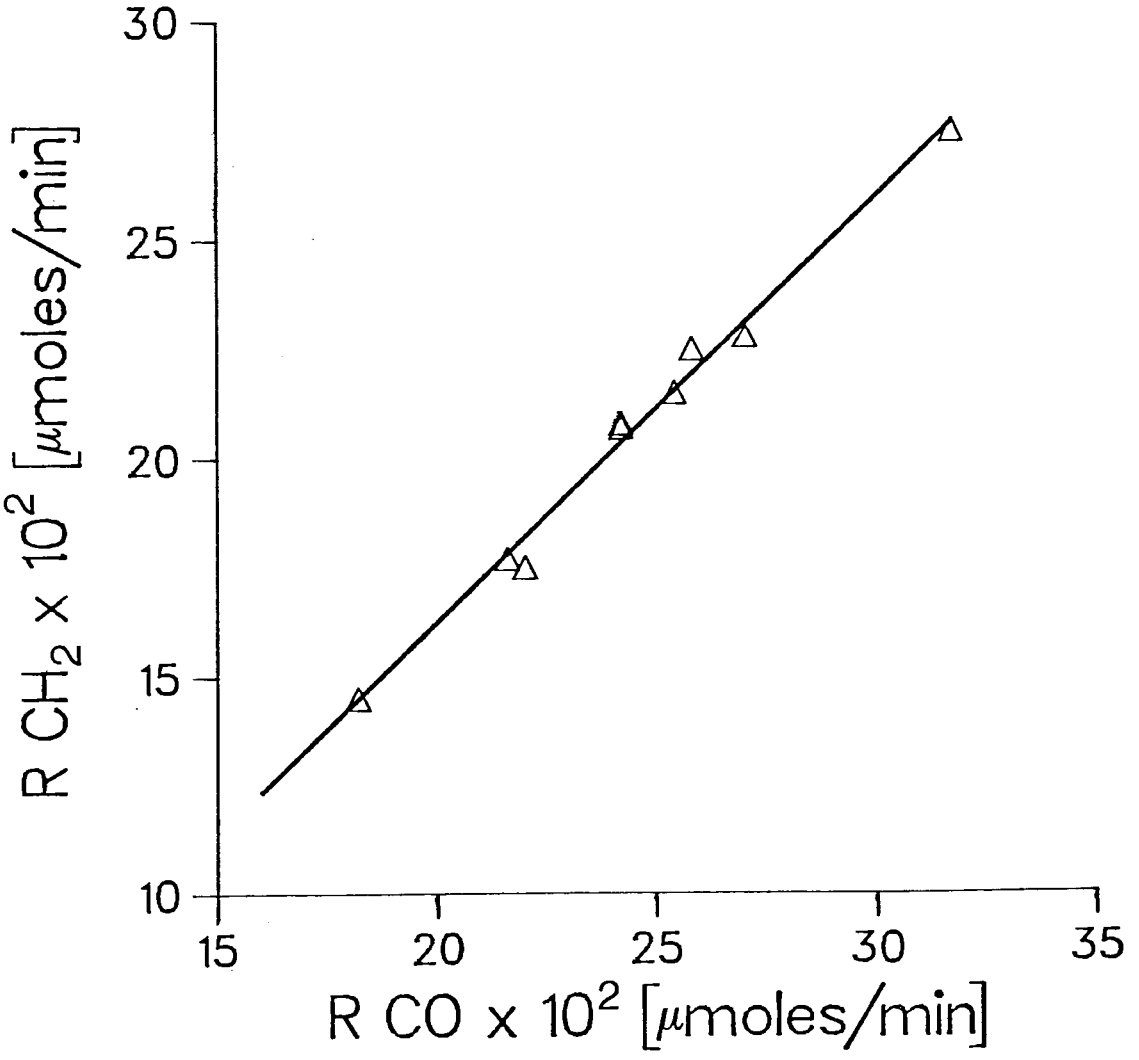

Fig. II-8. A Plot of R_{CO} vs. R_{CH_2} from Me_2SiF_2-Ketene Mixtures.

C. Deactivation of Excited Ketene by the Silanes.

Quantitative studies have shown that excited ketene is collisionally deactivated by ketene and by inert gases. The data obtained with the silanes can be treated to assess the role of these compounds in the deactivation process (II-6b). According to the proposed scheme, the carbon monoxide produced can be divided into two parts: one which represents the carbon monoxide produced by the primary process ($R_{CO\ PRIM}$) and another which represents the carbon monoxide produced by the secondary process ($R_{CO\ SEC}$).

$$\text{II-30} \quad R_{CO} = R_{CO\ PRIM} + R_{CO\ SEC}$$

The secondary carbon monoxide can be calculated from the rates of ethylene, acetylene, and ethane; from ethylene through Reactions II-7 and II-22, and from acetylene and ethane through the stoichiometric relationship II-31.

$$\text{II-31} \quad 4CH_2CO = C_2H_6 + C_2H_2 + 4CO$$

This relationship applies to the mechanistic proposal II describing ethane and acetylene formation but for the Kistiakowsky-Walter and the Russell-Rowland mechanisms, is strictly valid only for pure ketene because of Reaction II-23 which does not lead to secondary CO. In this case, II-31 is an approximation.

The secondary carbon monoxide may then be estimated from:

$$\text{II-32} \quad R_{CO\ SEC} = R_{C2H4} + R_{C2H6} + R_{C2H2}$$

Tables II-17, II-18, II-19 and II-20 show both secondary and primary carbon monoxide for each silane-ketene system calculated through II-32 and II-30.

Table II-20

Primary and Secondary CO: $MeSiF_3$-Ketene System.

P_{Sil} [torr]	$R_{CO\ SEC}$ [μmoles/min]×10²	$R_{CO\ PRIM}$ [μmoles/min]×10²
-	12.7	14.5
5.97	9.05	14.3
14.1	7.58	15.2
16.1	5.66	14.0
33.0	4.67	13.5
47.4	5.55	12.3
51.0	5.96	12.6

From the proposed scheme (Equations II-1 to II-6) the reciprocal of the rate of formation of primary carbon monoxide is given by

$$\text{II-33} \quad R^{-1}_{CO\ PRIM} = \frac{1}{I_{Abs}} \left\{ 1 + \frac{k_{6a}}{(k_3+k_4)} [K] + \frac{k_{6b}}{(k_3+k_4)} [Sil] \right\}$$

where $K \equiv S_o$. At low ketene pressures (less than 60 torr) it has been shown that $\Phi_{PRIM} = 1$ (30c, 31a) suggestive that Reaction II-6a is unimportant under the experimental conditions of the present study. Thus Equation II-33 simplifies to

$$\text{II-34} \quad R^{-1}_{CO\ PRIM} = \frac{1}{I_{Abs}} \left\{ 1 + \frac{k_{6b}}{(k_3+k_4)} [Sil] \right\}$$

Figures II-9, II-10, II-11 and II-12 are plots of $R^{-1}_{CO\ PRIM}$ against silane pressure for each system studied. A straight line as predicted by Equation II-34 provides a good representation of the data. Table II-21 summarizes the values of $k_{6b}/(k_3+k_4)$ obtained from the slope to intercept ratio of each plot.

Assuming Reaction II-6b occurs on every collision, the value of (k_3+k_4) can be determined. In Table II-21 are the estimated collision rate constants, and the values of (k_3+k_4) obtained with the data from each silane-ketene system. The latter agree within experimental error and fall into the reported range of 2.2×10^9 (31c) to 1.1×10^9 s^{-1} (30c).

Table II-21

$$^{m}S_o + Me_xSiF_{4-x} \xrightarrow{k_{6b}} S_o + Me_xSiF_{4-x}$$

Silane	$k_{6b}/(k_3+k_4)$ / L mol^{-1}	$k_z \times 10^{-11}$(a) / L mol^{-1}s^{-1}	$(k_3+k_4)\times 10^{-9}$ / s^{-1}
$MeSiF_3$	65±12	1.82	2.8±0.5
Me_2SiF_2	72±11	2.12	2.9±0.4
Me_3SiF	101±32	2.42	2.4±0.8
Me_4Si	116±16	3.09	2.7±0.4

(a) T = 295°K; collision diameters(b): ketene, 4 Å (30c, 31b); $MeSiF_3$, 5.80 Å; Me_2SiF_2, 6.54 Å; Me_3SiF, 7.22 Å; Me_4Si, 8.64 Å.

(b) It was assumed that the collision diameters of the Me_xSiF_{4-x} compounds are identical to those of the corresponding Me_xSiH_{4-x} compounds (44d).

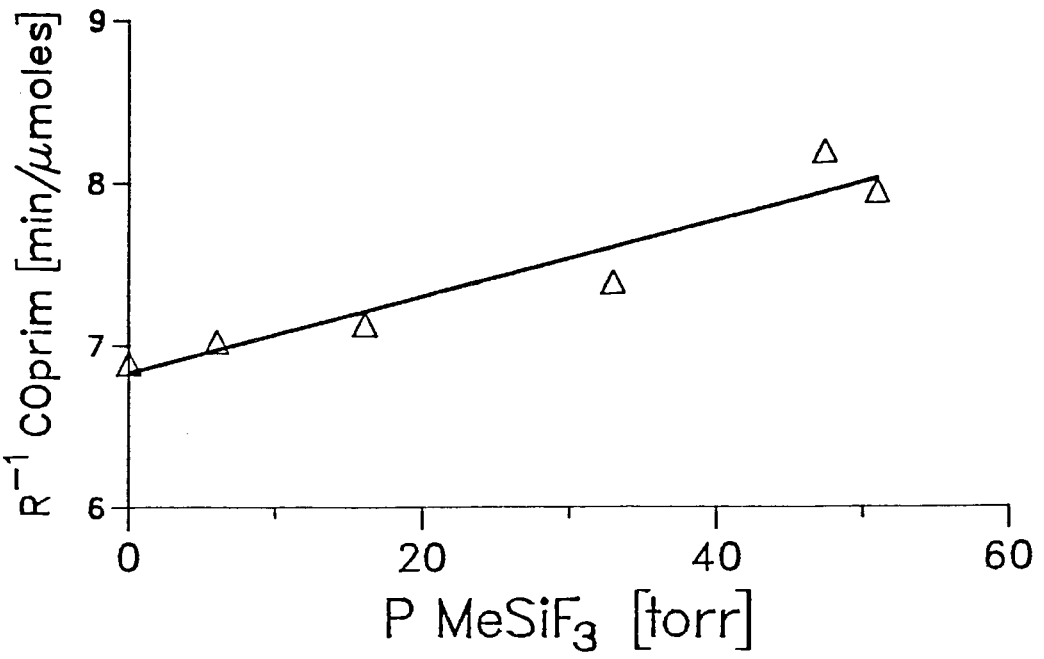

Fig. II-9. A plot of Reciprocal of Primary CO vs. $MeSiF_3$ Pressure from $MeSiF_3$-Ketene Mixtures.

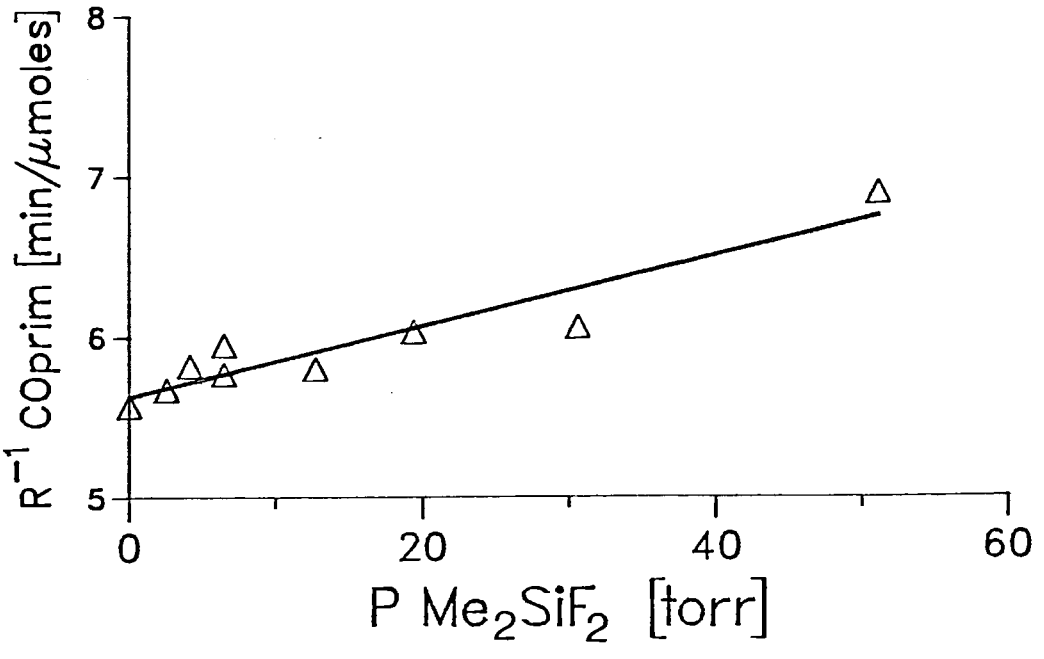

Fig. II-10. A plot of Reciprocal of Primary CO vs. Me_2SiF_2 Pressure from Me_2SiF_2-Ketene Mixtures.

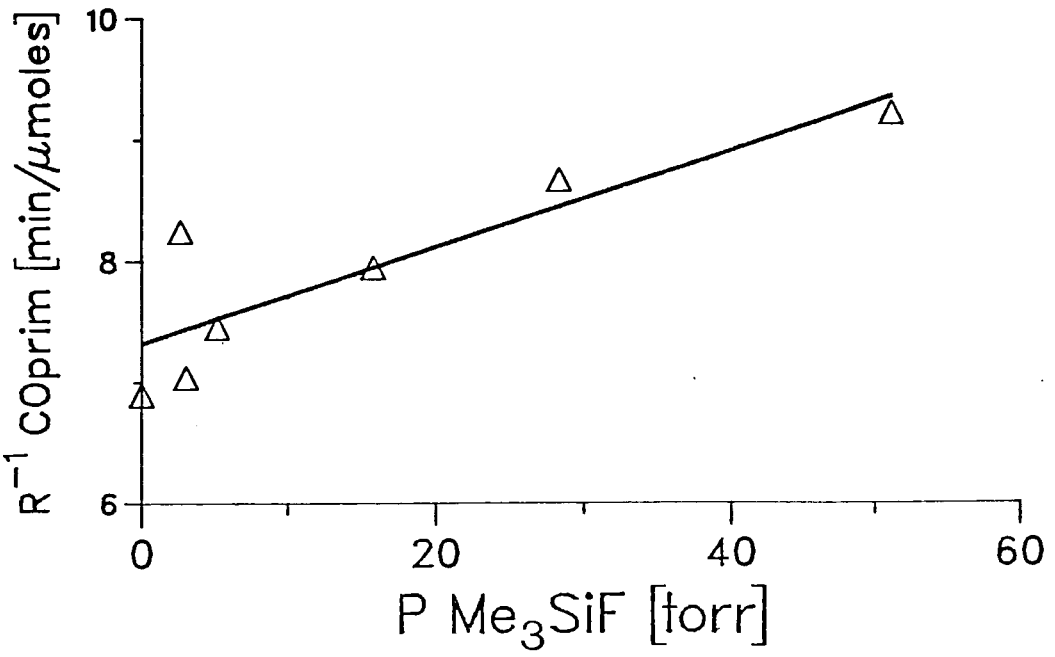

Fig. II-11. A Plot of Reciprocal of Primary CO vs. Me_3SiF Pressure from Me_3SiF-Ketene Mixtures.

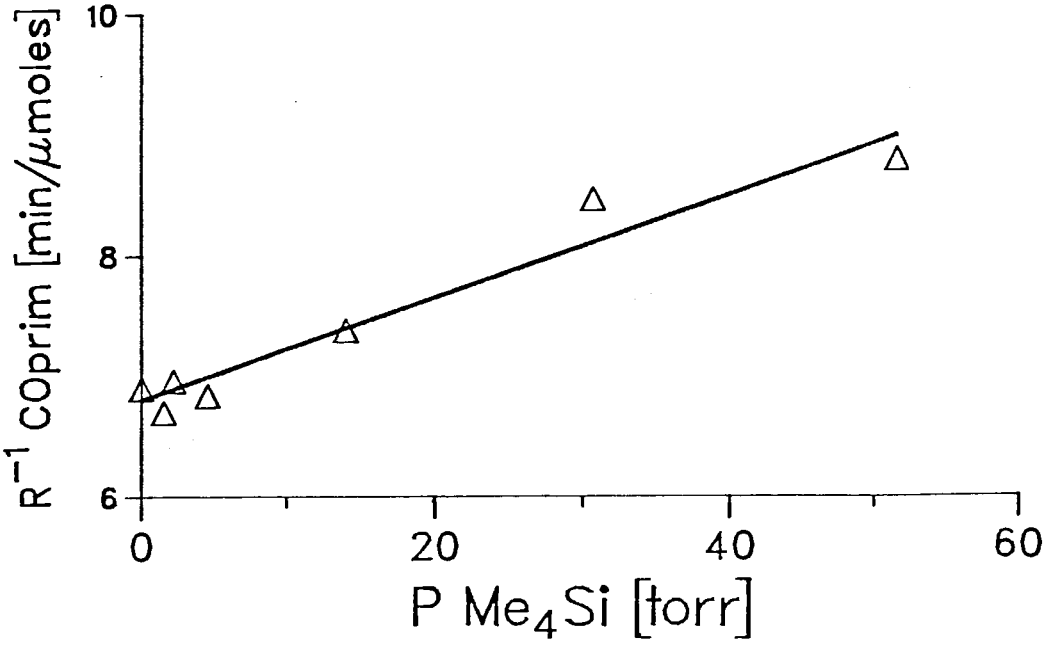

Fig. II-12. A plot of Reciprocal of Primary CO vs. Me_4Si Pressure from Me_4Si-Ketene Mixtures.

D. Reactivity of the Silanes toward Singlet Methylene: Me_xSiF_{4-x}-Ketene-NO Reaction Systems.

The reactivity of the Me_xSiF_{4-x} compounds toward singlet methylene may be determined from measurements of the reaction products formed by the competitive Reactions II-7 and II-21 in the presence of sufficient scavenger concentration to ensure complete removal of triplet methylene. Under such conditions, the proposed scheme may be simplified by omitting the reactions due to triplet methylene.

Thus, consideration of Reactions II-7, II-21a and II-21b yields the general expression:

$$\text{II-35} \quad \frac{R_{C_2H_4}}{R_{Si\ Products}} = \frac{k_7}{(k_{21a}+k_{21b})} \quad \frac{[K]}{[Me_xSiF_{4-x}]}$$

where R_{Si} products =

$$R_{EtMe_{x-1}SiF_{4-x}} + R_{Me_xSi(CH_2F)F_{3-x}}$$

From Reactions II-7 and II-21a

$$\text{II-36a} \quad \frac{R_{C_2H_4}}{R_{EtMe_{x-1}SiF_{4-x}}} = \frac{k_7}{k_{21a}} \quad \frac{[K]}{[Me_xSiF_{4-x}]}$$

and from Reactions II-7 and II-21b

$$\text{II-36b} \quad \frac{R_{C_2H_4}}{R_{Me_xSi(CH_2F)F_{3-x}}} = \frac{k_7}{k_{21b}} \quad \frac{[K]}{[Me_xSiF_{4-x}]}$$

Equation II-36b relates only to the case of Me_2SiF_2 where the corresponding insertion product is observed. The ratios of the rate constants may then be determined from the slopes of the appropriate plots. Thus, Fig. II-13 is a plot of $R_{C_2H_4}/R_{EtMe_{x-1}SiF_{4-x}}$ against $P_K/P_{Me_xSiF_{4-x}}$ with the data from Tables II-10, II-12, II-14 and II-16. Fig. II-14 is a separate plot of the complete data for the $MeSiF_3$-Ketene system; the yields of EtTFS obtained at the lower silane pressures have large errors due to a large uncertainty in measuring the ethyl derivative which was produced in very small amounts. The weighted least-squares line, slope = 6.90±0.56 and intercept = $(4.5\pm5.9)\times10^{-2}$, shows that within error limits the data represents Equation II-36a. Also, Equation II-36a is well represented by the data from the other ethyl derivatives. From the data of Table II-10, a plot of $R_{C_2H_4}/R_{DMFMFS}$ against $P_K/P_{Me_2SiF_2}$ is shown in Fig. II-15 and is in accord with Equation II-36b.

The ethyl derivatives formed in Reaction II-21a could result from insertion into either C-H or C-Si bonds. Work reported in the literature indicates that neither C-Si nor C-C bonds are attacked by singlet methylene (43,49). Thus, it is assumed that only C-H bonds are involved in the formation of the $Et_{Me_{x-1}SiF_{4-x}}$ compounds. The experimental data are consistent with methylene insertion into the C-H bonds of the methylfluorosilanes and only in the case of Me_2SiF_2 does singlet

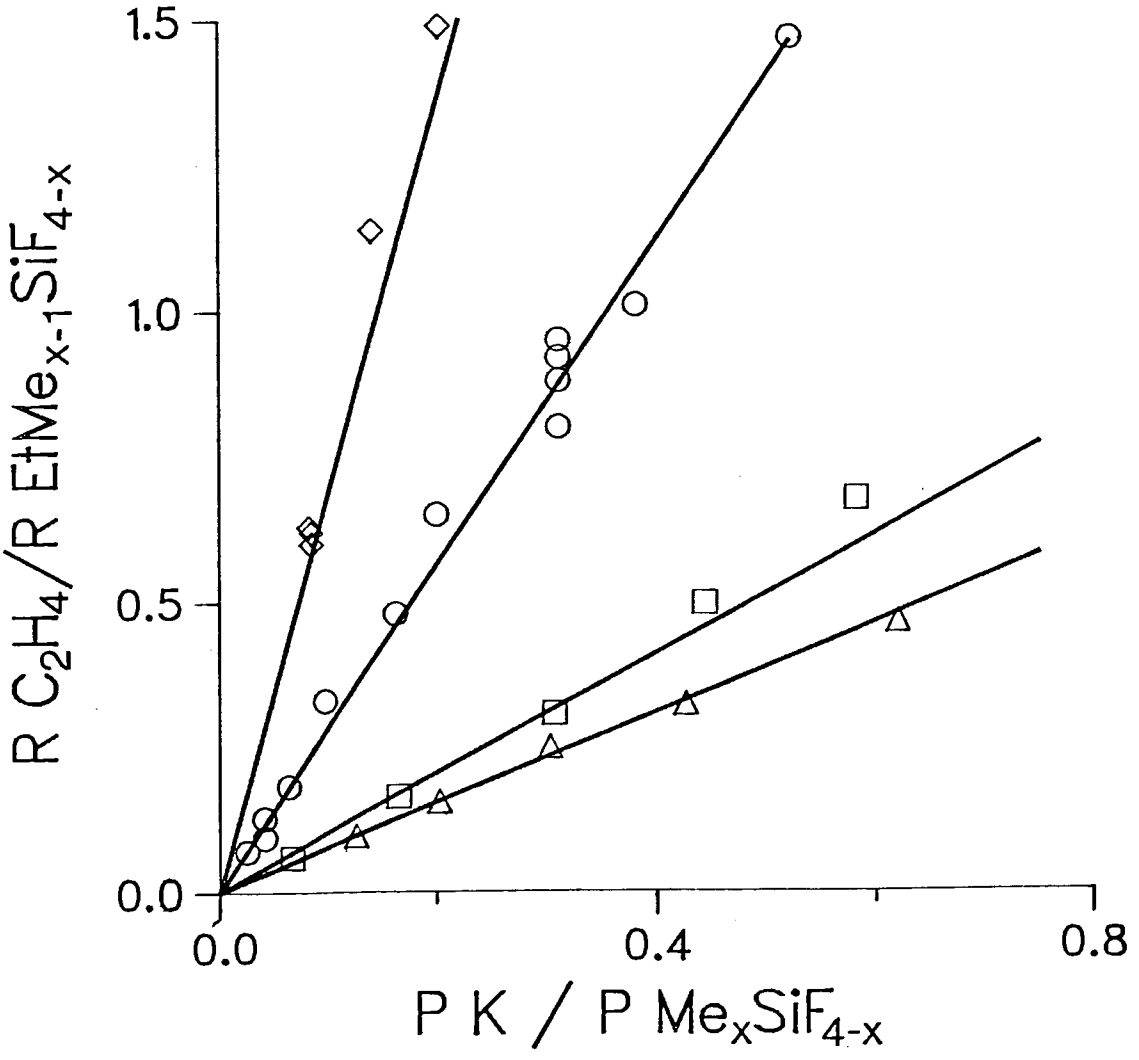

Fig. II-13. A Plot of $R_{C_2H_4}/R_{EtMe_{x-1}SiF_{4-x}}$ vs. $P_K/P_{Me_xSiF_{4-x}}$ from Δ, Me_4Si; □, Me_3SiF; O, Me_2SiF_2 and ◇, $MeSiF_3$ in Mixtures with Ketene and Nitric Oxide.

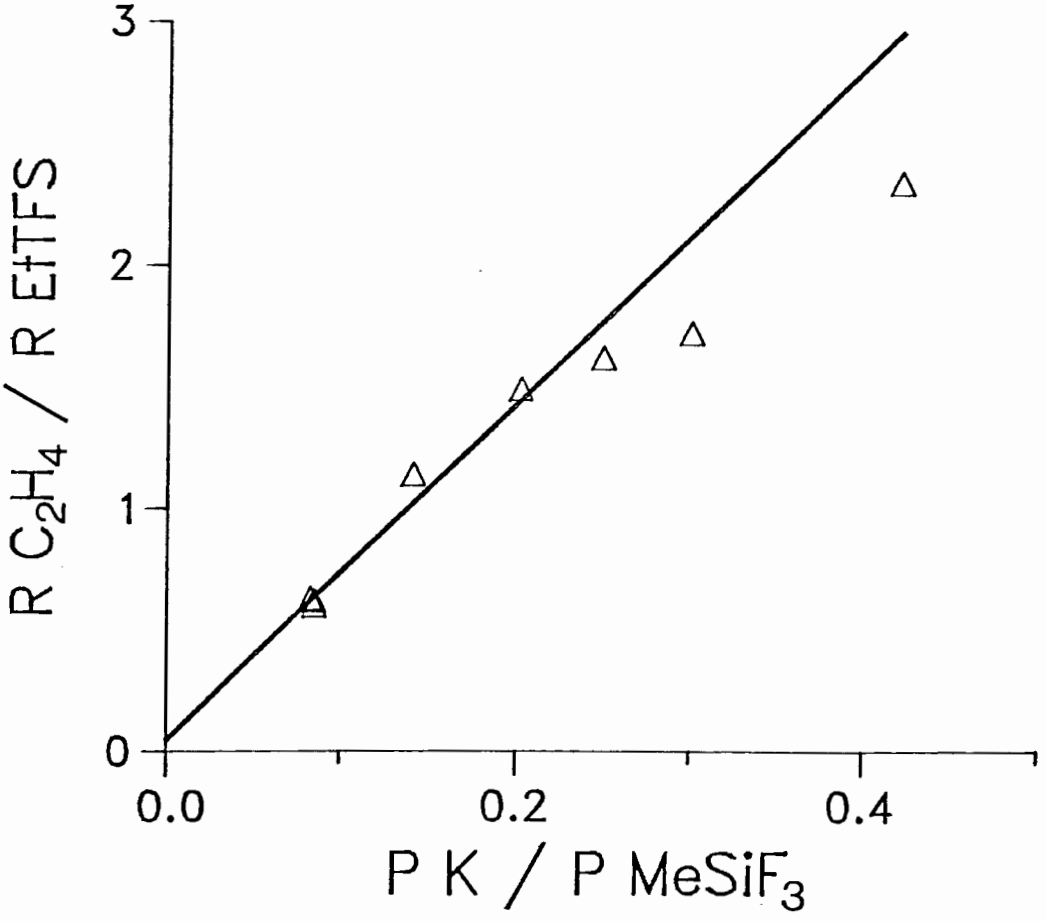

Fig. II-14. A Plot of $R_{C_2H_4}/R_{EtTFS}$ vs. P_K/P_{MeSiF_3} from $MeSiF_3$-Ketene-NO Mixtures.

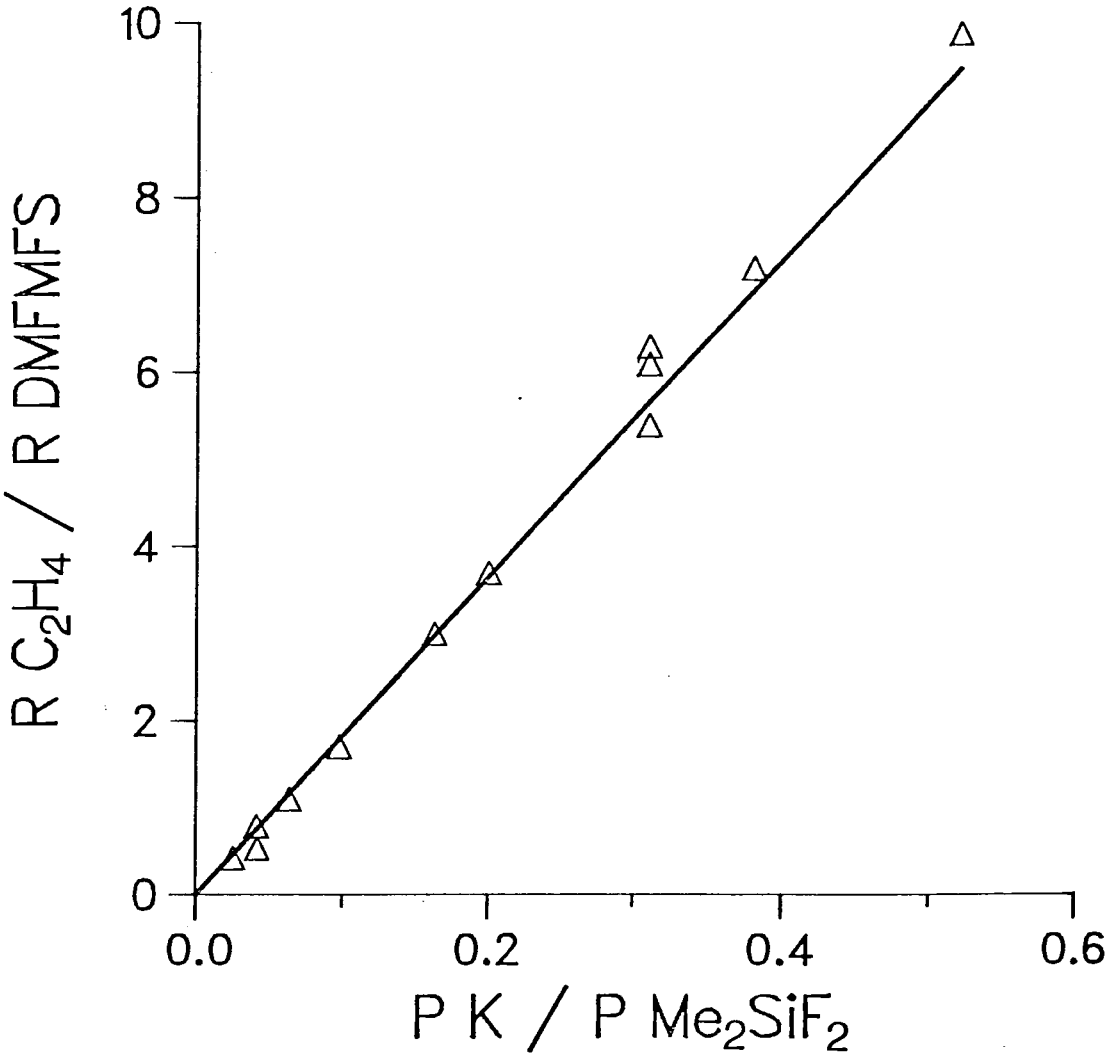

Fig. II-15. A Plot of $R_{C_2H_4}/R_{DMFMFS}$ vs. $P_K/P_{Me_2SiF_2}$ from Me_2SiF_2-Ketene-NO Mixtures.

methylene insert into the Si-F bond to produce the monofluoromethyl derivative. In accord to the proposal, the ratio R_{EtMDFS}/R_{DMFMFS} should be a constant, for both scavenged and nonscavenged Me_2SiF_2-ketene system; since

$$\text{II-37} \quad \frac{R_{EtMDFS}}{R_{DMFMFS}} = \frac{k_{21a}}{k_{21b}}$$

Fig. II-16 gives the dependence of the above ratio on the silane pressure. Despite large uncertainties in the values measured at low silane pressures due to the difficulties in determining small quantities of the DMFMFS in the presence of large amounts of unreacted silane, the results show that Equation II-37 applies over the pressure range studied.

The fact that R_{EtMDFS}/R_{DMFMFS} is unaffected, within error limits, by the presence of NO, suggests that when the scavenged and nonscavenged systems are compared, the decrease observed in the yields of EtMDFS and DMFMFS is due to the consumption of $^1CH_2$ which also reacts with nitric oxide. This decrease in the $^1CH_2$ will not affect reactivity determinations based on the competitive Reactions II-7 and II-21.

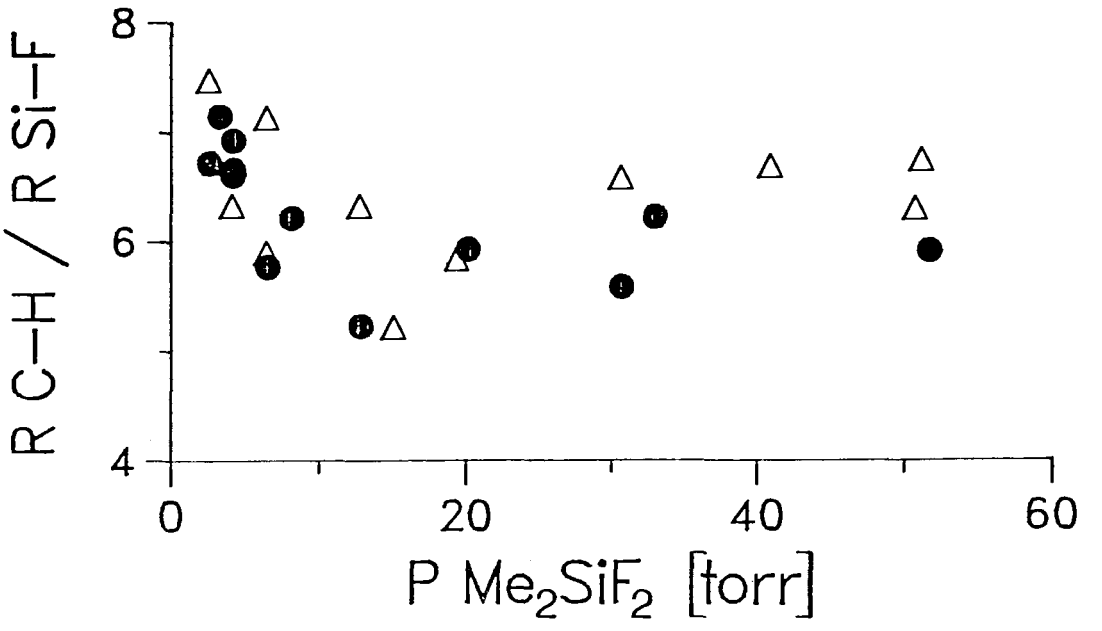

Fig. II-16. Pressure Dependence of the Ratio R_{EtMDFS}/R_{DMFMFS} (RC-H/RSi-F) from Me_2SiF_2-Ketene (Δ) and Me_2SiF_2-Ketene-NO (●) Mixtures.

From the slopes of the plots in Figures II-13, II-14 and II-15, the relative rates of total insertion into C-H and Si-F bonds of the Me_xSiF_{4-x} compounds may be determined (Equations II-36a and II-36b). These values as well as the 'per bond' relative reactivity values are given in Table II-22. These show that the total rate of insertion of singlet methylene into the C-H bonds of the Me_xSiF_{4-x} compounds follows the order expected from the increased number of C-H bonds in the series, that is

$$MeSiF_3 < Me_2SiF_2 < Me_3SiF < Me_4Si$$

Table II-22

Relative Rate Constants of Singlet Methylene Insertion at 22±1°C.

COMPOUND	Relative Rate (k_{21}/k_7)	
	Total	Per Bond
Insertion into the C-H bond		
$MeSiF_3$	0.145	0.048
Me_2SiF_2	0.355	0.058
Me_3SiF	0.971	0.108
Me_4Si	1.30	0.108
Insertion into the Si-F bond		
Me_2SiF_2	0.055	0.028

The per bond reactivity is such that

$$MeSiF_3 < Me_2SiF_2 < Me_3SiF = Me_4Si$$

Substitution of methyl groups by fluorine atoms into tetramethylsilane increases both the C-H and the Si-F bond dissociation energies (50,51) in going from Me_4Si to SiF_4. Table II-23 shows estimates of the C-H bond dissociation energies for the compounds of interest along with their relative reactivities to methylene insertion. Values of the Si-F bond dissociation energies for this series of compounds are not currently available but their trends are well established (51). Thus, a correlation of bond dissociation energy with per bond reactivity is

evident in the case of the compounds $MeSiF_3$, Me_2SiF_2 and Me_3SiF for insertion into C-H bonds; the larger the bond dissociation estimate, the slower the relative rate of insertion.

This trend is not observed in the case of Me_4Si as

TABLE II-23

Comparison of the Relative Reactivity of the Silanes to Methylene Insertion Scaled to $MeSiF_3$ = 1.0 with Estimated Bond Dissociation Energies.

Compound	Relative Reactivity		D_{C-H}[50]	D_{Si-F}[12]
	Total	Per Bond	kJ/mol	
		C-H		
$MeSiF_3$	1.0	0.33	418.4	
Me_2SiF_2	2.4	0.40	414.2	
Me_3SiF	6.6	0.73	410.0	≈807
Me_4Si	8.8	0.73	401.7	
		Si-F		
Me_2SiF_2	0.37	0.18		

compared to Me_3SiF in spite of the bond dissociation energy difference. The observed relative per bond ratio, 1:1, indicates that singlet methylene does not discriminate between these two compounds. A possible explanation is that Me_4Si is a more

sterically hindered molecule for methylene insertion into C-H than is the case in Me_3SiF. This steric effect would act in an opposite direction to the bond strength effect.

Insertion into the Si-F bond of Me_3SiF was not observed even though the bond dissociation energies are in the order $DMe_3Si\text{-}F < DFMe_2Si\text{-}F$ and insertion into Si-F bonds of Me_2SiF_2 was observed. Again, the results may be rationalized in terms of a steric effect. The Si-F bond is shorter than the Si-C bond (12) and is likely to be hindered by the methyl group in Me_3SiF and therefore will be less susceptible to methylene attack.

The discussion on steric effects may be exemplified by the proposal of Skell (52) and Doering (53) who postulated a triangular transition state for methylene insertion into C-H bonds, Figure II-17. Moreover, Gutsche and coworkers (54) suggested that the preferred pathway of methylene attack is midway between the C and H atoms and perpendicular to the C-H bond.

Thus, geometric requirements for the insertion reaction could account for some of the reactivity differences observed in this study.

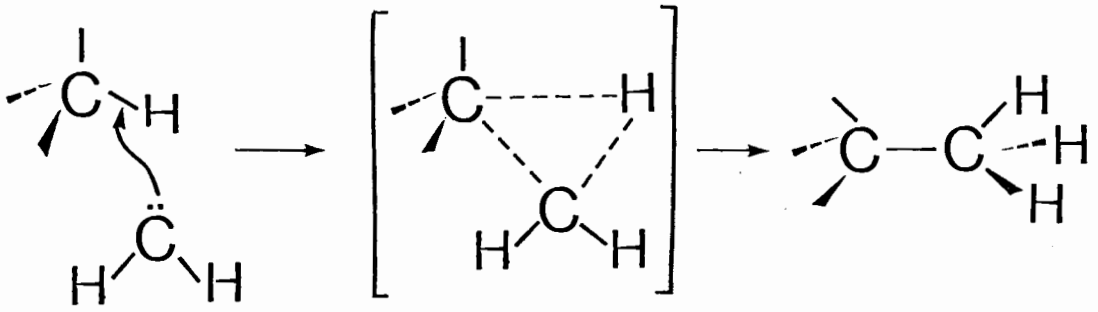

Fig. II-17. Doering-Skell Postulate for Methylene Insertion into C-H Bonds.

E. Me_xSiF_{4-x}-Ketene Reaction Systems (Absence of NO).

In the absence of NO, the participation of $^3CH_2$ needs to be considered in any kinetic analysis.

From the proposed mechanism, the ratio $R_{C_2H_4}/R_{Si\ Products}$ is given by

$$\text{II-38} \quad \frac{R_{C_2H_4}}{R_{Si\ Products}} = \frac{k_7}{k_{21}} \frac{[K]}{[Sil]} + \frac{k_{22}}{k_{21}} \frac{[K]}{[Sil]} \frac{[^3CH_2]}{[^1CH_2]}$$

where $K \equiv S_o$ and $R_{Si\ Products}$ corresponds to the overall rate of formation of Si-containing products.

Applying the steady state approximation to the intermediates, $^1CH_2$ and $^3CH_2$, yields cumbersome expressions when the proposed scheme is considered in full but simplified expressions are obtained when the reactions leading to minor products, ethane and acetylene, are neglected. This simplification is justified on the grounds that at most, 20% of the total methylene contributes to the formation of these products. Thus, the following equation is obtained when the steady state approximation is applied

$$\text{II-39} \quad \frac{[^3CH_2]}{[^1CH_2]} =$$

$$\frac{1}{k_{22}[K]} \left\{ \left(\frac{k_4}{k_3} (k_7 + k_{19})[K] + (k_{20} + k_{21})[Sil] \right) + k_{19}[K] + k_{20}[Sil] \right\}$$

A detailed derivation of expression II-39 is given in the appendix.

Substituting II-39 into II-38 yields

$$\text{II-40} \quad \frac{R_{C_2H_4}}{R_{Si\ Products}} =$$

$$\left(\frac{(k_7+k_{19})}{k_{21}} + \frac{k_4(k_7+k_{19})}{k_3k_{21}}\right)\frac{[K]}{[Sil]} + \frac{k_4(k_{20}+k_{21})}{k_3k_{21}} + \frac{k_{20}}{k_{21}}$$

Equation II-40 predicts that a plot of $R_{C_2H_4}/R_{Si\ Products}$ *vs.* $P_K/P_{Me_xSiF_{4-x}}$ will be a straight line with

$$\text{II-41} \quad \text{Slope} = \frac{(k_7+k_{19})}{k_{21}} + \frac{k_4(k_7+k_{19})}{k_3k_{21}}$$

and

$$\text{II-42} \quad \text{Intercept} = \frac{k_4(k_{20}+k_{21})}{k_3k_{21}} + \frac{k_{20}}{k_{21}}$$

Figure II-18 is a plot of $R_{C_2H_4}/R_{Si\ Products}$ *vs.* $P_K/P_{Me_xSiF_{4-x}}$ using data from Tables II-9, II-11, and II-13. The plot shows that indeed a straight line is a good representation in the case of each silane-ketene system. Also, as predicted by Equation II-40, each representation has a different slope and intercept. The corresponding values and standard deviations are

Compound	Slope	Intercept
Me_4Si	1.3±0.1	0.06±0.01
Me_3SiF	1.8±0.2	0.13±0.02
Me_2SiF_2	3.1±0.2	0.36±0.03

Hence the scheme proposed to account for the major products is consistent with the experimental observations.

An assumption that $k_{21} >> k_{20}$ leads to

II-43 Intercept = k_4/k_3

which is independent of the nature of the silane and contrary to the experimental results. Also, the assumption that $k_7 >> k_{19}$ leads to

$$\text{II-44} \quad \text{Slope} = \frac{k_7}{k_{21}}\left(1 + \frac{k_4}{k_3}\right)$$

In the case of each silane-ketene-NO system, k_7/k_{21} was obtained from the slopes of the plots of $R_{C_2H_4}/R_{Si}$ Products *vs.* $P_K/P_{Me_xSiF_{4-x}}$, thus k_4/k_3 may be obtained from the results for each silane system via,

$$\text{II-45} \quad \frac{k_4}{k_3} = \frac{(\text{slope})}{(\text{slope})_{NO}} - 1$$

The calculated values of k_4/k_3 using the data for Me_2SiF_2, Me_3SiF and Me_4Si are 0.27, 0.80 and 0.69 respectively. These differences are greater than can be accounted for by experimental error suggesting that the above approximation is incorrect and that the expression for k_4/k_3 is better represented by II-46 derived from II-41.

$$\text{II-46} \quad \frac{k_4}{k_3} = \frac{k_{21} \times \text{slope}}{(k_7 + k_{19})} - 1$$

The above experimental results therefore requires the inclusion of Equations II-19 and II-20 in the proposed mechanism.

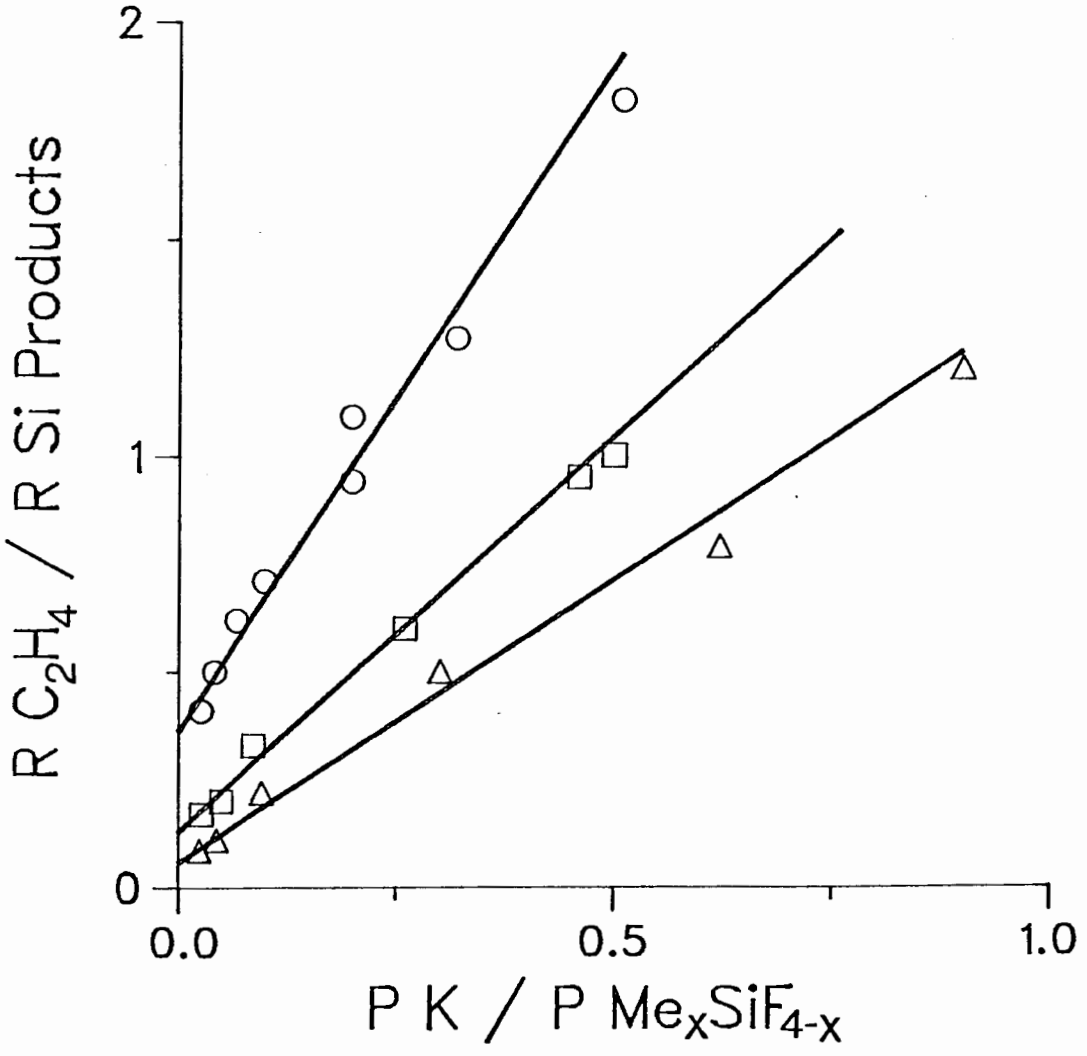

Fig. II-18. A Plot of $R_{C_2H_4}/R_{Si}$ Products vs. $P_K/P_{Me_xSiF_{4-x}}$ from Δ, Me_4Si; □, Me_3SiF and O, Me_2SiF_2 in Mixtures with Ketene.

II-6. CONCLUSIONS

The results of these studies are in agreement with those aspects of the mechanism of ketene photolysis at 313 nm which are well documented. Additional information may be summarized as follows:

1. Singlet methylene inserts into the C-H bonds of the methylfluorosilanes. The rate constant per bond for the insertion is in the order

$$Me_4Si = Me_3SiF > Me_2SiF_2 > MeSiF_3$$

2. Dimethylfluoromethylfluorosilane, $Me_2(F)SiCH_2F$, is formed via $^1CH_2$ insertion into the Si-F bond of Me_2SiF_2. The per bond reactivity of the Si-F bond is 2.1 times less than that of the C-H bond in this system.

3. The Me_xSiF_{4-x} compounds collisionally deactivate excited ketene and the corresponding rate constants are in the order

$$Me_4Si > Me_3SiF > Me_2SiF_2 > MeSiF_3$$

4. The interpretation of the experimental data requires that both ketene and the Me_xSiF_{4-x} compounds participate in the collisionally induced intersystem crossing of $^1CH_2$ to $^3CH_2$.

5. Ethane and acetylene are formed as minor products as a result of reactions of triplet methylene. If Reaction II-23

$$^3CH_2 + Me_xSiF_{4-x} \rightarrow CH_3 + CH_2Me_{x-1}SiF_{4-x}$$

is considered in conjunction with either the Kistiakowsky-Walter or the Russell-Rowland mechanisms, the trends in ethane and acetylene formation may be accounted for. An alternative mechanism involving $^3CH_2$ and $^1CH_2$ is also proposed but this proposal is purely speculative.

N_2O

APPENDIX

Derivation of Expressions for the Quantum Yields of N_2 and N_2O

From the proposed mehanism, the rate of nitrogen formation is given by Equation I-53

$$\text{I-53} \qquad R_{N_2} = k_{31}[(NO)_2{}^*] + k_{45}[SilNO\dagger][NO]$$

If $k_{45} >> k_{31}$

$$\text{I-54} \qquad R_{N_2} = k_{45}[NO][SilNO\dagger]$$

Applying the steady state approximation to the intermediate SilNO†

$$k_{42}[Sil][NO^*] = k_{44}[SilNO\dagger] + k_{45}[SilNO\dagger][NO] + k_{46}[SilNO\dagger][NO] + k_{47}[SilNO\dagger][Sil]$$

Hence,

$$\text{A-1} \qquad [SilNO\dagger] = \frac{k_{42}[Sil][NO^*]}{k_{44} + (k_{45} + k_{46}) + k_{47}[Sil]}$$

Applying the steady state approximation to the intermediate NO*

$$k_{27}[Hg^*][NO] = k_{29}[NO][NO^*] + k_{30}[NO][NO^*] + k_{42}[Sil][NO^*] + k_{43}[Sil][NO^*]$$

But, $I_{Abs} = k_{27}[Hg^*][NO]$.

Hence,

$$\text{A-2} \qquad [NO^*] = \frac{I_{Abs}}{(k_{29} + k_{30})[NO] + (k_{42} + k_{43})[Sil]}$$

Substituting the expression for [NO*] in Equation A-1 yields

A-3 $[SilNO\dagger] =$

$$\frac{I_{Abs}k_{42}[Sil]}{\{(k_{29}+k_{30})[NO] + (k_{42}+k_{43})[Sil]\}\{k_{44}+(k_{45}+k_{46})[NO] + k_{47}[Sil]\}}$$

Thus,

I-55 $\Phi_{N_2} \equiv \frac{R_{N_2}}{I_{Abs}} =$

$$\frac{k_{42}k_{45}[NO][Sil]}{\{(k_{29}+k_{30})[NO]+(k_{42}+k_{43})[Sil]\}\{k_{44}+(k_{45}+k_{46})[NO] + k_{47}[Sil]\}}$$

The rate of N_2O formation is given by Equation I-56.

I-56 $R_{N_2O} = k_{32}[(NO)_2^*][NO] + k_{49}[SilNO\dagger\dagger][NO]$

If $k_{49} >> k_{32}$

I-57 $R_{N_2O} = k_{49}[NO][SilNO\dagger\dagger]$

Applying the steady state approximation to the intermediate SilNO††

$$k_{43}[Sil][NO^*] = k_{48}[SilNO\dagger\dagger] + k_{49}[SilNO\dagger\dagger][NO] + k_{50}[SilNO\dagger\dagger][NO] + k_{51}[SilNO\dagger\dagger][Sil]$$

Hence,

$$[SilNO\dagger\dagger] = \frac{k_{43}[Sil][NO^*]}{k_{48}+(k_{49}+k_{50})[NO]+k_{51}[Sil]}$$

Replacing the expression for [NO*] given in A-2, the above equation becomes

$$[SilNO\dagger\dagger] = \frac{I_{Abs}k_{43}[Sil]}{\{(k_{29}+k_{30})[NO]+(k_{42}+k_{43})[Sil]\}\{k_{48}+(k_{49}+k_{50})[NO] + k_{51}[Sil]\}}$$

Thus,

I-58

$$\Phi_{N_2O} \equiv \frac{R_{N_2O}}{I_{Abs}} = \frac{k_{43}k_{49}[NO][Sil}{\{(k_{29}+k_{30})[NO]+(k_{42}+k_{43})[Sil]\}\{k_{48}+(k_{49}+k_{50})[NO] + k_{51}[Sil]\}}$$

Derivation of the Expression for the ratio $[^3CH_2]/[^1CH_2]$

From the scheme proposed on p.120, Equation II-38 is obtained:

$$\text{II-38} \qquad \frac{R_{C_2H_4}}{R_{Si\ Products}} = \frac{k_7}{k_{21}}\frac{[K]}{[Sil]} + \frac{k_{22}}{k_{21}}\frac{[K]}{[Sil]}\frac{[^3CH_2]}{[^1CH_2]}$$

Applying the steady state approximation to the intermediate $[^3CH_2]$

$$k_4[^mS_o] + k_{19}[^1CH_2][K] + k_{20}[^1CH_2][Sil] = k_{22}[^3CH_2][K]$$

Hence,

$$\text{A-4} \qquad [^3CH_2] = \frac{k_4[^mS_o] + \{k_{19}[K] + k_{20}[Sil]\}[^1CH_2]}{k_{22}[K]}$$

Applying the steady state approximation to the intermediate $[^1CH_2]$

$$k_3[^mS_o] =$$

$$k_7[^1CH_2][K] + k_{19}[^1CH_2][K] + k_{20}[^1CH_2][Sil] + k_{21}[^1CH_2][Sil]$$

Hence,

$$\text{A-5} \qquad [^1CH_2] = \frac{k_3[^mS_o]}{(k_7+k_{19})[K] + (k_{20}+k_{21})[Sil]}$$

Rearranging expression A-4 yields

$$\text{A-6} \qquad \frac{[^3CH_2]}{[^1CH_2]} = \frac{1}{k_{22}[K]}\left\{\frac{k_4[^mS_o]}{[^1CH_2]} + k_{19}[K] + k_{20}[Sil]\right\}$$

and substituting for $[^1CH_2]$ in Equation A-6 yields

$$\text{II-39} \qquad \frac{[^3CH_2]}{[^1CH_2]} =$$

$$\frac{1}{k_{22}[K]}\left\{\frac{k_4}{k_3}\left((k_7+k_{19})[K] + (k_{20}+k_{21})[Sil]\right) + k_{19}[K] + k_{20}[Sil]\right\}$$

Substituting the expression for the ratio $[^3CH_2]/[^1CH_2]$ into the second term of Equation II-38 yields

$$\text{A-8} \qquad \frac{k_{22}}{k_{21}}\frac{[K]}{[Sil]}\frac{[^3CH_2]}{[^1CH_2]} \equiv$$

$$\frac{k_4(k_7+k_{19})}{k_3k_{21}}\frac{[K]}{[Sil]} + \frac{k_{19}}{k_{21}}\frac{[K]}{[Sil]} + \frac{k_4(k_{20}+k_{21})}{k_3k_{21}} + \frac{k_{20}}{k_{21}}$$

Hence,

$$\text{II-40} \qquad \frac{R_{C_2H_4}}{R_{Si\ Products}} =$$

$$\left(\frac{(k_7+k_{19})}{k_{21}} + \frac{k_4(k_7+k_{19})}{k_3k_{21}}\right)\frac{[K]}{[Sil]} + \frac{k_4(k_{20}+k_{21})}{k_3k_{21}} + \frac{k_{20}}{k_{21}}$$

BIBLIOGRAPHY

1. E.W.R. Steacie, "Atomic and Free Radical Reactions", 2nd ed., Reinhold Publishing Co., New York (1954).

2. a) J.G. Calvert and J.N. Pitts, "Photochemistry", John Wiley and Sons, New York (1966).
b) H. Okabe, "Photochemistry of Small Molecules", John Wiley and Sons, New York (1978).
c) K.K. Rohatgi-Mukherjee, "Fundamentals of Photochemistry", John Wiley and Sons, New York (1978).
d) R.B. Cundall and A. Gilbert, "Photochemistry", T. Nelson and Sons, London (1970).

3. K.J. Laidler, J. Chem. Phys. 15, 712 (1947).

4. M.W. Zemansky, Phys. Rev. 36, 919 (1930).

5. a) J.R. Bates, J. Am. Chem. Soc. 54, 569 (1932).
b) A.J. Yarwood, O.P. Strausz, and H.E. Gunning, J. Chem. Phys. 41, 1705 (1964).
c) K. Yang, J. Am. Chem. Soc. 89, 5345 (1967).
d) J.V. Michael and G.N. Suess, J. Phys. Chem. 76, 482 (1974).

6. a) R.J. Cvetanovic, J. Chem. Phys. 23, 1208 (1955).
b) R.J. Cvetanovic, "Progress in Reaction Kinetics", Vol 2, Pergamon Press, London (1964).

7. a) Y. Rousseau and H.E. Gunning, Can. J. Chem. 41, 465 (1963).
b) M.G. Bellas, Y. Rousseau, O.P. Strausz, and H.E. Gunning, J. Chem. Phys. 41, 468 (1964).

8. R.J. Cvetanovic, W.E. Falconer, and K.R. Jennings, J. Chem. Phys. 35, 1225 (1961).

9. M.A. Nay, G.N.C. Woodall, O.P. Strausz, and H.E. Gunning, J. Am. Chem. Soc. 87, 179 (1965).

10. Y. Rousseau, O.P. Strausz, and H.E. Gunning, J. Chem. Phys. 39, 962 (1963).

11. a) S. Penzes, A.J. Yarwood, O.P. Strausz, and H.E. Gunning, J. Chem. Phys. 43, 4524 (1965).
b) S. Penzes, O.P. Strausz, and H.E. Gunning, ibid 45, 2322 (1966).

12. E. Colvin, "Silicon in Organic Synthesis', Butterworths (1981).

13. W.A. Noyes, J. Am. Chem. Soc. 53, 514 (1931).

14. R.J. Fallon, J.T. Vanderslice, and E.A. Mason, J. Phys. Chem. 63, 2082 (1959).

15. J.T. Vanderslice, E.A. Mason, and W.G. Maisch, J. Chem. Phys. 31, 738 (1959).

16. F.R. Gilmore, J. Quant. Spectry. Radiative Transfer 5, 369 (1965).

17. A.B. Callear and R.G. Norrish, Proc. Roy. Soc. (London) 266, 299 (1962).

18. O.P. Strausz and H.E. Gunning, Can. J. Chem. 39, 2549 (1961).

19. O.P. Strausz and H.E. Gunning, Can. J. Chem. 41, 1207 (1963).

20. R. Walsh, Acc. Chem. Res. 14, 246 (1981).

21. I.M.T. Davidson, C.E. Dean, and F.T. Lawrence, J. Chem. Soc., Chem. Comm., 52 (1981).

22. W.H. Atwell and D.R. Weyenberg, Angew. Chem., Int. Ed. Engl. 8, 469 (1969).

23. T.N. Bell, K.A. Perkins, and P.G. Perkins, J. Chem. Soc., Faraday Trans.I, 77, 1779 (1981).

24. K.A. Perkins and P.G. Perkins. Private communication to T.N. Bell.

25. I.M.T. Davidson and J.I. Mathews, J. Chem. Soc., Faraday Trans.I, 77, 2277 (1981).

26. a) R.G.W. Norrish and F.W. Kirkbride, J. Chem. Soc., 119 (1933).
b) R.G. Norrish, H.G. Crone and O.D. Saltmarsh, ibid., 1533 (1933).

27. a) H.M. Frey, Progr. Reaction Kinetics 2, 131 (1964).
b) W. Kirmse, "Carbene Chemistry", Academic Press, 2nd Ed., New York (1971).
c) P.P. Gaspar and G.S. Hammond, Carbenes Vol. II, Chapter 6, M. Jones and R. Moss (eds.), John Wiley and Sons, Inc., (1975), and references therein.

28. a) K. Knox, R.G. Norrish and G. Porter, J. Chem. Soc., 1477 (1952).
b) R.N. Dixon and G.H. Kirby, Trans. Faraday Soc. 62, 1406 (1966).
c) J.W. Rabalais, J.M. McDonald, V. Scherr and P.S. McGlynn, Chem. Rev. 71, 73 (1971).
d) A.H. Laufer and R.A. Keller, J. Am. Chem. Soc. 93, 61 (1971).

29. V.A. Zabransky and R.W. Carr, J. Phys. Chem. 79, 1618 (1975).

30. a) A.N. Stratchan and W.A. Noyes, J. Am. Chem. Soc. 76, 3258 (1954).
b) A.N. Stratchan and D.E. Thornton, J. Phys. Chem. 70, 952 (1966).
c) A.N. Stratchan and D.E. Thornton, Can. J. Chem. 46, 2353 (1968).

31. a) B.T. Connelly and G.B. Porter, Can. J. Chem. 36, 1640 (1958).
b) G.B. Porter and B.T. Connelly, J. Chem. Phys. 33, 81 (1960).
c) G.A. Taylor and G.B. Porter, J. Chem. Phys. 36, 1406 (1962).

32. a) F.S. Rowland, C. McKnight and E.K.C. Lee, J. Am. Chem. Soc. 89, 469 (1967).
b) R.L. Russell and F.S. Rowland, J. Am. Chem. Soc. 92, 7508 (1970).

33. G.B. Kistiakowsky and N.W. Rosenberg, J. Am. Chem. Soc., 72, 321 (1950).

34. G.B. Kistiakowsky and T.A. Walter, J. Phys. Chem. 72, 3952 (1968).

35. R.L. Russell and F.S. Rowland, J. Phys. Chem. 83, 2073 (1979).

36. A.H. Laufer and A.M. Bass, J. Phys. Chem. 78, 1344 (1974).

37. P.S.T. Lee, R.L. Russell and F.S. Rowland, Chem. Comm., 18 (1970).

38. W.B. deMoore and S.W. Benson, Adv. Photochem. 2, 219 (1964).

39. G. Herzberg, Proc. Royal Soc. (London) 262A, 291 (1961).

40. M.L. Halberstadt and J.R. McNerby, J. Am. Chem. Soc. 89, 3417 (1967).

41. R.A. Moss and M. Jones, "Reactive Intermediates", Vol. 2, R.A. Moss and M. Jones (Eds.), John Wiley and Sons, p.59 (1981).

42. K.A.W. Kramer and A.N. Wright, J. Chem. Soc., 3604 (1963).

43. a) J.W. Simons and C.J. Mazac, Can. J. Chem. 45 , 1717 (1967).
b) J.W. Simons and C.J. Mazac, J. Am. Chem. Soc. 90, 2484 (1968).
c) W.L. Hase, W.G. Brieland and J.W. Simons, J. Phys. Chem. 73, 4401 (1969).
d) W.L. Hase and J.W. Simons, J. Chem. Phys. 54, 1277 (1971).

44. M.J. Pilling and J.A. Robertson, J. Chem. Soc., Faraday Trans. I, 73, 968 (1977).

45. W. Braun, A.M. Bass, and M. Pilling, J. Chem. Phys. 52, 5131 (1970).

46. A.I. Vogel, "A Text-Book of Practical Organic Chemistry", Longmans, 3d Ed., p.372 (1961).

47. E.S. Alexander, R.N. Haszeldine, N.J. Newlands, and A.E. Tipping, J. Chem. Soc. (A), 2285 (1970).

48. S.A. Banyard, C.E. Canosa-Mas, M.D. Ellis, H.M. Frey and R. Walsh, J. Chem. Soc., Chem. Comm., 1156 (1980).

49. a) R.T. Conlin, P.P. Gaspar, R.H. Levin and M. Jones, J. Am. Chem. Soc. 94, 7165 (1972).
b) W.J. Baron, M.R. DeCamp, M.E. Hendrick, M. Jones, R.H. Levin, and M.B. Sohn, "Carbenes", Vol. I, M. Jones and R.A. Moss (Eds.), John Wiley and Sons, New York (1973).

50. T.N. Bell and A.E. Platt, J. Phys. Chem. 75, 603 (1971).

51. T.N. Bell, R. Berkley, A.E. Platt and A.G. Sherwood, Can. J. Chem. 52, 3158 (1974).

52. a) P.S. Skell and R.C. Woodworth, J. Am. Chem. Soc. 78, 4496 (1956).
b) P.S. Skell and A.Y. Garner, ibid., 78, 5430 (1956).

53. W.E. Doering and H. Prinzbach, Tetrahedron 6, 24 (1959).

54. C.D. Gutsche, G.L. Bachman, W. Udell and S. Bauerlein, J. Am. Chem. Soc. 93, 5172 (1971).